Cellular responses mediated by the transcription factor STAT1 in murine inflammatory diseases

Dissertation

In partial fulfilment of the requirements for the degree

"Doctor rerum naturalium (Dr. rer. nat.)"

of the Georg-August-Universität Göttingen

within the "Molecular Medicine" study program

of the Georg-August University School of Science (GAUSS)

submitted by

Theresa Riebeling

born in Schwalmstadt

Göttingen 2016

Members of the thesis committee:

Prof. Dr. mult. Thomas Meyer (supervisor)

Email: thomas.meyer@med.uni-goettingen.de

Postal Adress: Institute of Psychosomatic Medicine and Psychotherapy
University Medical Centre Göttingen
Georg-August-University Göttingen
Waldweg 33
37073 Göttingen

Prof. Dr. rer. nat. Susanne Lutz (second member of the thesis committee)

Email: susanne.lutz@med.uni-goettingen.de

Postal Adress: Institute of Pharmacology and Toxicology
University Medical Centre Göttingen
Georg-August-University Göttingen
Robert-Koch-Straße 40
37075 Göttingen

Prof. Dr. med. Dörthe Katschinski (third member of the thesis committee)

Email: doerthe.katschinski@med.uni-goettingen.de

Postal Adress: Institute of Cardiovascular Physiology
University Medical Centre Göttingen
Georg-August-University Göttingen
Humboldtallee 23
37073 Göttingen

Date of Disputation: 27 October 2016

AFFIDAVIT

Here I declare that my doctoral thesis entitled

“Cellular responses mediated by the transcription factor STAT1 in murine inflammatory diseases”

has been written independently with no other sources and aids than quoted.

Theresa Riebeling
Göttingen, September 2016

List of publications

Riebeling T, Staab J, Herrmann-Lingen C, Meyer T. DNA binding reduces the dissociation rate of STAT1 dimers and impairs the interdimeric exchange of protomers. *BMC Biochem* 2014;15:28.

Staab J, **Riebeling T**, Koch V, Herrmann-Lingen C, Meyer T. The two interfaces of the STAT1 N-terminus exhibit opposite functions in IFNγ-regulated gene expression. *Mol Immunol* 2015;67(2 Pt B):596-606.

Table of contents

Abbreviations VI
Acknowledgements XIII
Abstract XV
List of tables XVIII
List of figures XIX
1 Introduction 1
1.1 STAT1 – A key transcription factor in immunity and inflammation 1
1.2 JAK/STAT signalling, the actin cytoskeleton and the ERM-proteins 11
1.3 Objectives of this project 15
2 Materials and methods 16
2.1 Materials 16
2.1.1 Chemicals and reagents 16
2.1.2 Culture media 18
2.1.3 Drugs 19
2.1.4 Kits 19
2.1.5 Equipment 20
2.1.6 Disposables 21
2.1.7 Water 22
2.1.8 Sterilization of material 22
2.1.9 Oligonucleotides and primers 22
2.1.10 Enzymes and recombinant proteins 24
2.1.11 Antibodies 25
2.1.12 Plasmids and constructs 27
2.1.13 Cell lines 27
2.1.14 Animals 28
2.1.15 Software 28
2.2 Methods 30
2.2.1 Cell culture 30
2.2.2 Protein biochemistry 32
2.2.3 DNA analysis 36

2.2.4 RNA analysis 40
2.2.5 Primary cell isolation 41
2.2.6 Animal experiments 42
2.2.7 Classical histology 45
2.2.8 Immune staining techniques 46
2.2.9 Statistical analysis 48
3 Results 49
3.1 N-terminus-mediated intradimeric interactions are dispensable for protomer exchange kinetics of STAT1 49
3.1.1 DNA-binding kinetics do not differ among native STAT1 and GFP-tagged STAT1 50
3.1.2 Native and GFP-tagged STAT1 form hetero-tetrameric complexes *ex vivo* 52
3.1.3 The rate of protomer exchange is reduced through binding to DNA 53
3.1.4 The exchange of STAT1 protomers is a process independent of intradimeric N-terminal interactions 55
3.2 Gene expression of ezrin is weakly induced by STAT1 59
3.2.1 Unique GAS motif in the promoter region of the human ezrin gene was identified 59
3.2.2 STAT1 readily binds to the tandem GAS motif as a dimer but poorly as a tetramer 60
3.2.3 STAT1 associates to the *EZR* promoter in Jurkat cells 62
3.2.4 IFNγ-activated STAT1 induces *EZR* gene transcription 63
3.2.5 No evidence of IFNγ-induced ezrin expression in leukemia cell lines 65
3.2.6 *Ex vivo* analysis of STAT1-deficient and STAT1-F77A mutant mice does not show decreased ezrin protein expression 68
3.3 Assessment of the role of IFNγ-dependent STAT1 signalling in myocardial infarction 71
3.3.1 General characteristics of the study cohort and infarct survival 71
3.3.2 H&E staining did not reveal differences in the size of the infarcted area 73
3.3.3 Mice carrying the STAT1-F77A mutant are protected from adverse cardiac remodelling 75
3.3.4 STAT1 expression is reduced in hearts of STAT1-F77A knockin mice compared with the wildtype on day 3 following myocardial infarction 80
3.3.5 Immune histochemistry shows an accumulation of cells expressing tyrosine-phosphorylated STAT1 in the inflammatory infiltrate 82
3.3.6 No evidence of altered recruitment of neutrophils, monocytes or T cells to areas of myocardial infarction was observed in STAT1-F77A mutant mice 84

3.4 STAT1 deficiency delays onset of EAE upon challenge with lipopolysaccharide 88
3.4.1 STAT1 knockout mice are protected upon LPS challenge 89
3.4.2 Onset of clinical symptoms of EAE is delayed in STAT1 knockout mice injected with LPS 90
3.4.3 Cells from STAT1 knockout mice show increased proliferation upon MOG_{35-55} peptide stimulation 92
3.4.4 STAT1 knockout cells produce increased amounts of IL-17A and IFNγ 94
4 Discussion 97
5 References 115
Curriculum vitae 133

Abbreviations

A	Adenine
AF	Alexa Fluor dye
APC	Allophycocyanin
APCs	Antigen-presenting cells
APS	Ammonium persulphate
ATP	Adenosine triphosphate
BDGP	Berkeley drosophila genome project
BSA	Bovine serum albumin
C	Cytosine
C3a	Complement C3 isoform a
CBP/p300	CREB-binding protein
CCL	C-C motif chemokine ligand
CCR2	C-C motif chemokine receptor type 2
CD	Cluster of differentiation
cDNA	Complementary deoxyribonucleic acid
CFA	Complete Freund's adjuvant
ChIP	Chromatin immunoprecipitation
CIS	Cytokine-inducible SH2-domain containing protein
CNS	Central nervous system
Comp	Competition
Con A	Concanavalin A
CREB	cAMP response element-binding protein
CXCL	C-X-C motif chemokine ligand
Cy	Cyanine
DAB	3,3'-diaminobenzidine
DMEM	Dulbecco's modified Eagle's medium
DMSO	Dimethyl sulphoxide
DNA	Deoxyribonucleic acid
dNTP	Deoxynucleotide triphosphates
DTT	Dithiothreitol
EAE	Experimental autoimmune encephalomyelitis

EDTA	Ehylenediaminetetraacetic acid
EF	Ejection fraction
EGF	Epidermal growth factor
EGTA	Ethylene glycol-bis(β-amimoethyl ether)-N,N,N',N'-tetraacetic acid
EH medium	Preservation medium
ELISA	Enzyme-linked immunosorbent assay
EMSA	Electrophoretic mobility shift assay
ERM	Ezrin, radixin, moesin
EZR	Ezrin
FACS	Fluorescence-activated cell sorting
F-actin	Filamentous actin
FAS	Fractional area shortening
FBS	Fetal bovine serum
FERM	Four-point-one, ezrin, radixin, moesin
FITC	Fluorescein isothiocyanate
FOXP3	Forkhead box P3
FS	Fractional shortening
G	Guanine
GAPDH	Glyceraldehyde 3-phosphate dehydrogenase
GAS	Interferon-γ activated site/sequence
GBP	Guanylate binding protein
GFP	Green fluorescent protein
GH	Growth hormone
GTP	Guanosine triphosphate
H&E	Haemalum and eosin
HEPES	4-(2-hydroxyethyl)-1-piperazineethanesulphonic acid
HMGB1	High mobility group box 1
HPV	Human papilloma virus
HSP	Heat-shock protein
i.p.	Intraperitoneal
ICAM	Intercellular adhesion molecule
IFIT1	Interferon-induced protein with tetratricopeptide repeats 1
IFN	Interferon

IFNAR	Interferon-α-receptor
IFNGR	Interferon-γ-receptor
IgE	Immunoglobulin E
IGF	Insulin-like growth factor
IgG	Immunoglobulin G
IL	Interleukin
iNOS	Inducible nitric oxide synthase
IRAK	Interleukin-1 receptor associated kinase
IRF	Interferon-regulatory factor
ISGF	Interferon-stimulated gene factor
ISRE	IFNα-stimulated gene response element
JAK	Janus kinase
KO	Knockout
LIF	Leukemia-inhibitory factor
LN	Lymph node
LPS	Lipopolysaccharide
L-selectin	Lymphocyte selectin
LV	Left ventricle
Ly49A	Killer cell lectin-like receptor, subfamily A, member 1
Ly-6C / Ly-6G	Lymphocyte antigen 6 complex, locus C/G
LY96	Lymphocyte antigen 96
MHC	Major histocompatibility complex
MI	Myocardial infarction
MOG_{35-55}	Myelin oligodendrocyte glycoprotein peptide, amino acids 35-55
MPO	Myeloperoxidase
MS	Multiple sclerosis
Mx-Cre	Cre-recombinase expressed under the control of the MX dynamin-like GTPase 1
MyD88	Myeloid differentiation primary response gene 88
n.d.	Not detectable
NEAA	Non-essential amino acid
NFκB	Nuclear factor κB
NK	Natural killer
NOS	Nitric oxide synthase

N-terminus	Amino-terminus
PAGE	Polyacrylamide gel electrophoresis
PBS	Phosphate-buffered saline
PCR	Polymerase chain reaction
PE	Phycoerythrin
p-ERM	Phosphorylated ERM protein
PI3K	Phosphatidylinositol-4,5-biphosphate 3-kinase
PIAS	Protein inhibitor of activated STATs
PKC	Protein kinase C
Poly-dIdC	Poly-deoxyinosinic-deoxycytidylic acid
p-STAT	Phosphorylated STAT protein
PTP1B	Protein tyrosine phosphatase 1B
PVDF	Polyvinylidene fluoride
qPCR	Quantitative polymerase chain reaction
Rac1	RAS-related C3 botulinum substrate 1
RAGE	Receptor of advanced glycation end products
Rap1	RAS-related protein 1
RAR	Retinoic acid receptor
ReMed	Restimulation medium
Rho	Ras homolog
RIPA	Radioimmunoprecipitation assay
RNA	Ribonucleic acid
ROCK	Rho associated coiled-coil containing protein kinase
RORγt	RAR-related orphan receptor γ t
ROS	Reactive oxygen species
RPMI	Roswell Park Memorial Institute medium
RV	Right ventricle
SDS	Sodium dodecyl sulphate
SH2	Src-homology
SHP	SH2-containing phosphatase
SLC9A1	Solute carrier family 9 member A1
SOCS	Suppressor of cytokine signalling
STAT	Signal transducer and activator of transcription
T	Thymine

TBE	Tris, boric acid, EDTA buffer
T-bet	T cell-specific T-box transcription factor
TBS(T)	Tris buffered saline (supplemented with Tween-20)
TBX21	T-box 21
TC	Tyrosine phosphatase
TCR	T cell receptor
TE buffer	Tris EDTA buffer
TEMED	Tetramethylethylenediamine
TGF	Transforming growth factor
Th	T helper
TLR	Toll-like receptor
TMB	3,3',5,5'-tetramethylbenzidine
TNF	Tumour necrosis factor
TRAF6	TNF receptor-associated factor 6
TSS	Transcription start site
TYK	Tyrosine kinase
Untr	Untreated
UV	Ultra violet
VCAM	Vascular cell adhesion molecule
Vol_d	Volume diastole
Vol_s	Volume systole
WT	Wildtype
ZO	Zona occludens
αS1 / αS3	Anti-STAT1/3 antibody

Units

%	Percent
°C	Degree Celsius
b	Base
bpm	Beats per minute
Bq	Becquerel
Da	Dalton
g	Gram
G	Gauge
h	Hour
l	Liter
m	Meter
M	mol/l
min	Minute
mol	Mole
rpm	Rounds per minute
sec	Second
x g	Times gravity
Ω	Ohm

Amino Acids

When referring to amino acids either the three letter code or the one letter code is used.

Amino Acid	Three letter code	One letter code
Alanine	Ala	A
Arginine	Arg	R
Asparagine	Asn	N
Aspartic acid	Asp	D
Cysteine	Cys	C
Glutamic acid	Glu	E
Glutamine	Gln	Q
Glycine	Gly	G
Histidine	His	H
Isoleucine	Ile	I
Leucine	Leu	L
Lysine	Lys	K
Methionine	Met	M
Phenylalanine	Phe	F
Proline	Pro	P
Serine	Ser	S
Threonine	Thr	T
Tryptophan	Trp	W
Tyrosine	Tyr	Y
Valine	Val	V

Acknowledgements

Now, at the end of my time as a doctorate student, there are a couple of people whom I would like to thank for their help and support during the past three-and-a-half years. Without these people, this piece of work would not have been possible.

I hold the deepest gratitude towards my supervisor Professor Thomas Meyer. Throughout the time of my doctorate he gave me the greatest support and contributed to this project with discussion, advice, ideas, and material. He markedly shaped my view on what it means to be a scientist. I truly admire his dedication and enthusiasm.

Moreover, I would like to thank the members of my thesis committee, Professor Dörthe Katschinski and Professor Susanne Lutz, for their input, help, ideas and support – and for joining my committee while I was already in the middle of my doctorate. I thank Professor Ali El-Armouche who helped to establish the myocardial infarction project during the early phase but then had to leave my thesis committee when he moved to his new position in Dresden. Furthermore, I thank Professor Uwe-Karsten Hanisch who helped in laying the foundation of this project. His early passing was a great loss.

I am grateful to Dr Aleksandar Ivetic, our partner within the IRTG 1816, his lab group, and the entire department of Cardiology at King's College in London for offering me the opportunity to stay, work and learn with and from them during a period of two months last year.

I would like to acknowledge the service unit of the SFB 1002. I thank Sabrina Wollborn and Sarah Zafar for doing a wonderful job in performing the myocardial infarction surgery with great care and skill, Roland Blume and Marcel Zoremba for providing me with clear echocardiographic images and Beate Knocke for teaching me how to evaluate them properly.

Moreover, I want to express my gratitude towards the entire lab group of Professor Alexander Flügel, especially towards Dr Fred Lühder for his help and support in getting the EAE project started, and the technicians Martina Weig, Adriane Stas, and Birgit Curdt for teaching me and helping me with the needed experimental techniques.

I would like to express my gratitude towards my co-workers at the lab of molecular psychocardiology here in Göttingen for being supportive and helpful during the past three years. I hold a deep gratitude towards Dr Julia Staab, our post-doc for her help, ideas and valued discussion, for sharing her experience and expertise, helping me to calm down when I

was worried and for performing the qPCR on the STAT1 F77A knockin model. I want to thank Asma Doudin for double-checking my results and wish her all the best for her doctorate. Furthermore, I thank our technicians Heike Hühn and Anke Gregus for their excellent technical support and maintenance of the lab.

During my doctorate, I was granted the pleasure of meeting several MD students and rotation students and was allowed to supervise a few bachelor theses. I want to thank all of them for providing a pleasant working atmosphere and bringing new ideas into the lab. There are two students who I want to mention especially: Johannes Wolff for acquiring the proliferation and ELISA data of the EAE experiments with me during his bachelor thesis and Priyanka Menon for immune staining a part of the paraffin sections shown in this thesis. It was a pleasure to work with and supervise them.

Special thanks go to the organizing team of the International Research Training Group (IRTG) 1816. Not only did they help me and my fellow students of the program with funding issues but also supported us by offering workshops, meetings, and seminars and by encouraging us to widen our scope beyond our projects. I thank Dr Christina Würtz, Katja El-Armouche, Fulya Ören, Gry Dihazi, and Ulrike Fischer for the terrific work they have done and for always having an open ear when problems occurred. Furthermore, I want to mention my fellow students of the IRTG 1816 program. I hope that we will keep in touch.

During the past three-and-a-half years I have experienced and received lots of support by people from different departments of the University Medical Centre in Göttingen. I want to thank everybody who helped me at some point of my thesis by providing me with some reagent, a protocol, a cell line, an idea, discussion or technical assistance. I am sorry that there is not enough room to mention all of these people.

Finally, I want to mention my sister Katharina and my aunt Eva for proof-reading this thesis. I thank my parents, family, friends and my fiancé for being supportive, encouraging me to do a doctorate, and for their love, help and care at all times.

Abstract

The intracellular transduction of interferon signals from the plasma membrane to the nucleus is mediated by signal transducer and activator of transcription 1 (STAT1) which acts in tetrameric form as a transcription factor in immune responses. In this project, the protomer exchange between STAT1 dimers was studied under kinetic aspects and this process was identified as a potential rate-limiting step in the STAT1 activation/inactivation cycle. The data support an alternative mechanism for the transition between the parallel and anti-parallel conformation of STAT1 dimers based on the dissociation and subsequent reassociation of protomers which does not require reciprocal interactions within the N-terminal domain dimer to stabilize an intermediate conformational state. However, binding to high-affinity STAT-specific target sequences, termed gamma-activated sites (GAS), critically interfered with the exchange dynamics. A tandem GAS element in the promoter of the human gene coding for the cytoskeletal protein ezrin was identified *in silico* as a putative STAT1 target sequence, and was confirmed to bind dimeric STAT1 on each motif to moderately induce gene transcription. However, mice carrying either an N-terminal substitution mutation of STAT1 affecting cooperative DNA binding or a complete functional knockout of the *Stat1* gene did not present with altered expression of ezrin and moesin in bone marrow cells compared with mice expressing the wildtype molecule. In a model of myocardial infarction performed by ligation of the left anterior descending coronary artery, male mice expressing the IFNγ-irresponsive STAT1 mutant displayed higher survival rates, whereas females were protected from adverse cardiac remodelling in the early remodelling phase. The inflammatory infiltrate showed a mild increase in tyrosine-phosphorylated STAT1, while the pool of total STAT1 was significantly reduced in the infarcted areas of knockin animals as compared to their wildtype littermates. In experimental autoimmune encephalomyelitis used as a model for a T helper cell-induced autoimmune disease, cells obtained from lymphatic organs of STAT1-deficient animals at the time of disease onset were hyperproliferative and secreted high amounts of IFNγ and IL-17A. Injection of these mice with lipopolysaccharide during the induction phase of experimental autoimmune encephalomyelitis completely abolished this proliferative phenotype. In summary, the findings demonstrate the role of cooperative DNA binding and tetramer formation of STAT1 in orchestrating complex immunological processes, even in the absence of infectious agents and, furthermore, highlight the function of tyrosine-phosphorylated STAT1 as a key factor facilitating the cross-talk between innate and adaptive immunity.

STAT1-vermittelte zelluläre Antworten in murinen entzündlichen Erkrankungen

Die intrazelluläre Weiterleitung von Interferonsignalen von der Zytoplasmamembran zum Zellkern wird vermittelt über den Signaltransduktor und Aktivator der Transkription 1 (STAT1), welcher in seiner tetrameren Form als Transkriptionsfaktor an Immunantworten beteiligt ist. In diesem Projekt wurde der Protomerenaustausch zwischen STAT1-Dimeren unter kinetischen Gesichtspunkten untersucht und dabei dieser Prozess als ein potentiell geschwindigkeitsbestimmender Schritt des Aktivierungs-/Inaktivierungs-Zyklus von STAT1 identifiziert. Die Daten unterstützen einen alternativen Mechanismus für den Wechsel zwischen der parallelen und antiparallelen Konformation von STAT1-Dimeren basierend auf der Dissoziation und nachfolgenden Reassoziation von Protomeren, bei dem reziproke Interaktionen innerhalb des N-terminalen Domänendimers zur Stabilisierung eines intermediären Konformationsübergangs nicht benötigt werden. Durch Bindung an spezifische DNA-Zielbereiche, als Gamma-aktivierte Sequenzen (GAS) bezeichnet, wird die Dynamik des Protomerenaustauschs wesentlich beeinträchtigt. In der Sequenz des für das zytoskelettale Strukturprotein Ezrin kodierenden humanen *EZR*-Gens wurde mittels *in silico* Analyse ein doppeltes GAS-Motiv als mögliche STAT1-Zielsequenz identifiziert und die Bindung von STAT1-Dimeren an jedes der beiden Elemente sowie eine moderate Geninduktion bestätigt. Allerdings zeigen Mäuse mit einer N-terminalen Substitutionsmutation von STAT1, welche die kooperative DNA-Bindung beeinträchtigt, sowie auch ein kompletter funktioneller Knockout des *Stat1*-Gens keine veränderte Expression von Ezrin und Moesin in Knochenmarkszellen verglichen mit Mäusen, die das Wildtyp-Molekül exprimieren. In einem Myokardinfarktmodell durch Ligatur des Ramus interventricularis anterior zeigen männliche Mäuse mit Expression der Interferon-γ-irresponsiven STAT1-Mutante höhere Überlebensraten, während weibliche Tiere vor den nachteiligen Effekten des kardialen Remodellings in der frühen Phase geschützt sind. In entzündlichen myokardialen Infiltraten dieser Tiere wurde ein geringfügig höheres Expressionsniveau an tyrosinphosphoryliertem STAT1 nachgewiesen, während die Gesamtproteinmenge an STAT1 gegenüber dem Wildtyp reduziert war. Zellen aus lymphatischen Organen STAT1-defizienter Tiere mit experimenteller autoimmuner Enzephalomyelitis, die als Modell einer T-Helfer-Zell-vermittelten Autoimmunerkrankung verwendet wurde, zeigten einen hyperproliferativen Phänotyp und sezernierten größere Mengen an IFNγ und IL-17A. Injektion dieser Mäuse mit Lipopolysaccharid während der Induktionsphase der experimentellen autoimmunen

Enzephalomyelitis hob den hyperproliferativen Phänotyp vollständig auf. Zusammenfassend demonstrieren die Ergebnisse aus dieser Arbeit die Bedeutung einer kooperativen DNA-Bindung und Tetramerstabilisierung von STAT1 im Zusammenspiel komplexer immunologischer Prozesse auch in Abwesenheit infektiöser Pathogene und unterstreichen zudem die Schlüsselrolle von tyrosinphosphoryliertem STAT1 bei der Verknüpfung zwischen angeborenem und erworbenem Immunsystem.

List of tables

Table 1: List of chemicals and reagents 16

Table 2: List of media 18

Table 3: List of drugs 19

Table 4: List of kits 19

Table 5: List of equipment 20

Table 6: List of disposable materials 21

Table 7: List of hybridised oligonucleotides 23

Table 8: List of oligonucleotide primers for genotyping 23

Table 9: List of oligonucleotide primers for ChIP 24

Table 10: List of oligonucleotide primers for quantitative PCR (qPCR) 24

Table 11: List of enzymes 24

Table 12: List of recombinant proteins 25

Table 13: List of primary antibodies 25

Table 14: List of secondary antibodies 26

Table 15: List of plasmids and constructs 27

Table 16: List of cell lines 27

Table 17: List of mouse lines 28

Table 18: List of software 28

Table 19: Clinical scores for EAE 43

Table 20: Endpoint calculation of echocardiography data 45

Table 21: Criteria for distribution scores 47

Table 22: Criteria for density scores 48

Table 23: GAS motifs surrounding the transcription-start site (TSS) in the promoter of the human EZR gene 59

Table 24: GAS motifs surrounding the TSS of the murine EZR gene sequence 60

Table 25: Survival rates of mice after undergoing myocardial infarction surgery at day 3 post-myocardial infarction 72

List of figures

Figure 1: Model of tetramer stabilization of STAT1 binding to DNA 3

Figure 2: Proposed mechanisms for STAT1 conformational change 49

Figure 3: Native STAT1 and STAT1-GFP both favour tetrameric binding to tandem GAS sites 50

Figure 4: Competition assay showing the dissociation kinetics of STAT1 dimers from single GAS elements 51

Figure 5: Native STAT1 and STAT1-GFP can form hetero-tetramers 52

Figure 6: STAT1 hetero-tetramers consisting of two homodimers are formed on tandem GAS sites 53

Figure 7: Untagged and GFP-tagged STAT1 form hetero-tetramers with 3:1 and 1:3 stoichiometry when unbound to DNA 54

Figure 8: Binding of STAT1 to DNA hinders the exchange of protomers 55

Figure 9: Protomer exchange kinetics of dimers does not differ between the wildtype STAT1 and the F77A mutant 56

Figure 10: Amino-terminal interactions are dispensable for monomer exchange of STAT1 58

Figure 11: EMSA showing STAT1 binding to tandem GAS elements in the human EZR promoter 62

Figure 12: ChIP analysis of STAT1 association to the EZR promoter in IFNγ-treated Jurkat cells 63

Figure 13: Real-time PCR results from Jurkat cells and HL-60 cells treated with IFNγ for 2 h, 6 h, and 10 h, respectively 64

Figure 14: Real-time PCR results of Jurkat cells treated with IFNα and IFNγ showing induction of the EZR gene 65

Figure 15: Expression of ezrin and moesin in Jurkat and HL-60 cells treated with IFNα or IFNγ 66

Figure 16: Expression and phosphorylation of ezrin and moesin in HL-60 cells treated with IFNα or IFNγ. 67

Figure 17: *Ex vivo* analysis of baseline expression of ezrin and moesin in bone marrow cells from wildtype, STAT1-deficient and STAT1-F77A mice 69

Figure 18: Phosphorylation levels of ezrin and moesin in bone marrow from wildtype, STAT1-deficient and STAT1-F77A knockin mice treated *ex vivo* with interferons. 70

Figure 19: Kaplan-Meier survival analysis of mice subjected to experimental myocardial infarction 73

Figure 20: H&E staining of acute myocardial infarction 74

Figure 21: Evaluation of the extent of inflammation according to H&E staining of sections of paraffin-embedded cardiac tissue three days after myocardial infarction 75
Figure 22: Increase in left ventricular diameter after myocardial infarction 76
Figure 23: Increased left ventricular cross-sectional area due to myocardial infarction 77
Figure 24: Increase in end-diastolic and end-systolic volume after myocardial infarction ..78
Figure 25: The reduced cardiac function after myocardial infarction is blunted in mice with impaired STAT1 tetramer stabilization.....79
Figure 26: Expression and phosphorylation of STAT1 and STAT3 in heart tissue from STAT1-F77A knockin mice on day 3 after myocardial infarction.....81
Figure 27: Staining of tyrosine-phosphorylated STAT1 in heart sections on day 3 after myocardial infarction or sham operation 83
Figure 28: Analysis of the relative numbers of regulatory T cells in lymph node and spleen of the STAT1-F77A mouse line 84
Figure 29: Reduced activation of two known IFNγ-target genes by STAT1-F77A in reconstituted U3A cells 85
Figure 30: Staining of myeloperoxidase (MPO) on day 3 following myocardial infarction or sham operation.....86
Figure 31: Staining of CD68 following ligation of the left ascending coronary artery or sham operation on day 3.....87
Figure 32: Expression of CD3 in infarcted heart tissue on day 3 follow-up.....88
Figure 33: Survival before onset of EAE upon LPS challenge 89
Figure 34: Clinical scores in STAT1-deficient and wildtype mice treated with and without LPS injection 91
Figure 35: Mean date of EAE onset.....92
Figure 36: Relative proliferation rates of cells derived from lymphatic organs challenged with MOG_{35-55} peptide or concanavalin A 93
Figure 37: IL-17A concentrations in the supernatants of spleen and lymph node cells from MOG_{35-55}-immunised mice in the presence or absence of LPS challenge.....95
Figure 38: Dysregulated IFNγ production in the supernatants of primary cells from lymphatic organs of STAT1 knockout animal cells immunized with MOG_{35-55} peptide in the presence or absence of LPS co-stimulation.....96

1 Introduction

1.1 STAT1 – A key transcription factor in immunity and inflammation

Signal transducer and activator of transcription 1 (STAT1) belongs to a family of latent signal-dependent transcription factors that is highly conserved among mammals and is involved in a plethora of cellular processes including immunity, cell growth, differentiation and apoptosis (Levy and Darnell, 2002). The protein was first described in the early 1990s as part of a complex that was phosphorylated in response to interferon-α (IFNα) and IFNγ (Fu, 1992; Shuai et al., 1992).

STAT family proteins are thought to have evolved with the development of the first multicellular organisms. They were reported to be present in *Dictyostelium discoideum* and *Drosophila melanogaster* but were not found in *Saccharomyces cerevisiae* (Yan et al., 1996; Kawata et al., 1997). In mammals, there are seven different forms of STAT proteins, namely STAT1, STAT2, STAT3, STAT4, STAT5a, STAT5b and STAT6. In mice, the genes for these proteins cluster in three regions: *Stat1* and *Stat4* at the proximal region of chromosome 1, *Stat2* and *Stat6* at the distal region of chromosome 10 and *Stat3*, *Stat5a* and *Stat5b* at the distal region of chromosome 11 (Copeland et al., 1995). In humans, the genes encoding *STAT1* and *STAT4* are localised in a head to tail tandem orientation to the long arm of chromosome 2, *STAT3*, *STAT5a* and *STAT5b* are localized to chromosome 17, and *STAT2* and *STAT6* are both found on chromosome 12 (Darnell, 1997).

Upon activation by extracellular signalling ligands at the plasma membrane, STAT proteins exert their roles as transcription factors in the nucleus and modulate cytokine-dependent gene expression (Darnell, 1997). Among the signalling molecules are a variety of cytokines including interferons, interleukins, growth factors, and hormones (Abroun et al., 2015).

The characteristic structure of members of the STAT protein family is a modular set-up of an amino-terminal, a coiled-coil, a DNA-binding, a Src-homology (SH2), and a transactivation domain (from amino- to carboxy-terminus). The molecular weight of mammalian STAT proteins ranges between 80 kDa and 113 kDa (Darnell, 1997; Levy and Darnell, 2002). Conserved among the STAT transactivation domains is a tyrosine residue that is phosphorylated by Janus kinases (JAKs) upon activation. In STAT1, this residue is located at position 701, while the corresponding position in the STAT3 molecule is located at 705

(Shuai et al., 1993a; Kaptein, 1996). By differential splicing or proteolysis, all STAT proteins except for STAT2 have been found to be expressed with different isoforms of different protein size and slightly different regulation. In the case of STAT1 and STAT3, a full-length α- and a truncated β-isoform are expressed. Both β-isoforms lack a serine residue which is conserved among full-length STAT1, STAT3, STAT5a and STAT5b. Phosphorylation of this serine residue has been shown to boost STAT1 transcriptional activity rendering the β-isoforms less active (Schindler et al., 1992a; Schaefer et al., 1995; Wang et al., 1996; Decker and Kovarik, 2000; Horvath, 2000; Lödige et al., 2005).

The three-dimensional structures of STAT1 and STAT3 dimers bound to DNA were determined using crystallographic analyses. The data revealed the nature of STAT-DNA binding including the dimerization of the two protomers via reciprocal interactions of their SH2 domains and the binding interface interacting with the DNA (Becker et al., 1998; Chen et al., 1998). However, these structural analyses failed to determine the structure of the N-terminal domain and parts of the transactivation domain. Combination of the models of STAT1 and STAT4 for which crystallography of the N-terminus had been successful led to a model that predicted interactions of the N-termini within a dimer (Baden et al., 1998; Vinkemeier et al., 1998; Chen et al., 2003b). Crystallographic analysis of unphosphorylated STAT1 confirmed these predictions based on the hybrid model and showed that unphosphorylated cytosolic STAT1 forms tetrameric complexes as dimers of dimers. These studies identified two different conformational states of STAT1 dimers that would both be supported by N-terminal interactions and showed that phosphorylated STAT1 favoured the more open parallel alignment, while unphosphorylated STAT1 was more likely to acquire the more condensed antiparallel state (Mao et al., 2005; Wenta et al., 2008). STAT1 dimers in the parallel conformation were assumed to interact with the receptor and shown to bind to DNA.

The main role in stabilizing this conformational state was attributed to the SH2 domain. Stabilization of the antiparallel state is mainly achieved through a combination of N-terminal domain interactions and interactions of the coiled-coil domain with the DNA-binding domain of the partner protomer. It was proposed that phosphorylated STAT1 dimers in the parallel conformation are a poor substrate for phosphatases and cannot leave the nucleus unless they are dephosphorylated (Meyer et al., 2003). This suggests that a conformational shift is a main constituent of the STAT1 activation-inactivation cycle. It was predicted that interactions of the N-termini facilitate the shift from the parallel to the antiparallel conformational state and

that the phenylalanine at position 77 plays a major role (Mao et al., 2005; Zhong et al., 2005; Mertens et al., 2006; Wenta et al., 2008).

Second to the SH2 domain, the amino-terminal domain is the most highly conserved domain among the STAT proteins. However, domain exchange experiments have shown that it is not interchangeable. In STAT1, the amino-terminal domain spans the first 135 amino acids (Strehlow and Schindler, 1998; Murphy et al., 2000) and through this domain, protein-protein interactions between two STAT1 molecules are facilitated. Based on structural data and targeted mutagenesis, a conserved phenylalanine residue was identified at position 77 in STAT1 and at position 81 in STAT5 that is essential for the formation of tetramers (John et al., 1999; Meyer et al., 2004). Mutation of this residue in STAT1 to alanine resulted in severely impaired cooperative DNA binding and reduced expression of some but not all STAT1 target genes. Furthermore, the STAT1 N-terminus provides a surface to interact with other modulating factors such as the CREB-binding protein (CBP/p300) and protein inhibitor of activated STAT1 (PIAS1) (Leung et al., 1996; Darnell, 1997; Horvath, 2000; Shuai, 2000). In summary, DNA-bound tetramers and higher-order oligomers of STAT1 are formed by reciprocal amino-terminal interactions.

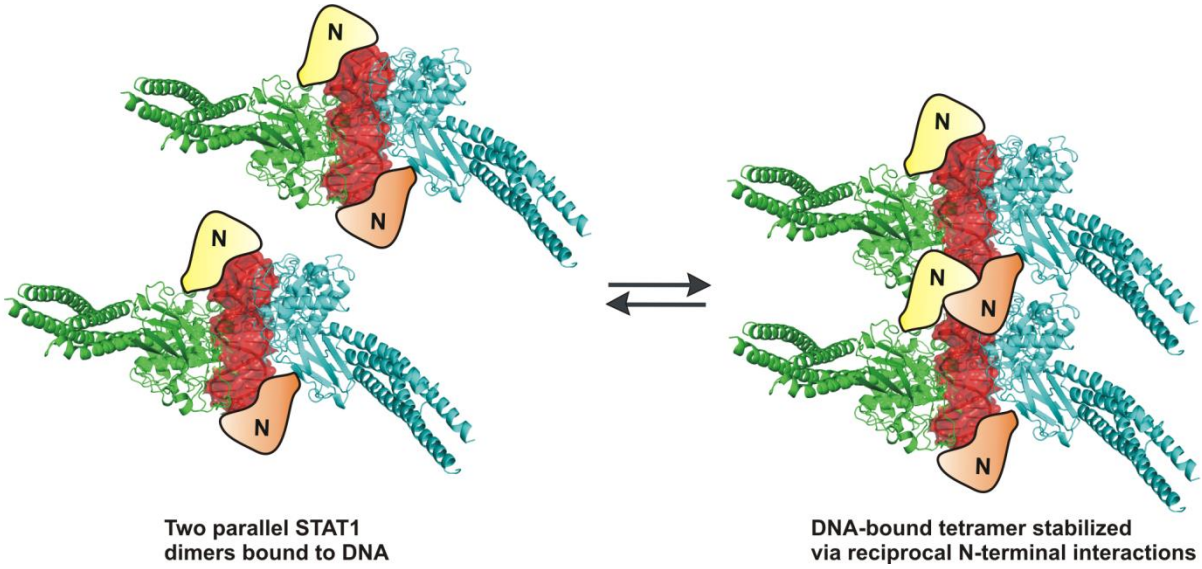

Figure 1: Model of tetramer stabilization of STAT1 binding to DNA. *Shown are STAT1 dimers in parallel alignment (blue and green) bound to the DNA double helix (red). The N-termini (N) of two dimers interact to facilitate cooperative DNA binding.*

The coiled-coil domain of STAT1 consists of 181 amino acids and forms a structure of four α-helices. It contains a leucine-rich nuclear export signal that is pivotal for the STAT1

activation cycle (Begitt et al., 2000). In addition, the coiled-coil domain forms an interface for interactions with the DNA-binding domain of a partner molecule in order to stabilize the anti-parallel dimer conformation. Targeted mutagenesis of the residues Q340, G384, Q408 of the DNA-binding domain and residue F172 disrupts these interactions and led to the destabilization of the antiparallel conformational state and prolonged tyrosine phosphorylation (Begitt et al., 2000; Mao et al., 2005; Mertens et al., 2006).

The DNA-binding domain contains the interface for the interaction of STAT1 with target sequences on DNA. Through several distinct residues, STAT1 interacts with the major as well as the minor groove of the DNA-double helix (Chen et al., 1998). Besides the DNA binding activity, this domain also provides the nuclear localisation sequence needed for the interaction with importin-α-5 to facilitate nuclear import of the phosphorylated STAT1 dimer (Fagerlund et al., 2002; McBride et al., 2002; Meyer et al., 2002).

The STAT1 linker domain spans the amino acids 488 to 575 (Chen et al., 1998). A variety of residues have been identified in the linker domain of STAT1 as well as of STAT3 which upon mutation, alter DNA-binding kinetics and affect gene transcription. It is believed that by interactions of the linker domain with the SH2 domain and the DNA-binding domain, the process of association to and release from DNA is regulated (Yang et al., 2002; Hüntelmann et al., 2014; Mertens et al., 2015). Furthermore, the measles virus phosphoprotein was found to interact with the STAT1 linker domain, thereby, preventing JAK1-induced activating phosphorylation, indicating that the linker domain is a target of viral pathogens during immune evasion (Devaux et al., 2013).

The SH2 domain is highly conserved among the STAT family members and provides the surface for the dimerization of tyrosine-phosphorylated STAT1 molecules. For this interaction, the arginine residue at position 602 is most critical since it interacts with the phosphorylated tyrosine residue 701 of the partner protomer to form a parallel STAT1 dimer (Shuai et al., 1993b; Chen et al., 1998; Wenta et al., 2008).

The transactivation domain of STAT1 spans a region of 67 amino acids and holds the critical phosphorylation site at position 701 as well as the serine residue at position 727 that can be phosphorylated to enhance transcription. The truncated STAT1β isoform lacks transcriptional activation, despite the fact that this isoform is able to dimerize, become tyrosine-phosphorylated and bind to DNA. Due to its low levels of conservation among the different STAT1 variants, the transactivation domain is believed to mediate target gene

specificity (Shuai et al., 1992; Schindler et al., 1992b; Darnell, 1997; Decker and Kovarik, 2000).

STAT1 is activated mainly by interferon signalling. Interferons are classified into three different subgroups. The type I interferons (IFNα, IFNβ and some related molecules) are known to be essential in orchestrating an antiviral defence. The only mammalian type II interferon is IFNγ. It has been identified as a main actor in antibacterial, -fungal and -parasite immunity but plays only a limited role in antiviral activity. Type III interferons classified as different isoforms of IFNλ were discovered in 2003. They were found to carry out their main tasks in supporting epithelial barrier function and in immunity against some RNA viruses (Kotenko et al., 2003; Sheppard et al., 2003; Zhang et al., 2008; Lazear et al., 2015).

Interferon signalling is initiated by binding of the cytokine to the extracellular domain of its cognate receptor. Type I interferons bind to the interferon-α receptor (IFNAR) which is comprised of two subunits, IFNAR1 and IFNAR2 (Novick et al., 1994; Platanias, 2005). Extracellular IFNγ is detected by the interferon-γ receptor (IFNGR) (Langer and Pestka, 1988). IFNAR and IFNGR are both class-II cytokine receptors. They contain an extracellular ligand-binding domain and a transmembrane domain which spans the membrane once. Proteins with tyrosine-kinase activity are bound to the intracellular carboxy-terminal domain of interferon receptors (Bach et al., 1997). Upon binding of the ligand to its receptor, the two receptor subunits dimerize. Janus kinases become activated which enables them to recruit and phosphorylate STAT proteins at a conserved tyrosine residue near the carboxy-terminus to induce activation. The Janus kinases are a relatively small family of tyrosine kinases consisting of only four members, namely JAK1, JAK2, JAK3 and TYK2 (tyrosine kinase 2). They are non-covalently bound to cytokine receptors via a four-point-one, ezrin, radixin, moesin (FERM) domain (Yamaoka et al., 2004). To facilitate differential regulation of type I and type II interferon signalling, IFNAR recruits STAT1 as well as STAT2, while IFNGR exclusively recruits STAT1 (Shuai et al., 1993b; Darnell, 1997). In the case of STAT1, the transcription factor is recruited from a pool of monomers and unphosphorylated dimers located in the cytosolic and nuclear compartment of the resting cell (Yang and Stark, 2008).

Following phosphorylation of STAT1 and STAT2, two different complexes are formed. The STAT1 homodimer is formed by interactions of the SH2 domains of two phosphorylated STAT1 monomers. The interferon-stimulated gene factor 3 (ISGF-3), a complex formed of phosphorylated STAT1 and STAT2 together with interferon-regulatory factor 9 (IRF9), is exclusively induced in response to type I interferon signalling. Both complexes interact with

importin-α5 and readily accumulate in the nucleus within minutes after activation (Fagerlund et al., 2002). Once inside the nucleus, the imported complexes facilitate transcription of interferon-responsive genes by association to target sequences in promoter and enhancer regions. STAT1 homodimers bind with high affinity to a palindromic sequence, the so-called interferon-gamma-activated site (GAS). The ISGF-3 complex binds to a different sequence, termed IFNα-stimulated response element (ISRE) (Darnell et al., 1994; Horvath, 2000).

STAT inactivation is catalysed by phosphatases located in the cytosol and in the nucleus. In the cytosol, the most prominent tyrosine phosphatases are SH2-containing phosphatase 1 (SHP-1), SHP-2, and protein tyrosine phosphatase 1B (PTP1B). In the case of STAT1 and STAT3, an important mechanism of inactivation is dephosphorylation in the nucleus by the T cell protein tyrosine phosphatase TC-45 (Hoeve et al., 2002; Levy and Darnell, 2002; Rawlings et al., 2004).

The most well-studied inhibitory mechanism to counteract JAK/STAT signalling is by the expression of suppressor of cytokine signalling (SOCS) proteins. These proteins are components in a negative feedback loop since most SOCS protein encoding genes are known targets of STAT-regulated gene transcription (Starr and Hilton, 1999; Levy and Darnell, 2002). Eight members of the SOCS protein family have been characterized and termed SOCS1-SOCS7 and cytokine-inducible SH2-domain containing protein (CIS). Some SOCS proteins execute their action of JAK/STAT signal inhibition by binding to the catalytic subunit of the receptor-bound JAKs, thereby hindering the autophosphorylation of the kinases. CIS has a different mode of action in competing with STAT proteins for the receptor binding site. The best studied of the SOCS protein family are SOCS1 and SOCS3 since the genetic knockout of these factors in mice results in complex and distinct impairments of immune regulation (Alexander, 2002; Rawlings et al., 2004; Linossi and Nicholson, 2015).

Another system of JAK/STAT signal inhibition functions through the expression of PIAS. This class of proteins has been shown to interact with numerous signalling pathways, the JAK/STAT and nuclear factor κB (NFκB) pathway being the best studied. They are thought to interact with dimeric STAT complexes by blocking the DNA-binding activity to prevent STATs from binding to promoters and, additionally, by the recruitment of co-repressors to stop the initiation of transcription. PIAS regulation does not affect all STAT-inducible genes to the same extent, indicating a mechanism of differential regulation. While some genes have been shown to be upregulated in PIAS1 knockdown, other genes remain unaffected (Liu et al., 2004; Shuai, 2006).

To study the function of STAT proteins in more detail, several different genetic knockout models for members of the STAT protein family have been generated. Since STAT1 mediates the intracellular signal transduction of both type I and type II interferons, the complete functional knockout of this transcription factor results in a complete absence of the typical response to IFNα, IFNβ and IFNγ. These mice show a high susceptibility to a large variety of microbial pathogens while remaining otherwise healthy and indistinguishable from wildtype littermates when kept under pathogen-free conditions (Durbin et al., 1996; Meraz et al., 1996). Using an *ex vivo* ischemia/reperfusion model of Langendorff perfusion of the heart, it was demonstrated that STAT1-deficient mice displayed reduced infarct size. Cardiomyocytes of the STAT1-knockout mouse line favoured autophagy over apoptosis signalling, resulting in higher cell survival rates in the peri-infarct region (McCormick et al., 2012).

The STAT1-F77A knockin mouse lacks the critical phenylalanine residue located in the N-terminus which is needed to facilitate tetramer stabilization. Owing to the exchange of this amino acid residue to alanine, cooperative DNA binding is rendered impossible. The F77A point mutation leaves type I interferon signal transduction mostly unaffected, but results in severely impaired transcriptional activation upon IFNγ signalling. Mice lacking N-domain-mediated tetramer stabilization are protected from viral infection and have a lower mortality under treatment with lipopolysaccharide (LPS). However, the transgenic mouse line showed higher rates of mortality when infected with *Listeria monocytogenes,* indicating impairments in antibacterial but not antiviral response (Begitt et al., 2014).

For some STAT proteins, especially for STAT1, it has been shown that they upregulate their own expression in a self-inducing manner. Upon IFNγ stimulation, the intracellular levels of unphosphorylated STAT1 are increased and remain elevated for more than one day. During this time, a set of immunomodulatory genes, among them several genes important in antiviral immune regulation, are overexpressed, as shown in fibroblasts and mammary gland epithelial cells (Cheon and Stark, 2009). A genetic knockin of *Stat1* which is constitutively unphosphorylated at this critical tyrosine residue was generated. The resulting mutant displayed a reduced and delayed response to type I and type II interferons. Furthermore, mice expressing tyrosine-phosphorylation-dead STAT1 were more susceptible to infection with *Legionella pneumophila* but not to *Listeria monocytogenes* compared with the complete functional knockout of STAT1 (Majoros et al., 2016).

As a component of the ISGF-3 complex, STAT2 is needed to transduce type I interferon signals. Mice lacking STAT2 protein expression are viable, but show a distinct

immunological phenotype in being more susceptible to a broad range of viral pathogens (Park et al., 2000).

The physiological role of STAT3 cannot be evaluated using a complete functional knockout in mice, since this factor contributes to embryonal development, and STAT3-deficiency is lethal between embryonic day 6.5 and 7.5 (Takeda et al., 1997b). Using a conditional knockout in Mx-Cre mice, 90 % knockdown efficiency in the liver and 70 % knockdown efficiency in the bone marrow were achieved. These mice showed a markedly reduced production of liver acute phase proteins in response to lipopolysaccharide (LPS) while overall cytokine signalling – pro- as well as anti-inflammatory – was prolonged (Alonzi et al., 2001). A cardiomyocyte-specific deletion of *Stat3* resulted in an increased susceptibility to cardiac damage, higher rates of apoptosis in response to inflammation, and the development of cardiac fibrosis and dysfunction in old age (Jacoby et al., 2003; Hilfiker-Kleiner et al., 2004).

STAT4 is the main transducer of interleukin-12 (IL-12) signalling – a strong inducer of differentiation towards the Th1 lineage in $CD4^+$ T cells. While developing normally and being fertile, STAT4 knockout mice display increased numbers of Th2 cells accompanied by a blockade of the development of Th1 cells (Kaplan et al., 1996b; Takeda and Akira, 2000; Wurster et al., 2000).

Genetic knockout of *Stat5a* has led to the identification of its role as a signal transducer in mammopoiesis and lactogenesis. While being indistinguishable from wildtype littermates, homozygous STAT5a-deficient mice did not lactate, indicating that, in the process of mammary gland development, STAT5a has a non-redundant role that STAT5b cannot compensate for despite its high sequence homology (Liu et al., 1997). Functional knockout of STAT5b led to a resistance to growth hormone (GH) pulses resulting in dwarfism, elevated plasma GH, low plasma insulin-like growth factor 1 (IGF1), and obesity (Udy et al., 1997). A redundant role for STAT5a and STAT5b in T cells was identified using a double mutant. Peripheral T cells failed to proliferate in response to IL-2 signalling (Moriggl et al., 1999). Using STAT5a-STAT5b double knockin N-domain mutant mice in which STAT5 proteins form dimers but not tetrameric complexes, Lin and coworkers identified a set of cytokine-regulated genes whose expression required STAT5 tetramers (Lin et al., 2012). Moreover, the authors demonstrated that the STAT5-double knockin mice had reduced numbers of cluster of differentiation 4-positive ($CD4^+$)/$CD25^+$ T cells, natural killer (NK) cells, and $CD8^+$ T cells

resulting in impaired cytokine-mediated proliferation. These findings demonstrated that tetramerization of STAT5 is critical for cytokine responses and normal immune function.

STAT6 is activated by IL-4 and IL-13 signalling, stimuli that induce the differentiation of Th2 cells. A mouse model of a complete functional knockout of STAT6 resulted in severely impaired humoral immune responses caused by altered T-helper cell differentiation (Kaplan et al., 1996a; Shimoda et al., 1996; Takeda et al., 1997a).

IL-10 deficiency in mice is associated with increased expression of IFNγ, C-X-C motif chemokine ligand 9 (CXCL9) and CXCL10 upon central nervous system (CNS) infection with murine cytomegalovirus. Surprisingly, infiltration of the brain by natural killer (NK) cells and $CD8^+$ T cells was decreased. Expression of L-selectin/CD62L was elevated on $CD8^+$ T cells obtained from murine cytomegalovirus-infected animals, and migration along a CXCL10 gradient was impaired (Cheeran et al., 2009).

Knockout of the PIAS1 gene was described as a transgenic model for impaired JAK/STAT inhibition (Liu et al., 2004). Mice deficient in PIAS1 expression displayed a set of STAT1-regulated genes that were constitutively upregulated (guanylate binding protein 1 [*Gbp1*], *Cxcl9*, *Cxcl10*), while others remained unaffected (*Irf1*, nitric oxide synthase 2 [*Nos2*], *Socs1*). Genetic knockout of *Pias1* was partly embryonically lethal, and homozygous pups were smaller than wildtype littermates, while being protected from bacterial infection and showing a stronger antiviral response.

The phenotypes of the above-mentioned transgenic mouse models with impaired JAK/STAT signalling underscore that this signalling pathway plays a major role in innate and adaptive immunity. In summary, type I interferon signalling is known to activate the ISGF-3 complex which induces the transcription of several genes involved in antiviral immunity. Studies using mutants with defective type I interferon signalling have shown that the formation of ISGF-3 is required for protection against a variety of viral pathogens (Horvath, 2000; Levy and Darnell, 2002; Jouanguy et al., 2007). The type II interferon IFNγ was identified to be involved in a variety of immunity- and inflammation-related processes including macrophage and T cell activation. The list of IFNγ-target genes includes genes coding for antiviral and microbicidal molecules, such as major histocompatibility complex (MHC) molecules, cytokines, chemokines, and phagocytic receptors (Stark, 2007; Hu and Ivashkiv, 2009). In innate immunity, IFNγ not only directly activates macrophages but low-dose stimulation was shown to sensitize macrophages resulting in an even more pronounced

STAT1-dependent response to type II interferon and to inflammatory signals acting through toll-like receptor 4 (TLR4) (Hu et al., 2002).

Signal transduction via STAT3 often acts as a counterbalance to STAT1 signalling. The activation of STAT3 signalling is induced by a variety of factors, among others IL-6, IL-10, epidermal growth factor EGF, and leukemia-inhibitory factor LIF (Wegenka et al., 1993; Riley et al., 1999; Abroun et al., 2015). STAT3 has been attributed a role in several immunological processes, such as autoimmune disease, cancer, and anti-fungal immunity. Dominant negative STAT3 mutations lead to a disease termed hyper-IgE syndrome, which is accompanied by chronic mucocutaneous candidiasis (Nefedova et al., 2004; Frisullo et al., 2006; Harada et al., 2007; Cypowyj et al., 2012).

Within the context of adaptive immunity, STAT1- and STAT3-dependent signal pathways are both important in the lineage decision of $CD4^+$ T helper (Th) cells. IFNγ, IL-12, STAT1 and STAT4 form a positive feed-forward loop to induce the master transcription factor of the Th1 cell fate, T-box transcription factor 21 (TBX21/T-bet) (Afkarian et al., 2002). Differentiation towards the Th17 lineage is induced by a combination of IL-6 and transforming growth factor β (TGFβ) signalling which leads to the induction of the master regulator of the Th17 program, RAR-related orphan receptor γ t (RORγt) in a STAT3-dependent manner (Bettelli et al., 2006; Ivanov et al., 2006; Korn et al., 2007; Yang et al., 2007). In contrast, regulatory T cells counteract the pro-inflammatory responses executed by Th1, Th2 and Th17 cells. This $CD4^+$ T cell lineage is induced by a combination of TGFβ, IL-2 and IL-10 (Chen et al., 2003a; Zheng et al., 2004; Fontenot et al., 2005). IFNγ- or STAT1-deficient $CD4^+$ T cells are more prone to develop towards the regulatory T cell fate (Caretto et al., 2010).

Although STAT1- and STAT3-dependent signal pathways induce different and often opposing reactions, stimulation of cells with IFNγ can induce STAT3 phosphorylation, and, vice versa, IL-6 - among other activators of STAT3 signalling - also induces STAT1 activation. This effect is especially pronounced in the absence of either of the two STAT proteins (Stark, 2007). Some activators of STAT signalling display a cell type-specific differential regulation of STAT gene induction, e.g. IFNβ is a strong inducer of STAT1 phosphorylation in monocytes and $CD8^+$ T cells but a poor inducer in $CD4^+$ T cells and B cells. In all four cell types, IFNβ also induces a pronounced STAT3 and STAT5 activation, suggesting that canonical STAT signalling cascades are not applicable to all cell types (van Boxel-Dezaire et al., 2010). The effects of differential regulation and opposing functions were

recently shown for other cytokines, including IL-21 and IL-27 (Peters et al., 2015; Wan et al., 2015).

1.2 JAK/STAT signalling, the actin cytoskeleton and the ERM-proteins

Numerous studies have reported that interferons are engaged in the regulation of cell shape via the actin cytoskeleton. In intestinal epithelial cells, IFNγ reduces the expression of the zona occludens protein ZO-1 and induces rearrangements of the apical actin cytoskeleton which results in increased paracellular permeability of the monolayer (Youakim and Ahdieh, 1999). During embryonic development, transient IFNγ production accompanied reorganization and re-gain of polarity of trophectoderm cells which had been treated with a protein kinase C agonist (Marcelo and Lefèvre, 2002). Rearrangements of the cytoskeleton have been of interest within the context of activation of different subsets of leukocytes. IL-2, as well as, type I interferons were shown to increase mobility of MHC-I and Ly49A at the cell membrane of NK cells (Bagawath-Singh et al., 2016).

Recruitment to the site of inflammation strongly depends on well-orchestrated cytoskeletal rearrangements. In experiments using a Boyden chamber, it has been demonstrated that complement C3 isoform a (C3a) in combination with IFNα and IFNγ was more potent in inducing F-actin-mediated migration than C3a alone (Gutzmer et al., 2004). Activation of T cells by antigen-presenting cells (APCs) involves rearrangements of the actin cytoskeleton (Valitutti et al., 1995). Migration in response to a chemotactic stimulus is strongly dependent on the correct distribution of signalling molecules and specific proteins to the correct location of the polarized cell (Niggli, 2014). T cells derived from mice deficient for the actin-bundling protein leukocyte plastin did not form proper immunological synapses with antigen-presenting cells resulting in reduced activation, proliferation and cytokine production and less severe symptoms in experimental autoimmune encephalomyelitis (EAE). This shows that proper lamellipodia formation is necessary for T cell activation (Wang et al., 2010).

Not only activation and recruitment of leukocytes are impaired in this context but also the process of migration within the tissue strongly depends on the formation of cellular protrusions that interact with matrix proteins. IFNβ and IFNγ but not IFNα are known to alter actin and paxillin cytoskeletal arrangement, thereby, inhibiting the contact of cell protrusions to fibronectin in U937 cells which hinders migration (Surin et al., 2000). Immature B cells were shown to exclude themselves from antigen-enriched sites in lymphatic organs in an

IFNγ/PI3K/PKCα-dependent mechanism which induced actin-cytoskeleton rearrangements that impaired migration (Flaishon et al., 2001). The cytokines C-C motif chemokine ligand 2 (CCL2), CXCL9, CCL5, IL-8 and CXCL10 induce microglial migration towards sites of brain inflammation. This migratory process is accompanied by reorganization of F-actin (Cross and Woodroofe, 1999).

In the context of infection with intracellular bacteria, the actin cytoskeleton is often exploited by the pathogen to facilitate bacterial movement. In fighting infection of the intracellular bacterium *L. monocytogenes*, IL-6 was shown to impair the recruitment of actin by the bacterium, while IL-6 and IFNγ both increased the expression of inducible nitric oxide synthase (iNOS) which helps in the defence against intracellular bacteria via production of reactive nitrogen species (Ouadrhiri et al., 1999). The enzyme iNOS was found to be sequestered near the cell membrane to the actin cortex in macrophages where it acts as a first line of defence against intracellular bacteria (Webb et al., 2001).

One mechanism of signalling mediated by the actin cytoskeleton is through the ERM proteins ezrin, radixin and moesin. This class of proteins forms the link between several transmembrane factors and the actin cytoskeleton and is an evolutionary conserved class of cytoskeletal proteins. They are associated with the cytoskeleton and form the link between actin filaments and the intracellular domain of cell surface membrane-spanning proteins. They are involved in a diverse set of cellular processes such being the assembly of the mitotic spindle and stability of filopodia, lamellipodia, microvilli and adhesion sites. Besides facilitating structural integrity of the cell, they perform scaffolding functions which aid signal transduction in response to extracellular stimuli (Takeuchi et al., 1994; Lamb et al., 1997; Furutani et al., 2007; Fehon et al., 2010; Vilmos et al., 2016).

Structurally, ERM proteins contain a highly conserved FERM domain at the N-terminus, an α-helical domain at the centre which is predicted to form coiled coils and an actin-binding domain at the carboxy-terminus. The FERM domain consists of three subunits - a ubiquitin-like fold, a four-helix bundle and a phosphotyrosine-binding-like domain – which assemble in a cloverleaf-like structure and facilitate binding to membrane-associated proteins. The C-terminal and α-helical domain can fold over the FERM domain in order to cover the interaction sites (Hamada et al., 2000; Bretscher et al., 2002; Pore and Gupta, 2015).

ERM proteins have been attributed several roles in immune mediation such as B and T cell activation and migration. Their role includes the scaffolding of cell-surface molecules as well

as intracellular signal transmission (Pore and Gupta, 2015). Ezrin, moesin and radixin bind to filamentous but not to globular actin. In most leukocyte subsets, only ezrin and moesin were identified while radixin was not detected (Pestonjamasp et al., 1995; Ivetic and Ridley, 2004). In T cell activation, the ERM proteins are known to have a role in sequestering membrane proteins that are not directly associated with T cell receptor (TCR) signalling to the distal pole complex (Chauhan and Moore, 2011). During the process of leukocyte extravasation, an accumulation of intercellular adhesion molecule 1 (ICAM1), vascular cell adhesion molecule 1 (VCAM1), ezrin and moesin regulated by Rho/p160 ROCK signalling was needed at the apical pole of the endothelial cells to allow for leukocyte adhesion and transmigration (Barreiro et al., 2002). During the process of diapedesis, Thr567-phosphorylated ezrin is involved in uropod formation and the sequestration of CD44 to the polar cap at the rear end of transmigrating lymphocytes (Lee et al., 2004). T cells derived from patients with systemic lupus erythematosus exhibit higher adhesion and migration capacity, while overexpressing CD44 and Thr567-phosphorylated ezrin. Transfection of healthy donor T cells with a constitutively active form of ezrin resulted in increased adhesion and migration (Li et al., 2007). However, recent experiments using $CD4^+$ T cells that lacked ezrin and moesin showed that ERM proteins were mostly dispensable for migration and diapedesis but severely impaired the interaction with β1-integrin and homing to the lymph nodes (Chen et al., 2013).

In the context of innate immunity, moesin was shown to co-precipitate with toll-like receptor 4, lymphocyte antigen 96 (LY96) and CD14 in macrophages. Blockade of moesin using a neutralizing antibody resulted in reduction of TLR4 signal transduction via myeloid differentiation primary response protein 88 (MyD88), interleukin-1 receptor-associated kinase 1 (IRAK1) and TNF receptor-associated factor 6 (TRAF6) (Zawawi et al., 2010). Treatment of peripheral blood monocyte-derived macrophages with IFNγ was associated with increased expression of P-glycoprotein and induced a polar redistribution of P-glycoprotein co-localized with ezrin and actin on cell pseudopodia. These results were shown exclusively for macrophages and could not be confirmed for monocytes and lymphocytes (Puddu et al., 1999).

Although expression of the ERM genes is tissue specific, some redundancy has been shown in their function. Mice with a global genetic knockout of moesin developed normally, were fertile and did not show impairments in processes relying on ERM signalling such as platelet aggregation or the formation of stress fibres (Doi et al., 1999). However, moesin deficiency in mice led to an impairment in the slow rolling of neutrophils, resulting in reduced

recruitment in a peritonitis model (Matsumoto and Hirata, 2016). Mutations in the moesin gene in humans have been linked to primary immunodeficiency (Lagresle-Peyrou et al., 2016). Genetic knockout of radixin in mice led to the birth of healthy appearing pups. However, in these mice, the secretion of bilirubin was hindered leading to high serum concentrations of conjugated bilirubin and liver injury (Kikuchi et al., 2002). Ezrin deficiency in mice results in severe defects in the development of the gastrointestinal system. Usually, these mice die within the first two weeks post-natal (Tamura et al., 2005). Knockdown of ezrin in trophoblast giant cells identified a non-redundant role of ezrin in an immunological context and was shown to be required for sequestering heat-shock protein 70 (HSP70) and facilitating phagocytosis of bacterial pathogens (Watanabe et al., 2009).

Overexpression and increased activity of ezrin have been implicated in the context of cancer. Increased ezrin protein expression in solid tumours has been associated with poor prognosis and increased formation of metastasis (Elzagheid et al., 2008; Leiphrakpam et al., 2014; Cetin et al., 2015). Using hepatocellular carcinoma cell lines, it was shown that its overexpression was associated with an increased ability to migrate, suggesting a role in the formation of metastases (Zhang et al., 2006). In Epstein-Barr virus-associated nasopharyngeal carcinoma, ezrin overexpression was linked to increased motility and invasiveness (Endo et al., 2009). In non-small cell lung cancer cells, interactions of phosphorylated ezrin with the EGF receptor were shown to boost transcription of oncogenic target genes of EGF signalling (Saygideğer-Kont et al., 2016).

ERM phosphorylation is regulated by small GTPases. Deletion of the small GTPase Ras-associated protein 1 (Rap1) in T cells resulted in reduced homing to lymph nodes and increased invasion of the intestinal mucosa by an ERM phosphorylation-dependent mechanism (Ishihara et al., 2015). Interactions of the Ras homolog (Rho) family GTPases and the ERM proteins have been implicated in the regulation of several factors involved in migration and cell adhesion such as CD44 and solute carrier family 9 member A1 (SLC9A1) (Okamoto et al., 1999; Denker and Barber, 2002). Besides Ras-related C3 botulinum toxin substrate 1 (Rac1), also RhoA was shown to be involved in endothelia interaction with extracellular matrix proteins in an ERM-dependent manner (Menager et al., 1999). Transient signalling via the TCR results in reduced ERM phosphorylation in a Rac-dependent manner which affects polarity and motility of T cells. This mechanism stalls T cells in their current position and might allow for the establishment of a proper immunological synapse (Cernuda-Morollón et al., 2010).

1.3 Objectives of this project

STAT1 displays a variety of ways of facilitating signalling: the tyrosine-phosphorylated molecule binds to STAT2 and IRF9 to mediate IFNα signalling, while in IFNγ signalling homodimers of STAT1 are formed. The un-phosphorylated homodimer has recently been shown to be transcriptionally active and, in addition, STAT1 exerts also non-transcriptional effects. The STAT1-F77A knockin mouse is a useful tool to distinguish signalling mediated by the homo-tetramer from other types of signalling. Up to now, this mouse model has been studied mainly within the context of infectious disease. In this project, the focus is shifted from the context of infectious disease where the immune system is activated in order to fight a pathogen towards non-infectious inflammatory diseases. The mouse models of myocardial infarction and EAE are well-established procedures that will be focused on in this investigation. The aim of this study is to increase our understanding of the role of STAT1 in these immunological processes.

This project will assess the role of the N-terminal domain in the transition between the two STAT1 conformational states. Thereafter, the contribution of interferon-activated STAT1 signalling on the expression of the ERM proteins will be studied. In order to evaluate the recruitment of immune cells to sites of myocardial inflammation *in vivo*, experimental ligation of the left anterior descending artery will be performed in STAT1-F77A knockin mice and the effect will be compared to their wildtype littermates. In addition, the role of STAT1 expression in EAE will be studied.

2 Materials and methods

2.1 Materials

2.1.1 Chemicals and reagents

Table 1: List of chemicals and reagents

Name	Company
Agarose	Carl Roth, Karlsruhe, Germany
Ampicillin	Sigma-Aldrich, Taufkirchen, Germany
APS (ammonium persulphate)	Carl Roth
Bromophenol blue	Fisher Bioreagents, Pittsburgh, USA
BSA (bovine serum albumin) Fraction V	Carl Roth
Complete Mini proteinase inhibitor cocktail	Roche, Rotkreuz, Switzerland
Concanavalin A	Sigma-Aldrich
DAB (3,3'-diaminobenzidine)	Sigma-Aldrich
Desoxy-ATP (adenosine triphosphate) [^{33}P]-labelled	Hartmann Analytic, Braunschweig, Germany
DMSO (dimethyl sulphoxide)	Applichem, Darmstadt, Germany
dNTP (deoxynucleotide triphosphates)	Carl Roth
DTT (dithiothreitol)	Applichem
EDTA (ethylenediaminetetraacetic acid)	Sigma-Aldrich
EGTA (ethylene glycol-bis(β-amimoethyl ether)-N,N,N',N'-tetraacetic acid)	Carl Roth
Entellan	Merck Millipore, Darmstadt, Germany
Eosin Y	Merck Millipore
Ethanol, 99.8 %	Carl Roth
Ethidium bromide solution 0.625 g/ml	VWR Life Science, Erlangen, Germany
FBS (fetal bovine serum) Superior	Biochrom, Berlin, Germany
Ficoll	Amersham Bioscience, Freiburg, Germany
Fluoromount G	Southern Biotech, Birmingham, USA
Formaldehyde solution, 37 %	Carl Roth
Glycerol, ROTIPURAN® ≥99,5 %, p. a.	Carl Roth
Glycine	Carl Roth
H_2O_2 (hydrogen peroxide) solution (30 %)	Carl Roth

H_2SO_4 (sulphuric acid)	Carl Roth
[^{3}H]-Thymidine (tritiated thymidine) (37 MBq/ml)	MP Biomedicals, Eschwege, Germany
HEPES (4-(2-hydroxyethyl)-1-piperazineethanesulphonic acid), Pufferan ≥99,5 %, p. a.	Carl Roth
HEPES, cell culture grade	Carl Roth
Hoechst 33258	Sigma-Aldrich
Igepal CA-630	Sigma-Aldrich
Isopropanol	Carl Roth
Kanamycin	Sigma-Aldrich
KCl (potassium chloride)	Merck Millipore
L-glutamine	Thermo Fisher
LiCl (lithium chloride)	Carl Roth
LPS	Sigma-Aldrich
Lymphocyte separation medium	PAA, Pasching, Austria
Mayer's haemalum	Merck Millipore
MegaTran 1.0	Origene, Rockville, USA
Mercaptoethanol	Sigma-Aldrich
Methanol	Merck Millipore
$MgCl_2$ (magnesium chloride)	Sigma-Aldrich
$Na_3C_6H_5O_7$ (trisodium citrate)	Carl Roth
NaCl (sodium chloride)	Carl Roth
NaCl, 0.9 %	B. Braun, Melsungen, Germany
$NaHCO_3$ (sodium bicarbonate)	Carl Roth
NaN_3 (sodium azide)	Thermo Fisher
Na-Pyruvate (sodium pyruvate)	Thermo Fisher
Na_3VO_4 (sodium orthovanadate)	Acros Organics, Geel, Belgium
NEAA (non-essential amino acids)	Thermo Fisher
PBS (phosphate buffered saline)	Life Technologies, Carlsbad, USA
Pefabloc	Roche
Penicillin/streptomycin	Biochrom
Pertussis toxin	List Biological Laboratories, Campbell, USA
Phenol/chloroform/isoamylalcohol (25:24:1)	Carl Roth

Poly-dIdC (poly-deoxyinosinic-deoxycytidylic acid)	Sigma-Aldrich
Protein A Agarose/Salmon Sperm DNA	Merck, Darmstadt, Germany
Puromycin	Sigma-Aldrich
RIPA (radioimmunoprecipitation assay) buffer, 10 x	Merck
Rotiphorese Gel 30 (Acrylamid/Bisacrylamid (37.5:1)-solution)	Carl Roth
Rotiphorese Gel 40 (Acrylamid/Bisacrylamid (29:1)-solution)	Carl Roth
Roti-Plast Paraffin	Carl Roth
SDS (sodium dodecyl sulphate)	Carl Roth
SDS PAGE (polyacrylamide gel electrophoresis) running buffer, 10x	Carl Roth
Sodium acetate	Carl Roth
Sodium deoxycholate	Applichem
TEMED (tetramethylethylenediamine)	Carl Roth
Tris-base	Carl Roth
Tris-HCl	Carl Roth
Triton X-100	Carl Roth
Tween-20	Carl Roth
Xylene	Merck Millipore

2.1.2 Culture media

Table 2: List of media

Name	**Company**
DMEM (Dulbecco's modified Eagle's medium) (Glucose 4.5 g/l, 580 mg/l L-Glutamin, 110 mg/l Na-pyruvate)	Biochrom
DMEM (Glucose 4.5 g/l, without L-Glutamin, 110 mg/l Na-pyruvate)	Biochrom
LB medium (Luria/Miller)	Carl Roth
RPMI (Roswell Park Memorial Institute medium) 1640	Lonza, Basel, Switzerland

2.1.3 Drugs

Table 3: List of drugs

Name	Company
Cepetor (medetomidine, 1 mg/ml)	Cp-pharma, Burgdorf, Germany
CFA (complete Freund's adjuvant)	Difco Laboratories, Detroit, USA
Fentanyl (0.05 mg/ml)	Rotexmedica, Trittau, Germany
Flumazenil (0.5 mg/ml)	Inresa Arzneimittel, Freiburg im Breisgau, Germany
Isoflurane	Abbvie, Chicago, USA
Ketamine	Medistar, Ascheberg, Germany
Midazolam (5 mg/ml)	Rotexmedica
Novalminsulfon (metamizol, 500 mg/ml)	Zentiva Pharma, Berlin, Germany
Revertor (atipamezole hydrochloride (5 mg/ml)	Cp-pharma
Temgesic (buprenorphine hydrochloride 0.324 mg/ml)	Reckitt Benckiser, Slough, UK
Xylariem (xylazine hydrochloride)	Ecuphar, Greifswald, Germany

2.1.4 Kits

Table 4: List of kits

Name	Company
ABsolute Blue QPCR SYBR Green Mix	Thermo Fisher, Waltham, USA
Bio-Rad Protein Assay Kit II	Bio-Rad, Hercules, USA
Mouse IFNγ Enzyme-linked immunosorbent assay (ELISA) MAX Deluxe	Biolegend, San Diego, USA
Mouse IL-17 ELISA MAX Deluxe	Biolegend
PE anti-mouse/rat/human FOXP3 Flow kit	Biolegend
PeqGold total RNA Kit	VWR Life Science
Qiagen Plasmid Maxi Kit	Qiagen, Hilden, Germany
Thermo Scientific Verso™ cDNA Synthesis Kit	Thermo Fisher

2.1.5 Equipment

Table 5: List of equipment

Name	Company
Bandelin Sonopuls	Bandelin electronic, Berlin, Germany
BioBeam 8000, gamma irradiation device	STS, Braunschweig, Germany
Biological safety cabinet class II, Herasafe KS 9	Thermo Fisher Scientific, Langenselbold, Germany
BioPhotometer plus	Eppendorf, Hamburg, Germany
Cell harvester Filter Mate	Perkin Elmer, Waltham, USA
Centrifuge 5804 R	Eppendorf
Embedding machine EG1160	Leica, Wetzlar, Germany
Filter mate cell harvester	Perkin Elmer
FLA-5100 scanner	Fuji, Düsseldorf, Germany
Flow cytometer FACSCalibur	BD, Heidelberg, Germany
Freezing container	Nalgene, Rochester, USA
Incubator B 5061 EC-CO_2	Heraeus, Hanau, Germany
Speedmill tissue homogenizer	Analytic Jena, Jena, Germany
Luminescence counter MicroBeta TriLux	Perkin Elmer, Waltham, USA
Microcentrifuge 5415 R	Eppendorf
Microscope, fluorescent, Axiovert 200M	Zeiss Oberkochen, Germany
Microscope, inverted, Axiovert 40 CFL	Zeiss
Microscope, BX51	Olympus, Tokyo, Japan
Microtome SM 2000 R	Leica
Mini Vent type 845	FMI GmbH, Seeheim-Jungenheim, Germany
Multifuge 1S-R	Heraeus
Neubauer-modified counting chamber	Paul Marienfeld, Königshofen, Germany
Odyssey CLx imaging system	LI-COR, Bad Homburg, Germany
Orbital shaker	VWR Life Science
Pipettes, Type Research (P1000, P200, P100, P10, P2.5)	Eppendorf
Power supply unit	Biometra, Göttingen, Germany
Real-time cycler Mastercycler epgradient S	Eppendorf
Rocker Duomax 1030	Heidolph, Schwabach, Germany
Semi-dry blotting cell	Peqlab Biotechnologie, Erlangen, Germany

SDS PAGE gel running system	Biometra
Steel Mesh, pore size 40 µm	UMG factory, Göttingen, Germany
Sonicator UW 2070	Bandelin electronic
Sunrise ELISA Reader	Tecan, Männedorf, Switzerland
Surgical forceps	Fine Science Tools, Heidelberg, Germany
Surgical scissors	Fine Science Tools
Thermo shaker TS1	Biometra
Tissue Dehydration System TP1028	Leica
Tuberculin metal/glass syringe	Hartenstein, Würzburg, Germany
UVsolo TS imaging system	Analytic Jena
Vevo® 2100 System	Visualsonics, Toronto, Canada
Waterbath GFL	Schuett biotec GmBH, Göttingen, Germany

2.1.6 Disposables

Table 6: List of disposable materials

Name	**Company**
Cell culture flasks, T75	Sarstedt, Nümbrecht, Germany
Cell culture plates, 6-well, 24-well, 96-well	Sarstedt
Cell Scraper 25 cm	Sarstedt
Cryovials	Nunc, Roskilde, Denmark
Ethilon 9-0 BV-4 5.0 mm 3/8c EH7448G surgical silk	Ethicon, Norderstedt, Germany
FACS tubes	BD
Falcon tubes, 15 ml, 50 ml	Sarstedt
Filter mat A	Perkin Elmer, Waltham, USA
Glass capillary intraEND 100 µl	Brand, Wertheim, Germany
Glass cover slip	Thermo Fisher
Glass microscope slide	Thermo Fisher
Illustra-MicroSpin-G-25 column	GE Healthcare, Little Chalfont, UK
Injection needles	B. Braun, Melsungen, Germany
InnuSpeed lysis tubes A	Analytic Jena
Insulin Syringe, 29 G	B. Braun, Melsungen, Germany
MaxiSorp ELISA plates, 96-well, flat bottom	Nunc
MeltiLex A scintillator sheets	Perkin Elmer

Microreaction tube, 0.2 ml, 1.5 ml, 2 ml	Eppendorf
Petri Dishes, 10 cm	Corning, New York, USA
Pipette Tips (P1000, P100, P10)	Sarstedt
Prolene 6-0 C-1 13 mm 3/8c 8889H surgical silk	Ethicon, Norderstedt, Germany
PVDF (polyvinylidene fluoride) membrane Immobilon-P	Merck Millipore
Round bottom tubes, 14 ml	BD
Serological pipettes, 5 ml, 10 ml	Sarstedt, Nümbrecht, Germany
Syringe, 20 ml, 10 ml	BD, Heidelberg, Germany

2.1.7 Water

Most solutions referred to in this study were produced using double-distilled H_2O. This quality was reached using the PURELAB Plus purification system (Elga Labwater, Celle, Germany). Water with a resistivity of 18.2 MΩ*cm was produced.

If DNase-, RNase- and proteinase-free water was specifically recommended for the application, Molecular Biology Grade Water (5 Prime, Hilden, Germany) was used.

2.1.8 Sterilization of material

Laboratory equipment and solutions used in cell culture or other highly sensitive settings were sterilized using the 5075 ELV autoclave (Tuttnauer Europe B.V., Breda, the Netherlands).

If heat sterilization was not recommended for a solution, filter-sterilization was performed using a Minisart NY 25 syringe filter (Sartorius, Göttingen, Germany).

2.1.9 Oligonucleotides and primers

All oligonucleotide primers were purchased from Sigma-Aldrich. The online platforms primer3plus and NCBI blast were used to design primers. For the genotyping of the STAT1 knockout mouse line, sequences were taken from (Meraz et al., 1996)). All oligonucleotides were reconstituted in DNase-, RNase-, proteinase-free water and stored at -20°C.

2.1.9.1 Hybridised oligonucleotides

Nucleotides were reconstituted at a concentration of 200 µmol/l. Hybridization was achieved through mixing equal parts of complementary oligos, heating to 95°C for 5 min and slow cooling to room temperature.

Table 7: List of hybridised oligonucleotides

Name		Sequence
2xGAS	Sense	5'-TTT TCG TTT CCC CGA AAT TGA CGG ATT TCC CCG AAA C-3'
	Antisense	5'-TTT TGT TTC GGG GAA ATC CGT CAA TTT CGG GGA AAC G-3'
EZR long	Sense	5'-TTT TCA AAC AAA AAA ACT TAA TTC CTA GAA TTT CAG AGA AAT CCC ATG GAG CTT TTT-3'
	Antisense	5'-TTT AAA AAG CTC CAT GGG ATT TCT CTG AAA TTC TAG GAA TTA AGT TTT TTT GTT TG-3'
EZR short	Sense	5'-TTT TTA ATT CCT AGA ATT TCA GAG AAT C-3'
	Antisense	5'TTT TGA TTT CTC TGA AAT TCT AGG AAT TA-3'
EZR M1	Sense	5'-TTT TTA ATA GCT ACT ATT TCA GAG AAT C-3'
	Antisense	5'-TTT TGA TTT CTC TGA AAT AGT AGC TAT TA-3'
EZR M2	Sense	5'-TTT TTA ATT CCT AGA ATT AGA GAC TAA TC-3'
	Antisense	5'-TTT TGA TTA GTC TCT AAT TCT AGG AAT TA-3'
EZR M3	Sense	5'-TTT TTA ATA GCT ACT ATT AGA GAC TAA TC-3'
	Antisense	5'-TTT TGA TTA GTC TCT AAT AGT AGC TAT TA-3'
EZR M4	Sense	5'-TTT TTA ATT CCT AGT ATT ACA GAG AAA TC-3'
	Antisense	5'-TTT TGA TTT TC TGT AAT ACT AGG AAT TA-3'
M67	Sense	5'-TTT TCG ACA TTT CCC GTA AAT CTG-3'
	Antisense	5'-TTT TCA GAT TTA CGG GAA ATG TCG-3'

Grade of purification: Desalted

2.1.9.2 Oligonucleotide primers

Primers used for genotyping and chromatin immunoprecipitation (ChIP) were reconstituted to a concentration of 100 µmol/l. Primers used in quantitative real-time polymerase-chain reaction (qRT-PCR) were reconstituted to the concentration of 50 µmol/l.

Table 8: List of oligonucleotide primers for genotyping

Gene		Sequence
Stat1-F77A	Forward	5'-CGC GAA TTG CTA ATA AAA CAA G-3'
	Reverse	5'-TGC TGC TGA GTC CAA ATA AAG-3'
Stat1 wt	Forward	5'-GGC TGA CCT TGG AAC TTG TG-3'
	Reverse	5'-AAG AGT CAG CAG GGG TCT GA-3'

neomycin	5’-AGC GCA TCG CCT TCT ATC-3’

Grade of purification: Desalted

Table 9: List of oligonucleotide primers for ChIP

Gene		Sequence
EZR	Forward	5’-GAA GCC AGA CGT TGA GAA CC-3’
	Reverse	5’-CCG AAG CTC TGG TTA AGT GG-3’
IRF1	Forward	5’-CTT CGC CGC TAG CTC TAC AAC AG-3’
	Reverse	5’-GCT CCG GGT GGC CTCGGT TCG-3’

Grade of purification: Desalted

Table 10: List of oligonucleotide primers for quantitative PCR (qPCR)

Gene		Sequence
ccl2	Forward	5’-CCA GTC ACC TGC TGT TAT AAC-3’
	Reverse	5’-TGG AAT CCT GAA CCC ACT TCT-3’
cxcl10	Forward	5’-ATT CTG AGC CTA CAG CAG AG-3’
	Reverse	5’-GCT TGC AGG AAT AAT TTC AA-3’
ezr	Forward	5’-CAG AGA GAG AGC TCT CGG AG-3’
	Reverse	5’-TGG CAG TGT ATT CTG CAA GC-3’
gapdh	Forward	5’-GAA GGT GAA GGT CGG AGT C-3’
	Reverse	5’-GAA GAT GGT GAT GGG ATT TC-3’
ifit1	Forward	5’-CAG AAG CCC AGA CTT ACC TG-3’
	Reverse	5’ATA GGC AGA GAT CGC ATA CC-3’
irf1	Forward	5’-AGC TA GCT GTG CGA GTG TA-3’
	Reverse	5’-TAG CTG CTG TGG TCA TCA GG-3’
stat1	Forward	5’-CCG TTT TCA TGA CCT CCT GT-3’
	Reverse	5’-TGA ATA TTC CCC GAC TGA GC-3’

Grade of purification: HPLC

2.1.10 Enzymes and recombinant proteins

Table 11: List of enzymes

Name	Company
ExtrAvidin (streptavidin-peroxidase)	Sigma-Aldrich
InnuTaq DNA polymerase	Analytic Jena

InnuTaq HOT-A DNA polymerase	Analytic Jena
Klenow fragment	New England Biolabs, Ipswich, USA
Proteinase K	Carl Roth
Taq polymerase	Ares Bioscience GmbH, Cologne, Germany
Trypsin	PAA, Pasching, Austria
Tsp509I	Thermo Fisher

Table 12: List of recombinant proteins

Name	**Company**
IFN-α, human, recombinant from *E. coli*	Biomol, Hamburg, Germany
IFN-α, murine, recombinant from *E. coli*	Abcam, Cambridge, Germany
IFN-γ, human, recombinant from *E. coli*	Biomol
IFN-γ, murine, recombinant from *E. coli*	Biomol
Myelin oligodendrocyte glycoprotein peptide amino acids 35-55 (MOG_{35-55})	Institute for Medical Immunology Charité Berlin, Berlin, Germany

2.1.11 Antibodies

Table 13: List of primary antibodies

Name	**Company**	**Cat-No.**
Acetyl-histone H3	Merck-Millipore, Darmstadt, Germany	17-10112
CCR2 AF700, clone 475301	R&D Systems, Wiesbaden, Germany	FAB 5538N
CD3	Bio-Rad, Hercules, USA	MCA 1477
CD4 PE, clone GK1.5	BD Pharmingen, Erembodegem, Belgium	557308
CD4 PE/Cy5, clone H129.19	Biolegend, San Diego, USA	130312
CD4 PE e610, clone RM4-5	eBioscience, Frankfurt a. M.,Germany	61-0042-80
CD8α PE/Cy7, clone 53-6.7	Biolegend	100722
CD11b FITC, clone M1/70	Biolegend	101206
CD25 FITC, clone 7D4	BD Pharmingen	553070
CD44 PE, clone IM7	BD Pharmingen	553134
CD62L FITC, clone MEL-14	Biolegend	104405
CD68	Bio-Rad	MCA 1957T
Ezrin	Cell Signaling Technology, Cambridge, UK	3145

Ezrin/radixin/moesin	Cell Signaling Technology	3142
Glyceraldehyde 3-phosphate dehydrogenase (GAPDH), clone 14C10 rabbit mAB	Cell Signaling Technology	2118
Ly-6C APC/Cy7, clone HK1.4	Biolegend, San Diego, USA	128025
Ly-6G PE, clone RB6-8C5	BD Pharmingen	553128
Myeloperoxidase	Thermo Fisher	PA5-16672
NK-1.1 APC/Cy7, clone PK136	Biolegend	108723
Normal rabbit IgG	Merck-Millipore	12-370
Phospho-ERM (ezrin [Thr567]/radixin [Thr564]/moesin [Thr558])	Cell Signaling Technology	3141
p-STAT1, clone 58D6	Cell Signaling Technology	9167
p-STAT3	Cell Signaling Technology	9131
STAT1, (C-24)	Santa Cruz, Dallas, USA	sc-345
STAT1α p91, (M-23)	Santa Cruz	sc-591
STAT3, (H-190)	Santa Cruz	sc-7179
TCRβ FITC, clone H57-597	BD Pharmingen	553171

Table 14: List of secondary antibodies

Name	**Company**	**Cat-No.**
Biotinylated anti-rabbit IgG (H+L) derived from goat	Vector Laboratories Inc, Burlingame, USA	BA-1000
Biotinylated anti-rat IgG (H+L) derived from rabbit	Vector Laboratories Inc, Burlingame, USA	BA-4001
Goat anti-rat secondary antibody, Alexa-Fluor 647 conjugated	Thermo Fisher	A-21247
Donkey anti-rabbit secondary antibody, IRDye 800CW conjugated	LI-COR Biosciences, Bad Homburg, Germany	926-32213

2.1.12 Plasmids and constructs

Table 15: List of plasmids and constructs

Name	Description	Reference
pSTAT1	Full-length human STAT1 cloned into the pcDNA3.1 mammalian expression vector (Thermo Fisher)	(Begitt et al., 2000)
pSTAT1-DE92/96RR	pSTAT1 double missense mutation with exchange of aspartate 92 and glutamate 96 to arginine	(Staab et al., 2015)
pSTAT1-F77A	pSTAT1 point mutation with exchange of phenylalanine 77 to alanine	(Meyer et al., 2004)
pSTAT1-GFP	Recombinant human STAT1α (aa 1-746) protein fused to green fluorescent protein (GFP) at the carboxy-terminus cloned into the pEGFP-N1 vector (Clontech Laboratories Inc, Mountain View, USA)	(Begitt et al., 2000)
pSTAT1-GFP-F77A	pSTAT1-GFP encoding the F77A point mutation as a STAT1 GFP fusion protein	(Meyer et al., 2004)

2.1.13 Cell lines

Table 16: List of cell lines

Name	Characteristics	Origin
HeLa	Human adherent epitheloid cervix carcinoma cell line; positive for HPV16	(Scherer et al., 1953) Kind gift from Professor Uwe Vinkemeier, Nottingham
HL-60	Human suspension cell line derived from peripheral blood promyeloblast leukemia	(Collins et al., 1977) Kind gift from Professor Matthias Dobbelstein, Göttingen
Jurkat	Human suspension cell line derived from T lymphocyte leukemia	(Gillis and Watson, 1980) Kind gift from Professor Matthias Dobbelstein, Göttingen
U3A	Human adherent epitheloid fibrosarcoma line; deficient in STAT1 expression	(McKendry et al., 1991) Kind gift from Professor Uwe Vinkemeier, Nottingham

2.1.14 Animals

Some of the experiments in this project were performed in mice as a model organism. Mice were kept in individually ventilated cages in the animal facilities of the University Medical Centre, Göttingen. All experiments performed were in line with the current law and approved by the Lower Saxony State Office for Consumer Protection and Food Safety (*Niedersächsisches Landesamt für Verbraucherschutz und Lebensmittelsicherheit*, LAVES).

Table 17: List of mouse lines

Name	Characteristics	Origin
STAT1-F77A knockin	Mouse line carrying a point mutation resulting in a substitution of alanine in position 77 for phenylalanine on a C57Bl6/N background (Charles Rivers, Sulzfeld, Germany)	(Begitt et al., 2014)
STAT1 knockout	Mouse line with deletion of several exons of STAT1 resulting in a complete functional knockout; obtained on an 129/Sv background and backcrossed for more than six generations onto a C57BL6/N (Charles Rivers, Sulzfeld, Germany) genetic background	(Meraz et al., 1996) Purchased from Taconic Farms, Cologne, Germany

2.1.15 Software

Table 18: List of software

Name	Description	Distributor
AnalySIS^B	Life science imaging software	Olympus
CellQuestPro	Operating and analysis software for cell sorter	BD
CorelDRAW 12	Vector Graphics editor	Corel Corporation, Ottawa, Canada

Fiji	Add-on to the ImageJ software with focus on biological-image analysis	Public domain; add-on to ImageJ (Schindelin et al., 2012)
IBM SPSS, Version 23	Statistics software	IBM, Armonk, USA
ImageJ	Java-based image processing program	Public domain; developed at NIH by Wayne Rasband (Schneider et al., 2012)
Magellan6	Operating and analysis software for ELISA reader	Tecan, Mannedorf, Switzerland
Microsoft Excel	Spreadsheet analysis program	Microsoft Corporation, Redmond, USA
Realplex ep	Operating software for Eppendorf real-time cycler	Eppendorf
SigmaPlot	Statistics software	Systat Software GmbH, Erkrath, Germany
TINA v 2.0	Operating software for FLA-5100 scanner	Raytest, Straubenhardt, Germany
Vevo® 2100 Software	Operating and analysis software for the Vevo® 2100 imaging system	Visualsonics, Toronto, Canada

2.2 Methods

2.2.1 Cell culture

2.2.1.1 Unfreezing of established tumour cell lines

To unfreeze established tumour cell lines (namely U3A, HeLa, Jurkat and HL-60), a cryovial containing 1.5 x 10^6 cells was taken from the -80°C freezer and quickly thawed in a water bath at 37°C. As soon as most of the cell suspension was liquid, the content of the tube was transferred to 10 ml pre-warmed culture medium. This diluted suspension was centrifuged for 5 min at 65 x g at room temperature. The supernatant was discarded, the pellet was re-suspended in 10 ml pre-warmed culture medium and transferred to a T75 culture flask to allow the cells to attach and grow. The following culture media were used: for U3A cells DMEM (with L-glutamine) with 10 % FBS, 1 % penicillin/streptomycin, and 0.008 % puromycin and for HeLa, HL-60, and Jurkat cells RPMI 1640, supplemented with 10 % FBS and 1 % penicillin/streptomycin. Commercially obtained PBS (Gibco) was used for all cell-culture applications.

2.2.1.2 Freezing of established tumour cell lines

To freeze cells from an established tumour cell line, the cells were harvested by digestion of cell-cell junctions using trypsin after washing the cells with PBS for adherent cells or direct centrifugation of suspension culture cells. The incubation time with trypsin was 2 min for U3A cells and 4 min for HeLa cells. The cells were collected and spun down at 65 x g for 5 min. The supernatant was discarded, the pellet was resuspended in the respective freezing medium and aliquots of 1.5 x 10^6 cells in 1 ml freezing medium were transferred to cryotubes. The tubes were transferred to a freezing container to allow gradual cooling to -80°C and stored at -80°C. Culture medium supplemented with 20 % FBS and 10 % DMSO was used for freezing HeLa, HL60, Jurkat, and U3A cells.

2.2.1.3 Maintenance, passaging and seeding of established tumour cell lines

The established tumour cell lines were cultured in a humidified atmosphere at 37°C and 5 % CO_2 (HeLa, HL-60, Jurkat, and U3A cells). The cells were passaged every 2 to 3 days. For this, the suspension cells were pelleted by centrifugation at 65 x g for 5 min. The supernatant was discarded, and the pellet resuspended in culture medium. An aliquot was inoculated with fresh culture media in a new T75 flask (typical passage as 1:8 or 1:10 dilution). Adherent cells were washed with PBS and trypsinized. Trypsin activity was stopped by addition of twice the

amount of complete culture medium. An aliquot from this suspension was used to start a new passage in a T75 flask (typical passage as 1:8 or 1:10 dilution). For the plating, cells were counted before being seeded. For protein and RNA analysis, 250,000 cells were seeded in each well of a 6-well culture plate. This corresponds to a density of approximately 1.56×10^5 cells per cm^2.

2.2.1.4 Routine check for mycoplasma infection in established tumour cell lines

To check for infection with mycoplasma, cells were stained with Hoechst dye. Suspension cells were spun down at 100 x g and resuspended in methanol for a 15 min fixation. After having been spun down again, the cells were resuspended in Hoechst dye diluted 1:5,000 in methanol and incubated at 37°C for 15 min. Cells were spun down yet again, washed with PBS and resuspended in PBS. For the analysis, 50 µl of the cell suspension were placed on a glass microscope slide and covered with a cover slip. Adherent cells were fixed with 4 % formaldehyde in PBS for 15 min at room temperature. Cells were washed twice with PBS and once with H_2O and stained with Hoechst dye diluted 1:5,000 in PBS. Again, cells were washed twice with PBS, once with H_2O, and mounted using Fluoromount G mounting medium. Cells were routinely analysed for Hoechst staining in the cytoplasm to detect mycoplasma infection using the Axiovert 200M fluorescent microscope at 340 nm and a magnification of 40x.

2.2.1.5 Treatment of cultured cells with different stimuli

Prior to protein or RNA extraction, cultured cells were treated with different stimuli. To this end, the respective stimulus (e.g. IFNγ) was diluted in pre-warmed culture medium at the desired concentration for adherent cells or at five times the concentrations used for suspension cells. For adherent cells, the culture medium was replaced by the medium containing the stimulus. In the case of suspension cells, 25 % of the culture volume was added from the cytokine-containing medium. For the RNA extraction, culture medium was replaced with culture medium containing only 0.5 % FBS 16 h prior to the beginning of the stimulation, and stimulation with cytokines was also performed in low serum-culture medium. If not stated differently, treatment concentrations were as follows: human IFNγ; 50 ng/ml, human IFNα; 50 ng/ml, murine IFNγ; 5 ng/ml, and murine IFNα; 5 ng/ml. Treatment with vanadate was carried out using 0.8 mmol/l sodium vanadate and 0.2 mmol/l H_2O_2.

2.2.1.6 Transfection of cultured cells with plasmid DNA

Cultured eukaryotic cells were transfected with different vectors using MegaTran 1.0 according to the manufacturer's recommendation. For the 6-well plate scale, 160 µl of 150 mM NaCl solution were mixed with 1.6 µg of DNA and 4.8 µl of MegaTran 1.0 per well using a vortex and incubated at room temperature for 10 min. For each well, 160 µl of this solution was added to eukaryotic cells that had grown to 50-70 % confluence and blended with the culture supernatant by gentle agitation. Cells were cultured for a further 24 h before stimulation to allow for uptake and expression of the vector.

2.2.2 Protein biochemistry

2.2.2.1 Fractionated protein extraction

For protein extraction, cells grown in 6-well-culture plates or a single cell suspension were used. For suspension cells, the cells were collected and harvested by centrifugation for 4 min at 1,500 x g. They were washed with PBS and spun down again. The pellet was resuspended in 50 µl complete cytosolic protein lysis buffer (20 mM HEPES, 10 mM KCl, 1 mM EDTA, 100 µM Na_3VO_4, 10 % glycerol, 0.1 % IGEPAL CA-630, pH 7.4, supplemented with 1 % Complete proteinase inhibitor cocktail (reconstituted), 3 mM DTT, 0.4 mM Pefabloc) and incubated on ice for 5 min. In order to harvest adherent cells, they were washed twice with PBS, and 50 µl of complete cytosolic protein lysis buffer were added to the culture dish. The cells were incubated with the lysis buffer for 5 min, harvested using a cell scraper and then transferred to a 1.5 ml microreaction tube. The cells in complete cytosolic lysis buffer were spun down for 15 sec at 4°C and 16,100 x g. The supernatant was transferred to a fresh microreaction tube and centrifuged again for 5 min at 4°C and 16,100 x g. The resulting cleared supernatant was collected as cytosolic protein extract. The pellet from the initial centrifugation step was resuspended in 50 µl complete nucleic protein lysis buffer (20 mM HEPES, 420 mM KCl, 1 mM EDTA, 100 µM Na_3VO_4, 20 % glycerol, pH 7.4, supplemented with 1 % Complete proteinase inhibitor cocktail, 3 mM DTT, and 0.4 mM Pefabloc) and incubated on ice for 30 min. The lysate was centrifuged for 15 min at 4°C and 16,100 x g. The supernatant was collected as nucleic extract. Finally, the cytosolic and nucleic extracts were pooled. If the protein extracts were to be used in electrophoretic mobility shift assay (EMSA) analysis, they were stored without any further processing at -80°C. If the protein extracts were to be used in Western blotting analysis, 14.4 µl of 6x Laemmli buffer (350 mM Tris-HCl, 8 % SDS, 30 % glycerol, 10 % mercaptoethanol, 0.04 % bromophenol, pH 7.4) were added to the 80 µl pooled protein sample. The extracts were boiled at 95°C for 3 min and stored at -20°C.

2.2.2.2 Direct protein extraction from bone marrow cells

Proteins from treated murine bone marrow were obtained using a direct approach: Following isolation of the bone marrow and production of a single cell suspension, cells were collected by centrifugation for 4 min at 100 x g at 4°C. The cells were washed once with ice-cold PBS and collected using a second centrifugation step. The pellet was resuspended in 100 µl 2x Laemmli buffer (produced by diluting 6x Laemmli buffer in double-distilled H_2O) using a 29 G insulin syringe. The extracts were boiled at 95°C for 3 min and stored at -20°C until use. Before being loaded, these samples were diluted 1:1 in SDS-running buffer and again boiled for 3 min at 95°C.

2.2.2.3 Protein extraction from murine heart

In order to extract protein from murine heart, cardiac tissue was snap-frozen in liquid N_2 after removal of the heart from the mouse and separation of the lower third of the left ventricle (main infarcted area) from the rest of the organ. Protein extraction was achieved by splitting the acquired pieces of tissue in a mortar with liquid N_2. Roughly 40 mg of tissue were used for protein extraction. The tissue was placed in 800 µl complete RIPA buffer supplemented with 1 % complete protease inhibitor cocktail, 1 % PMSF (100 µM in isopropanol), and 1 mM Na_3VO_4 and homogenized using the Speedmill tissue homogenizer with innuSpeed lysis tubes A for 4 x 45 sec. The homogenized sample was incubated on ice for 30 min and transferred to a fresh reaction tube before sonication at 50 % amplitude, 70 % time for 3 x 30 sec. After sonication, debris was spun down at 12,000 x g for 20 min at 4°C. Supernatants were collected as protein extracts and stored at -80°C until use. When used for Western blotting experiments, 40 µg of protein were diluted in PBS (150 mM NaCl, 100 mM Na_2HPO_4, 15 mM K_2HPO_4, 30 mM KCl, pH 7.4) and 6x Laemmli buffer was added. These samples were boiled for 5 min at 95°C before being loaded.

2.2.2.4 Protein quantification using Bradford assay

To quantify protein concentrations in samples obtained from whole tissue, the Bradford method was used (Bradford, 1976). Briefly, protein samples were diluted in PBS to reach a total volume of 800 µl. Two hundred µl of the Bio-Rad protein assay dye reagent was added and incubated with the protein solution for 5 min. The solution was transferred to a semi-micro cuvette for spectrometric analysis at 595 nm using the BioPhotometer plus. The photometer was calibrated for concentrations ranging from 1-25 µg/ml using the BSA standard provided with the Bio-Rad Protein Assay Kit II.

2.2.2.5 Western blotting analysis

For Western blotting analysis, protein samples containing Laemmli buffer were loaded onto a two-phase 10 % SDS-PAGE gel. Polymerisation of the stacking gel was achieved by adding 25 % stacking gel buffer (500 mM Tris-HCl, 0.4 % SDS, pH 6.8), 16 % Rotiphorese Gel 30, 0.6 % APS, and 0.2 % TEMED in double-distilled H_2O. The separating gel was polymerised by mixing 25 % separating gel buffer (1.5 mM Tris-HCl, 0.2 % SDS, pH 8.8), 33.1 % Rotiphorese Gel 30, 0.03 % APS, and 0.16 % TEMED (in double-distilled H_2O). The samples were run at 11 mA using 1x SDS PAGE running buffer (25 mM Tris-Base, 192 mM glycine, 0.1% SDS, pH 8.6) and transferred onto a PVDF membrane using a semidry blotting technique at 80 mA for 90 min with transfer buffer (25 mM Tris-base, 150 mM glycine, 10 % methanol, pH 8.0). The resulting blot was blocked using 4 % BSA in Tris-buffered saline (TBS) (137 mM NaCl, 10 mM Tris-HCl, pH 7.4) supplemented with 0.1 % Tween-20 (TBST) and incubated overnight at 4°C with the primary antibody diluted in 4 % BSA in TBST. Then, the blot was washed five times for 5 min with TBST before being incubated with the diluted secondary antibody for 1 h in the dark at room temperature. It was washed 5 times with TBST, once with TBS and scanned using the LI-COR Odyssey CLx imaging system. For reblotting, the membrane was washed three times for 5 min and three times for 15 min in TBST. Thereafter, it was incubated overnight with a new primary antibody and developed the next day, as described above. If the first and second antigen to be detected were similar in molecular size, the blot was stripped from its first set of primary and secondary antibodies before analysis. To this end, the blot was incubated with stripping buffer (62.5 mM Tris-HCl, 2 % SDS, 0.7 % mercaptoethanol, pH 6.8) at 60°C for 60 min. Subsequently, it was thoroughly washed with tap water, then four times for 15 min in TBST, blocked again with 4 % BSA in TBST and incubated overnight with a different primary antibody.

The dilutions of primary antibodies were as follows: anti-ERM 1:1,000; anti-ezrin 1:2,000; anti-GAPDH 1:5,000; anti-phospho-ERM 1:1,000; anti-phosphotyrosine-STAT1 1:1,000; anti-phosphotyrosine-STAT3 1:1,000; anti-STAT1 1:1,000 and anti-STAT3 1:750. Dilution of the IRDye 800CW-conjugated donkey-anti-rabbit secondary antibody was 1:10,000.

2.2.2.6 Electrophoretic mobility shift assay

DNA binding of STAT1 was assessed using electrophoretic mobility shift assay (EMSA). For this technique, purified samples of native protein were incubated with radioactively labelled DNA probes in the presence of a non-specific competitor (poly-dIdC), and the reactions were run on a native polyacrylamide gel. The DNA probe (0.2 µl) was mixed with 1 µl poly-dIdC

(2 mg/ml), 1.3 µl DTT (100 mM), 3.5 µl H_2O and 2.5 µl 5x EMSA loading buffer (100 mM HEPES, 200 mM KCl, 5 mM $MgCl_2$, 2.5 mM EDTA, 0.5 mM EGTA, 20 % Ficoll) and incubated with 4.5 µl or adjusted amounts of protein extracts for the times indicated. The STAT1 C-24 antibody was used in a supershift reaction, while the STAT3 H-190 antibody was used as a negative control. This mixture was loaded onto an equilibrated non-denaturing 4.8 % TBE-polyacrylamide gel (12 % Rotiphorese Gel 40, 2.4 % TBE (89 mM Tris-base, 89 mM boric acid, 2 mM EDTA), 2 % APS, 0.1 % TEMED) and run at 400 V using 0.25x TBE. The gel was then pressed against Whatman blotting paper and vacuum-dried. The radioactive signals were detected using transfer of the signal to a phospho-imager film and read by the FLA-5100 scanner. For this reading, the software TINA v 2.0 was used.

2.2.2.7 Radioactive labelling of EMSA probes

Oligonucleotides intended for use in EMSA were annealed by mixing them at a concentration of 100 mmol/l in DNase-, RNase- and proteinase-free H_2O and heating the mixture to 95°C in a water bath. This was left to slowly cool to room temperature overnight to allow proper annealing and was then stored at -20°C until further use. Radioactive labelling was performed by an end-filling reaction using the Klenow fragment. Five units of the Klenow fragment derived from DNA polymerase I from *E. coli* were mixed with 5 µl 10x Eco-Pol buffer, 0.1 ng annealed oligonucleotides and 8 µl [^{33}P]-labelled ATP and incubated for 25 min at room temperature. Finally, an excess of non-radioactive dNTPs (6.5 mM of each dNTP) was added for a further 5 min, and the reaction was stopped by addition of 1 µl of 0.5 mM EDTA solution. Free nucleotides were eliminated by centrifugation at 700 x g for 3 min using an Illustra-MicroSpin-G-25 column.

2.2.2.8 ELISA

In order to quantify IL-17 and IFNγ production, culture supernatants of cells isolated from lymph node and spleen were collected after 72 h incubation in restimulation medium (ReMed) (5 % FBS, 0.0002 % mercaptoethanol in R_0 medium supplemented with 1 % NEAA, 1 % Na-pyruvate, 1 % L-glutamine, and 1 % penicillin/streptomycin) and analysed using ELISA technique. Cells isolated as described above were seeded in U-bottom 96-well plates at a density of 3 x 10^5 cells per well for the analysis of lymph node isolates and 6 x 10^5 cells per well for spleen cells, respectively. MOG_{35-55} at a final concentration of 20 µg/ml was used as a specific stimulus, while concanavalin A at a concentration of 1.25 µg/ml was used as control. Cells were incubated with the reagents at 37°C and 5 % CO_2. Each condition was analysed in

triplicate individually for every animal. After 72 h, supernatants were collected and stored at -80°C until analysis. Measurements were performed using the Mouse ELISA MAX Deluxe kits for IL-17A and IFNγ following the manufacturer's recommendations. Briefly, MaxiSorp ELISA plates were coated with 100 µl of the capture antibody provided, diluted 1:200 in coating buffer for 16 h at 4°C. Unspecific binding sites of the capture antibodies were blocked with Assay Diluent A for 1 h at room temperature. One hundred µl of diluted supernatants were added to the wells of the plate and incubated for 2 h at room temperature under mild agitation, each sample was applied in triplicate. Samples were diluted in Assay Diluent A in order to give values within the dynamic range of the assay. Standard curves were generated by inclusion of diluted IL-17A or IFNγ at concentrations of 15.6 pg/ml, 31.25 pg/ml, 62.5 pg/ml, 125 pg/ml, 250 pg/ml, 500 pg/ml and 1,000 pg/ml. Background values were acquired by measurement of pure Assay Diluent A. 100 µl of diluted detection antibody was added to each well and incubated for 1 h. Thereafter, the wells were incubated with the avidin-conjugated horseradish peroxidase for 30 min. Finally, 100 µl of freshly prepared TMB substrate solution was added and incubated with the plate in the dark for 20 min. The chromatic reaction was terminated by adding 100 µl 2 N H_2SO_4 to each well. A thorough rinse using PBS-Tween was performed between each of the steps. Absorbance at 450 nm and 570 nm was determined using the Sunrise ELISA plate reader. Difference values used for further analysis were calculated as the absorbance at 570 nm subtracted from the absorbance at 450 nm. Quantitative assessment of the data was performed using the standard curve.

2.2.3 DNA analysis

2.2.3.1 DNA extraction from tail biopsies

To extract DNA from mouse tissue samples (e.g. tail biopsy), the tissue sample was lysed in 500 µl tail extraction buffer (100 mM Tris, 5 mM EDTA, 200 mM NaCl, 0.2 % SDS, pH 8.5) and 10 µl proteinase K (20 mg/ml) overnight at 56°C and 250 rpm in a thermo-shaker. Proteinase K was inactivated by a 5 min incubation at 90°C. The lysate was centrifuged at 16,100 x g and 10°C for 15 min, 350 µl of the supernatant was collected, and the DNA was precipitated by adding 500 µl isopropanol. The sample was mixed thoroughly by vortexing and centrifuged for 5 min at 16,100 x g. The supernatant was discarded, the pellet was washed twice with 70 % ethanol, air-dried and finally resuspended in 50 µl TE buffer (10 mM Tris-base, 1 mM EDTA, pH 7.5). The DNA was heated to 48°C for 30 min and stored at 4°C overnight before analysis to allow complete resuspension.

2.2.3.2 Genotyping of STAT1-F77A knockin mice

Genotyping of STAT1-F77A knockin mice was achieved by PCR amplification and subsequent analysis of a restriction-fragment size polymorphism. The respective fragment was amplified using the primer pair stat1 F77A at a final concentration of 0.4 µmol/l, 2.5 µl of 10x reaction buffer, 0.5 µl of 50 mM $MgCl_2$ solution, 1 µl of dNTP mix (10 µmol/l), 17.25 µl of DNase-, RNase- and proteinase-free water and 0.25 µl of Taq polymerase for each sample. 1.5 µl of purified DNA solution was added. The reaction was transferred to a thermocycler and run with the following program: 95°C for 3 min, followed by 41 cycles of denaturation at 95°C for 15 s, annealing at 61°C for 15 s, and extension at 72°C for 15 sec with a final elongation at 72°C for 7 min. The resulting PCR product was run on a 1 % agarose gel at 85 mA for 45 min and analysed using the UVsolo TS imaging system to check for proper product amplification. A total of 5 µl of the product were incubated with 0.3 µl of Tsp509I, 1.5 µl of reaction buffer B and 7.2 µl of DNase, RNase- and proteinase-free water overnight at 65°C. The digested PCR product was tested using a 3 % agarose gel run at 85 mA for 60 min. Since the F77A mutation eliminates a Tsp509I-restriction site, fragment-length polymorphism was exploited for genotype analysis. Due to the loss of a Tsp509I site caused by mutation F77A, the STAT1F77A-derived PCR product showed an additional 234 bp fragment, which was cleaved into two fragments of similar size in the case of wildtype-derived DNA.

2.2.3.3 Genotyping of STAT1-KO mice

Genotyping of STAT1-KO mice was achieved by a PCR setup resulting in the amplification of a native or neomycin cassette-related fragment of the KO allele or both with a common upstream primer and a reverse primer located either in the deleted sequence or in the neomycin-resistance gene. For this purpose, the DNA was prepared and purified as described above. The PCR reaction included 2.5 µl of 10x buffer containing $MgCl_2$, 1 µl each of stat1 wildtype forward and reverse and neomycin primer, 0.625 µl of dNTP, 0.15 µl of innuTaq Hot A polymerase, 1 µl of DNA and 17.7 µl of DNase- RNase- and proteinase-free water. The PCR conditions were 95°C for 4 min, followed by 40 cycles of denaturation at 95°C for 45 s, annealing at 60°C for 45 s, and extension at 72°C for 210 sec with a final elongation at 72°C for 10 min. The resulting PCR product was run on a 1 % agarose gel at 85 mA for 45 min and visualized using the UVsolo TS imaging system. The PCR product from the native gene was 1.7 kb, while the corresponding product length of the transgene was 1.3 kb.

2.2.3.4 Plasmid amplification

For plasmid amplification, chemically competent bacteria of the *E. coli* strain DH5α were transformed using the heat-shock method (Cohen et al., 1972). Briefly, 100 µl of DH5α cells were slowly unfrozen and incubated on ice with 1 µg of the desired plasmid DNA. The bacteria were then exposed to a 30 sec heat shock at 42°C with a subsequent 2 min-incubation on ice. The reaction was transferred to 1 ml of antibiotic-free LB medium and incubated for 1 h at 37°C with 225 rpm of orbital agitation before being spread on a pre-warmed agarose plate containing either ampicillin (for the plasmids derived from pcDNA3.1) or kanamycin (for the plasmids derived from pEGFP-N1). After incubation lasting 16 h, a colony was picked and inoculated with 2 ml of LB medium containing the respective antibiotic and grown for 8 h, before 1 ml of this pre-culture was transferred to 100 ml of LB medium with antibiotic and incubated overnight. The bacteria grown in this culture were centrifuged at 6,000 x g for 15 min. For the isolation of plasmid DNA, the Qiagen Plasmid Maxi kit was used according to the manufacturers' instructions. The DNA was resuspended in DNAse-, RNAse- and proteinase-free water. The concentration was adjusted to 1 µg/µl after determination by UV spectrophotometry. Plasmid DNA was stored at -20°C.

2.2.3.5 ChIP analysis

For chromatin immunoprecipitation (ChIP), Jurkat cells were grown in 10 ml suspension culture until they reached 80 % confluence and treated with 50 ng/ml IFNγ for 45 min or left untreated. Cells were harvested, washed twice with PBS and resuspended in 1.5 % formaldehyde in PBS. Cells were fixed for 15 min before the reaction was stopped by adding 11 % of the volume of 2 M glycine solution. After 5 min incubation, the cells were washed twice with ice-cold PBS and resuspended in 750 µl FA-lysis buffer (50 mM HEPES, 140 mM NaCl, 1 mM EDTA, 1 % Triton X-100, 0.1 % sodium deoxycholate, 0.1 % SDS, pH 7.5). Cells were lysed for 20 min on ice. Subsequently, sonication was performed 20 times for 25 sec at 70 % time and 55 % amplitude. A total of 6.75 ml RIPA buffer (50 mM Tris-HCl, 150 mM NaCl, 2 mM EDTA, 1 % IGEPAL CA-630, 0.5 % sodium deoxycholate 0.1 % SDS, 1 % complete protease inhibitor cocktail (reconstituted), pH 8.0) and 60 µl of protein-A agarose/salmon sperm DNA were added for a preclearing step of 30 min with slow rotation. Agarose beads were removed by centrifugation at 700 x g for 1 min. Four hundred µl of each sample were collected as reference input and stored at -20°C until further analysis. Overnight incubation with the antibodies for pull-down was performed in a volume of 1.6 ml each at 4°C with constant rotation. The following primary and secondary antibodies were used with

their corresponding dilutions: anti-STAT1αp91 (M-23); 1:640, anti-acetyl histone; 1:320, and anti-rabbit immunoglobulin (IgG); 1:320. Incubation with 5 µl H_2O was included as a negative control. After 16 h of incubation, 40 µl of protein-A agarose/salmon sperm DNA was diluted 1:2 in TE-buffer and added to the sample. Incubation lasted 1.5 h at 4°C with constant rotation. Beads were centrifuged at 4°C and 700 x g for 1 min. The beads were washed in five consecutive steps with low salt buffer (20 mM Tris-HCl, 150 mM NaCl, 2 mM EDTA, 1 % Triton X-100, 0.1 % SDS, pH 8.1), high salt buffer (20 mM Tris-HCl, 500 mM NaCl, 2 mM EDTA, 1 % Triton X-100, 0.1 % SDS, pH 8.1), LiCl buffer (10 mM Tris-HCl, 250 mM LiCl, 1 mM EDTA, 1 % sodium deoxycholate, 1 % IGEPAL CA-630, pH 8.1), and TE buffer twice. The DNA/protein complex was eluted with a 1:1 mix of 2 % SDS solution and 200 mM $NaHCO_3$ solution in two consecutive steps in a total volume of 400 µl. Afterwards, 14 µl of 5 M NaCl solution were added and incubated at 65°C overnight with constant agitation. To each reaction, 7 µl of 0.5 M EDTA solution, 14 µl of 1 M Tris-HCl solution and 1 µl of proteinase K solution (20 mg/ml) were added and incubated with the sample for 1 h at 37°C. The enzyme was heat-inactivated for 20 min at 75°C. DNA was isolated using 360 µl phenol/chloroform/isoamyl alcohol (25:24:1). The phases were separated at 10,000 x g for 2 min. The aqueous phase was collected and supplemented with 35 µl of 3 M sodium acetate solution and DNA was precipitated by incubation with 800 µl isopropanol at -20°C for 1 h. The DNA was collected by centrifugation for 15 min at 16,100 x g and 4°C. The pellet was washed once in 70 % ethanol and left to air-dry before being dissolved in DNase-, RNase- and proteinase-free water. ChIP samples were stored at -20°C.

2.2.3.6 ChIP-analysis PCR

ChIP analysis was performed using classical PCR. For the reaction, innuTaq HOT-A DNA polymerase was used according to the manufacturer's recommendations. The reaction included 2.5 µl of 10x buffer containing $MgCl_2$, 1 µl of 10 mM forward and reverse primer each, 0.625 µl of dNTPs (10 mM), 0.15 µl of polymerase, 1.5 µl of DNA and 18.225 of µl DNase-, RNase- and proteinase-free water. The reaction was transferred to a thermocycler and run using the following protocol: 95°C for 4 min, followed by 38 cycles of denaturation at 95°C for 45 s, annealing at 61°C for 45 s, and extension at 72°C for 120 sec with a final elongation at 72°C for 10 min. The resulting PCR product was run on a 1 % agarose gel at 85 mA for 45 min and analysed using the UVsolo TS gel imaging system.

2.2.4 RNA analysis

2.2.4.1 RNA extraction from cell culture

For the extraction of RNA, the PeqGold total RNA kit was used according to the manufacturer's recommendation. Briefly, cells were cultured in starvation medium for 16 h and subsequently treated for the respective duration of time with the indicated cytokine. At the end of the incubation time, the cells were washed with PBS. Four hundred µl of lysis buffer T were added to each well. The lysed cells were transferred to the DNA-removing column and centrifuged at 12,000 x g for 1 min. The eluate was mixed with an equal volume of 70 % ethanol and transferred to an RNA-binding column. The column was centrifuged for 1 min at 10,000 x g, washed once with wash buffer 1 and twice with ethanol-supplemented wash buffer 2. The column was then centrifuged for 1 min to dry at 10,000 x g and 50 µl of DNase-, RNase- and proteinase-free water were added and incubated with the column for 3 min. The RNA was eluted during a 1 min centrifugation at 5,000 x g. The resulting RNA was used directly for cDNA synthesis or stored at -80 C.

2.2.4.2 Reverse transcription of RNA isolated using the PeqGold total RNA kit

To obtain cDNA from the isolated RNA samples, the RNA was reversely transcribed using the Verso cDNA Synthesis Kit from Thermo Fisher according to the manufacturer's instructions. For each sample, 4 µl of 5x cDNA synthesis buffer, 2 µl of dNTP mix, 1 µl of RNA primer (anchored Oligo dT), 1 µl of RT Enhancer, 1 µl of Verso Enzyme Mix and 3 µl of DNase-, RNase- and proteinase-free H_2O were mixed and added to 8 µl of the purified RNA. The amount of RNA necessary for sufficient yield of the cDNA synthesis had been determined empirically. The mix was transferred to the thermocycler and incubated for 30 min at 42°C. The reaction was stopped by heating the sample to 95°C for the duration of 2 min. The synthesised cDNA was stored at -20°C until use.

2.2.4.3 Real-time PCR

Endogenous gene transcription was analysed using quantitative PCR (qPCR) technique. The reactions were performed at 95°C for 4 min, followed by 38 cycles of denaturation at 95°C for 45 s, annealing at 61°C for 45 s, and extension at 72°C for 120 sec with a final elongation at 72°C for 10 min and the epgradient S real-time cycler. All primers used in qPCR were diluted to a working concentration of 5 µmol/l. A mastermix was prepared containing 10 µl of SYBR green, 0.28 µl of each primer and 9.44 µl of H_2O for each sample and 19 µl of this mix were added to each cavity of a ThermoFast semi-skirted 96-well-plate. One µl of the cDNA

solution was added to the reaction mix. Each reaction was performed in duplicate. The reaction was run with settings adjusted to Filter 520 nm 'SYBR', Filter 550 nm 'X', Sample Vol. '20 µl', Probe 'SYBR Green'. The following program was used: 95°C for 15 min, followed by 45 cycles of denaturation at 95°C for 15 sec, annealing at 55°C for 30 sec, and extension at 72°C for 30 sec. GAPDH was used as reference housekeeping gene. The program realplex ep was used to operate and adjust the settings of the real-time cycler. Data analysis was performed using the $2^{-\Delta\Delta C_T}$ method (Livak and Schmittgen, 2001).

2.2.5 Primary cell isolation

2.2.5.1 Isolation of bone marrow cells

Primary murine bone marrow cells were isolated from mouse femur and tibia. The mice were sacrificed by CO_2 inhalation. The fur, skin, muscle and fat were removed from the leg. The leg was cut at the hip joint, the femur separated from the hip bone through dislocation. The foot was removed, femur and tibia were separated from each other using a scalpel cut at the patella. The bones were washed in PBS, and potentially remaining tissue was removed using gauze drenched in PBS. The femurs and tibias were transferred to a cell-culture hood and sterilized for 15 sec in 70 % ethanol. Samples were then rinsed in PBS and transferred to DMEM supplemented with 10 % FBS and 1 % penicillin/streptomycin for short-time storage. The ends of the bones were cut using sterile surgical scissors. A syringe filled with medium carrying a 21 G needle was inserted into the bone and used to flush the bone marrow into a 50 ml falcon tube. The bone marrow was dispersed using a 23 G needle, passed through a 40 µm cell strainer and centrifuged for 5 min at 100 x g. The supernatant was discarded, and the cells were resuspended in medium at the desired density.

2.2.5.2 Isolation of splenocytes and T cells

Primary cells from spleen and lymph nodes were obtained from mice which had been immunized with MOG_{35-55}, in order to assess proliferation and production of cytokines. The mice were euthanized using CO_2, and the spleen as well as the inguinal and mesenteric lymph nodes were collected in ice-cold preservation medium (EH medium) (DMEM supplemented with glutamine and 25 mM HEPES). The organs were pressed trough a steel mesh to separate the cells and eliminate connective tissue. The resuspended cells were centrifuged at 100 x g for 6 min at 4°C, and the pellet was washed once using EH medium. The cells were resuspended in ReMed. Cell numbers were counted using a Neubauer chamber and the cell suspension diluted for seeding in proliferation and cytokine production assays.

2.2.5.3 Isolation of leukocytes from blood

To analyse the composition of leukocyte subsets in circulation, 100 µl of blood were taken from the retro-orbital sinus of mice using a glass capillary. The blood-filled capillary was transferred to a 1.5 ml reaction tube containing 400 µl of PBS/EDTA (1 mM EDTA in PBS) solution. Lymphocyte separation medium was carefully added as a sublayer and the samples were centrifuged for 20 min at 300 x g. The resulting buffy coat (~200 µl) was collected, transferred to 3 ml FACS buffer (2 % BSA, 308 mM NaN_3 in PBS) and used for further analysis.

2.2.5.4 Assessment of proliferation capacity

To evaluate whether primary cells derived from spleen and lymph nodes of MOG_{35-55}-immunized animals were able to proliferate upon an antigen stimulus, a proliferation assay was performed. The proliferation rate was assessed based on detection of [^{3}H]-thymidine incorporated into the DNA. To this end, cells isolated from treated mice as described above were seeded in U-bottom 96-well plates in 100 µl ReMed per well. Cell numbers were 3 x 10^5 for cells obtained from lymph nodes and 6 x 10^5 for spleenocytes. MOG_{35-55} at a concentration of 20 µg/ml and, as a positive control, concanavalin A at a concentration of 1.25 µg/ml were incubated with the samples at 37°C and 5 % CO_2. Each condition was analysed in triplicate individually for every animal. After 48 h, [^{3}H]-thymidine was added to a final decay rate of 685.19 Bq/ml culture supernatant and incubated with the cells for 16 h. For quantification of [^{3}H]-thymidine incorporation, cells were lysed and then transferred to a Filter Mat A using the Filter Mate cell harvester. Filter mats were washed six times with water and dried at 80°C for 90 min. A MeltiLex scintillator sheet was melted onto each filter mat. The mats were cooled to room temperature and radioactive decay was measured using the MicroBeta TriLux luminescence counter.

2.2.6 Animal experiments

2.2.6.1 Immunization with MOG_{35-55} peptide and treatment with LPS

For the induction of EAE, MOG_{35-55} peptide mixed with CFA was used. Mice were anaesthetized using a combination narcotic of 8 % ketamine and 4 % xylazine hydrochloride, in sterile 0.9 % NaCl. The animals were injected with 100 µl of MOG_{35-55} immunization paste (50 % MOG_{35-55} peptide, 50 % CFA), mixed and incubated at 4°C for 90 min prior to injection) subcutaneously in two different sites. Two hundred µl of pertussis toxin solution were applied intraperitoneal (i.p.), and mice were observed while recovering from narcosis.

Forty-eight hours after immunization with MOG_{35-55} immunization paste, the animals were injected with a second bolus of 200 µl pertussis toxin solution. Lipopolysaccharide (LPS) was injected i.p. 24 h after immunization with MOG_{35-55} immunization paste at a concentration of 5 µg/g body weight. Controls were injected with 0.9 % NaCl solution.

2.2.6.2 Clinical scores of EAE

Beginning on day 10 following immunization with MOG_{35-55} peptide, mice were observed daily to evaluate EAE disease progression. Scores were assigned following the parameters stated in Table 19. With a score of 4 and above, mice were offered powdered food and water at the bottom of the cage, with a score of 5 and above, mice were additionally kept on cotton mats to avoid sores. Upon reaching a score of 7 or higher or after losing more than 20 % of their original body weight, mice were euthanized. EAE experiments were approved by the LAVES (reference number 3392 42502-04-13/1227).

Table 19: Clinical scores for EAE

Score	Clinical signs
0	No clinical signs
1	Reduced tail tonicity
2	Flaccid tail paresis
3	Loss of righting reflex
4	Kinetic ataxia
5	Mild paresis of hind legs
6	Full paresis of one hind leg or partial paresis of both hind legs
7	Paraplegia with full paresis of both hind legs
8	Tetraparesis with (mild) paresis of the forelegs
9	Moribund
10	Dead

2.2.6.3 Surgery for myocardial infarction

Myocardial infarction was surgically introduced into STAT1-F77A knockin mice on a C57BL/6N background. Surgery was performed on healthy young adult animals at the age of 8-12 weeks. Three days before surgery, the drinking water of the animals was supplemented with 2 mg/ml metamizol to provide basic analgesia and to prevent avoidance of metamizol supplemented water after surgery. Mice were anaesthetized using 10 µl/g body weight

narcotic solution (5 % Cepetor, 10 % midazolam, 10 % fentanyl, in 0.9 % NaCl) i.p. and fixed in the supine position. Through a small incision of the trachea, a tube was inserted to provide artificial respiration. Respiration was set at 150 µl volume and 150 strokes/min. The skin on the chest was dissected with a lateral cut, the pectoral muscles were detached to expose the rib cage and the 4^{th} intercostal space was spread to expose the heart. The infarction was introduced by ligation of the left anterior descending artery using Ethilon 9-0 BV-4 5.0 mm 3/8c EH7448G surgical silk. Whitening of the cardiac apex was observed to control proper occlusion of the coronary vessel. After successful introduction of the infarction, retractors were removed and the skin was sutured using Prolene 6-0 C-1 13 mm 3/8c 8889H surgical silk. Narcotic antagonist (5 % Revertor, 10 % Flumazenil, in sterile 0.9 % NaCl) was injected i.p. at a dose of 10 µl/g body weight. Mice were given a buprenorphine solution (1 % Temgesic in sterile 0.9 % NaCl) at a dose of 15 µl/g body weight and left on a pre-warmed plate at 37°C until fully awake. Sham-operated mice underwent the same surgery but the suture around the coronary vessel was removed without occlusion of the left anterior descending artery. After surgery, gavage of metamizol through drinking water was continued. If analgesia was not sufficient, the mice were given buprenorphine (10 µl/g body weight) i.p. twice per day. Myocardial infarction experiments were approved by the LAVES (reference number 3392 42502-04-13/1226).

2.2.6.4 Echocardiographical assessment

Transthoracic echocardiography was performed ≤ 7 days before myocardial infarction (MI) surgery and 3 days after surgery for the acute phase testing and at 1 week and 4 weeks after surgery for the long-term observation cohort. Echocardiography was performed under 1.5 % isoflurane narcosis using the Vevo x2100 system equipped with a 30 MHz centre frequency ultrasound transducer. The long axis was visualized in B mode only, the short axis in B- and M-mode. Heart rates varied in the range of 320-450 bpm, respiration rates ranged from 100-150 per minute. Data analysis was performed using the Vevo 2100 software. In the long axis, the diastolic and systolic length was determined (L_s and L_d). In the short axis, left ventricular inner diameter ($LVID_s$ and $LVID_d$), anterior and posterior wall thickness and left ventricular interior area ($Area_s$ and $Area_d$) were measured in systole and diastole. In addition, the left ventricular exterior area was measured in systole only. From these data, fractional area shortening (FAS), fractional shortening (FS), ejection fraction (EF), end-diastolic (Vol_d) and end-systolic volume (Vol_s) were calculated.

Table 20: Endpoint calculation of echocardiography data

Measurement	Calculation
FAS	$(Area_d – Area_s) / Area_d * 100$
FS	$(LVID_d – LVID_s) / LVID_d * 100$
Vol_s	$(5 / 6) * (Area_s * L_s)$
Vol_d	$(5 / 6) * (Area_d * L_d)$
EF	$(Vol_d – Vol_s) / Vol_d * 100$

2.2.7 Classical histology

2.2.7.1 Paraffin embedding of tissue and organs

In order to prepare murine tissue and organs for histological and immunohistological analysis, organs were embedded in paraffin. Mice were sacrificed through cervical dislocation under isoflurane narcosis. Organs of interest were surgically removed and washed in PBS before being perfused for 96 h in 4 % formaldehyde solution at 4°C. Organs and tissue were transferred to pure PBS for 16 h and dehydrated using consecutive ascending concentrations of ethanol, pure xylene and finally paraffin. Paraffin perfused organs were cast in blocks using the EG1160 tissue embedder. To perform histological analysis, paraffin blocks were cut using the SM 2000 R microtome, stretched using a water bath at 45°C and dried at 50°C. Sections were of 5 µm in thickness.

2.2.7.2 H&E staining of paraffin embedded sections of murine heart

To gain an overall impression of tissue conditions, haemalum and eosin (H&E) staining was performed on paraffin embedded sections. For this purpose, tissue samples were first de-paraffinized and re-hydrated by incubation in xylene for twice 15 min and descending concentrations of ethanol (99 %, 96 %, 70 %, desalted H_2O) twice for 2 min each. Slides were stained with filtered Mayer's haemalum solution for 10 min and blued using running tapwater for 10 min. The slides were counterstained in 0.1 % eosin solution for 2 min, washed twice in desalted water and dehydrated using ascending concentrations of ethanol (70 %, 96 %, 99 %) twice for 2 min each followed by two 15 min incubation steps in xylene. The samples were mounted using Entellan and analysed using light microscopy.

2.2.8 Immune staining techniques

2.2.8.1 Fluorescence-activated cell sorting analysis

When performing fluorescence-activated cell sorting (FACS) analysis, cells of spleen, lymph nodes or circulating leukocytes were stained after producing a single cell suspension. If nothing else is stated, 5 x 10^5 cells were used for analysis. The cells were centrifuged at 185 x g for 8 min and 4°C and washed once with FACS buffer. They were stained after resuspension in 100 µl antibody mastermix (FACS buffer with antibodies) for 15 min at 4°C while being protected from light. Cells were washed again once using FACS buffer and were resuspended in 1 ml FACS buffer before analysis. Staining of nuclear forkhead box P3 (FoxP3) was performed using, the PE anti-mouse/rat/human FOXP3 Flow kit according to the manufacturer's recommendations. After having been stained for extracellular markers, the cells were incubated for 30 min with 400 µl Fix-Perm solution, protected from light throughout the entire staining. Cells were washed once in FACS buffer. Blocking was performed for 15 min in 2 % rat serum in perm buffer. One µl of FoxP3 antibody was then directly added and incubated with the cells for 30 min. Cells were washed twice in perm buffer and resuspended in 200 µl FACS buffer.

Sorting was performed using the FACSCalibur cell sorter. For analysis, the software CellQuestPro was used. A minimum of 30,000 cells was sorted for quantitative analysis. Four different reaction mixes staining for different leukocyte subsets were used for detection. One mix was targeted to identify different T cell-subsets and contained CD4 PE e610 (1:500), CD8 PE/Cy7 (1:333), CD44 PE (1:333), and CD62L (1:200). In a second reaction, myeloid cell subsets were identified using CD11b FITC (1:200), Ly-6C APC/Cy7 (1:500), CCR2 AF700 (1:20), and Ly-6G PE (1:1,000). The third staining was performed to identify NK and NKT cells using TCRβ FITC (1:200), CD4 PE (1:1,000), and NK-1.1 APC/Cy7 (1:250), and in the fourth reaction, regulatory T cells were quantified using CD25 FITC (1:200), CD4 PE/Cy5 (1:500) and the PE anti-mouse/rat/human FOXP3 Flow kit.

2.2.8.2 Immune staining using HRP-reaction

Immune staining for the detection of the protein localisation in tissue sections was performed using a peroxidase reaction. The tissue sections were de-paraffinized and re-hydrated by incubation in xylene twice for 15 min followed by a series of descending concentrations of ethanol (99 %, 96 %, 70 %, desalted H_2O) twice for 2 min each. Slides were boiled in citrate buffer (8.13 mM sodium citrate, pH 6.0) for 15 min, left to cool on ice and rinsed with double-distilled H_2O and PBS. A peroxidase block was performed using 3 % H_2O_2 in PBS for

20 min at 4°C. The tissue was blocked in 10 % FBS in PBS supplemented with 0.05 % Triton X-100 and incubated with the primary antibody in 10 % FBS in PBS for 16 h at 4°C. The antibody was removed and the tissue rinsed three times with PBS before the biotinylated secondary antibody diluted 1:200 in 10 % FBS in PBS was applied for 1 h at room temperature. After rinsing the slide four times with PBS, it was incubated with streptavidin-peroxidase diluted 1:1,000 in PBS for 1 h. Slides were developed using DAB. The 2.5 % stock solution of DAB was diluted 1:250 in PBS supplemented with 0.012 % H_2O_2 and incubated with the tissue until the chromatic reaction was clearly visible. The reaction was stopped by rinsing off the DAB with double-distilled H_2O. Nuclei were counterstained with Mayer's haemalum solution for 10 min and blued using running tap water for 10 min. The slides were washed twice in desalted water and dehydrated using ascending concentrations of ethanol (70 %, 96 %, 99 %) twice for 2 min each and two 15 min incubation steps in xylene. The samples were mounted using Entellan and analysed using light microscopy. Dilutions of primary antibodies were as follows: anti-phosphotyrosine-STAT1; 1:200, anti-myeloperoxidase (MPO); 1:200, anti-CD68; 1:75, and anti-CD3 1:200.

2.2.8.3 Evaluation of staining intensity

Ventricle myocardial infiltration was assessed using two independent measures, the distribution of cells staining positive and the density of these cells within the positive area. Both measures were scored on a scale from 0-4. The criteria applied for scoring the distribution are listed in Table 21. The criteria applied for scoring the density are listed inTable 22. For the evaluation of the H&E stained hearts, only the distribution criteria were applied.

Table 21: Criteria for distribution scores

Score	Characteristics
0	No specific staining
1	Less than half of the left ventricle
2	50 % to 90 % of the left ventricle
3	Entire left ventricle but little or no infiltration of the septum or right ventricle
4	Entire left ventricle and strong infiltration of the right ventricle or the septum

Table 22: Criteria for density scores

Score	Characteristics
0	No specific staining
1	Single cells at low density
2	Small accumulations, moderate density
3	Many or large accumulations
4	High, even density of positively stained cells

2.2.9 Statistical analysis

For statistical analysis, IBM SPSS and SigmaPlot were used. Means and standard deviations or standard errors were calculated from the data. Between-group differences were assessed using Student's *t*-test. A p value of .05 was chosen as level of significance.

3 Results

3.1 N-terminus-mediated intradimeric interactions are dispensable for protomer exchange kinetics of STAT1

It is known that STAT1 dimers need to undergo a conformational change from a parallel to an antiparallel alignment to be prone to inactivating dephosphorylation (Zhong et al., 2005). Mertens and colleagues have proposed a mechanism in which intradimeric N-terminal interactions facilitate the rotation of dimer partners from one of the conformational states to the other (Mertens et al., 2006) (Figure 2, model 1). Here, experimental data support an alternative mechanism to achieve conformational reorientation, namely, conversion of parallel to antiparallel STAT1 dimers is achieved through dissociation and re-association of STAT1 protomers (Wenta et al., 2008) (Figure 2, model 2). Kinetics of the dissociation of dimers and tetramers were investigated using EMSA technique, utilising native and GFP-tagged STAT1 protein derived from transfected U3A cells. Furthermore, the question as to whether N-terminal interactions – especially those facilitated by the phenylalanine residue at position 77 – are essential for this process has been addressed.

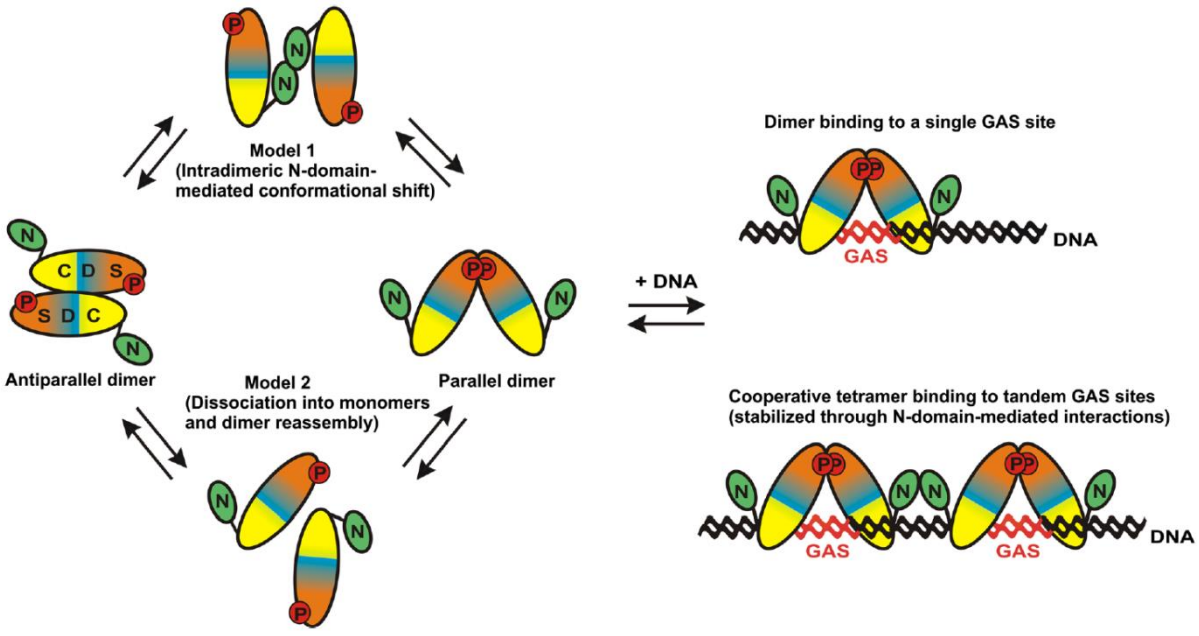

Figure 2: Proposed mechanisms for STAT1 conformational change. *Model 1 by Mertens et al,. 2006 suggested that the transition between two conformational states is facilitated through reciprocal N-terminal interactions. Model 2 is based on the dissociation and reassociation of STAT1 dimers. High-affinity DNA binding (dimeric as well as tetrameric) is only possible in the parallel form. N = N-terminus, C = coiled-coil domain, D = DNA-binding domain, S = SH2 domain, P = phosphate group.*

3.1.1 DNA-binding kinetics do not differ among native STAT1 and GFP-tagged STAT1

In order to assess the exchange kinetics of STAT1 protomers, an experimental system was established. The vectors pcDNA3.1, coding for full-length native STAT1, and pEGFP-N1, encoding a GFP-tagged STAT1 fusion protein, were utilized to introduce two different versions of the STAT1 gene into the STAT1-deficient cell line U3A. These two constructs differ in weight which makes it possible to distinguish them in EMSA readouts and in their ability of subcellular trafficking (Meyer et al., 2007). First, we evaluated whether they also differ with respect to their DNA-binding kinetics which would render them useless for the intended experiments.

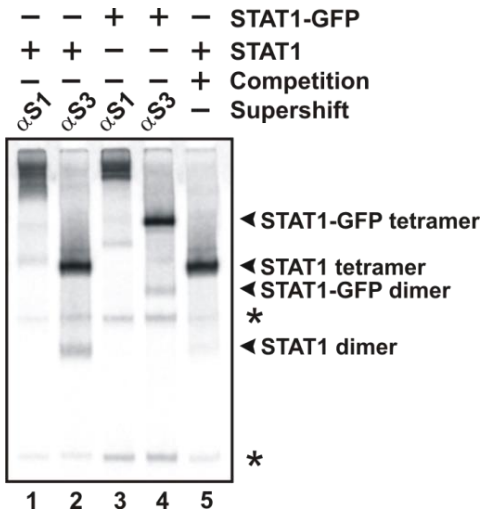

Figure 3: Native STAT1 and STAT1-GFP both favour tetrameric binding to tandem GAS sites. *EMSA confirmed the identity of recombinant STAT1 proteins interpreted to be the untagged (lane 1, lane 2 and lane 5) and the GFP-tagged variant (lane 3 and lane 4) using supershift reactions with either anti-STAT1 (lane 1 and lane 3) or anti-STAT3 (lane 2 and lane 4) antibody. Lane 5 shows the result of a competition experiment with unlabelled GAS elements added in 750-fold excess. The asterisk indicates an unspecific band.*

Protein extracts derived from U3A cells transfected with a construct carrying either the native *STAT1* gene or the gene for *STAT1* with a GFP-tag were incubated with the [^{33}P]-labelled 2xGAS probe and analysed by means of EMSA (Figure 3). Both STAT1 proteins bound to the probe specifically as dimeric and tetrameric complexes, as shown in lane 2 and lane 4 for native STAT1 and GFP-tagged STAT1, respectively. For both variants, the slower migrating complex corresponding to the tetrameric form was favoured over the dimeric complex, as indicated by stronger signal intensity in the autoradiograms. The specificity of the signal was confirmed by supershift reaction: Addition of a STAT1-specific antibody

significantly shifted the dimer and tetramer band (lane 1 and 3), whereas an antibody directed against STAT3 was unable to cause this effect (lane 2 and 4). Co-incubation with a 750-fold molar excess of an unlabelled 2xGAS oligonucleotide rapidly weakened the signal for dimeric STAT1 bound to the probe, while leaving the signal intensity for the tetramer almost unaffected. This highlights the higher stability of tetrameric complexes bound to DNA as compared to dimeric complexes – an effect highly dependent on reciprocal interactions between the STAT1 amino-termini (Vinkemeier et al., 1996; Begitt et al., 2014).

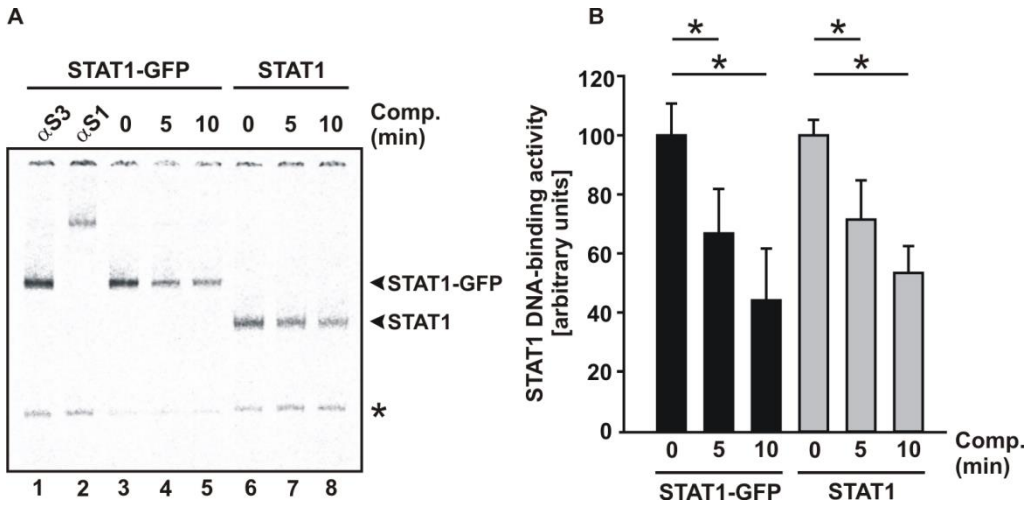

Figure 4: Competition assay showing the dissociation kinetics of STAT1 dimers from single GAS elements. *(A) Protein extracts from U3A cells transfected with plasmids coding for either wildtype or GFP-tagged STAT1 were incubated with [^{33}P]-labelled M67 for 15 min and subsequently co-incubated with a 750-fold molar excess of unlabelled M67 duplex for the indicated times. The asterisk indicates an unspecific band. (B) Densitometry of three independent experiments showing the results from the competition assay in A. Error bars represent the standard deviation. Asterisks indicate statistically significant differences.*

In order to compare the DNA-release kinetics of the two STAT1 variants, a competition with the untagged M67 oligonucleotide was performed (Figure 4). Protein extracts from IFNγ-treated U3A cells which had been transiently transfected with a plasmid coding for either native or GFP-tagged STAT1 were incubated on ice for 15 min with the radioactively labelled M67 probe which contained a single GAS element. A 750-fold molar excess of non-labelled M67 oligonucleotide was added 0, 5 and 10 min before the samples were loaded onto the non-denaturing polyacrylamide gel. As seen in lanes 6-8 of Figure 4A, DNA binding of native STAT1 was reduced with time owing to competition from unlabelled DNA. The same effect was observed for the STAT1-GFP molecule (lanes 3-5). Quantitative assessment of three independent experiments demonstrated that DNA-bound STAT1 dimers are released

relatively rapidly and that the dissociation kinetics of the native and the GFP-tagged STAT1 variants are comparable (Figure 4B).

3.1.2 Native and GFP-tagged STAT1 form hetero-tetrameric complexes *ex vivo*

Given the observation that native and GFP-tagged STAT1 both bind to DNA with similar kinetics, the next step was to observe whether the two variants were able to interact in order to form hetero-tetramers. Extracts from IFNγ-treated U3A cells expressing either recombinant GFP-tagged or untagged STAT1 were incubated with radioactively labelled 2xGAS probes. As a control, each of the protein variants was incubated with the DNA probe separately for 20 min on ice and the resulting samples were then combined immediately before being loaded onto the gel (Figure 5, lane 5). In this setting, the two homo-tetramers can be clearly distinguished. To allow interchange of dimers, a separate reaction was set up where the [^{33}P]-labelled 2xGAS probe was incubated with a mix of both extracts for 20 min before being loaded onto the gel (Figure 5, lane 6). In this setting of co-incubating the extracts with the probe, both bands corresponding to the homo-tetramers in lane 5 appeared again. Additionally, a third band appeared between the two homo-tetramers which was interpreted as a 2xGAS probe occupied by two homo-dimers each containing either GFP-tagged or untagged STAT1.

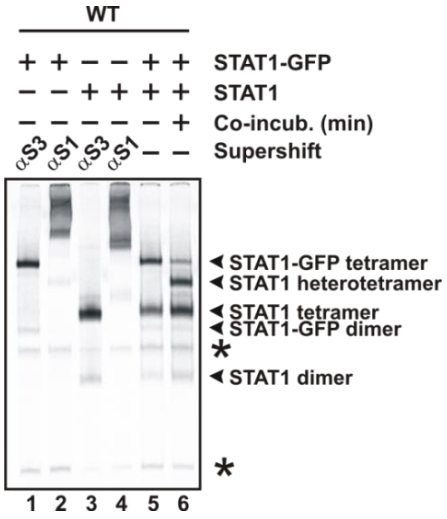

Figure 5: Native STAT1 and STAT1-GFP can form hetero-tetramers. *Extracts from U3A cells expressing native or GFP-tagged STAT1 were incubated with the [^{33}P]-labelled 2xGAS probe either separately (lane 5) or mixed together (lane 6) for 20 min. Asterisks indicate unspecific bands.*

To validate the identity of the additional band, a co-incubation of the extracts before loading with varying portions of both STAT1 variants was performed (Figure 6). Lane 1 and 2 correspond to lane 5 and 6 from Figure 5. In lanes 3 and 4, the amount of extracts from cells transfected to produce native STAT1 exceeded the extracts from lane 5 and 6 by the factor 5, while this relation was reversed for GFP-tagged STAT1. It becomes clear that, in lane 4, there is almost no signal from the band representing the STAT1-GFP homo-tetramer, whereas in lane 6, the signal from the native STAT1 homo-tetramer band was markedly reduced compared with the corresponding band in lane 2 and 5. This strong reduction in the signal intensity indicated that the newly formed tetrameric complex is indeed a hetero-tetramer consisting of two STAT1-GFP/STAT1-GFP and STAT1/STAT1 homodimers, respectively.

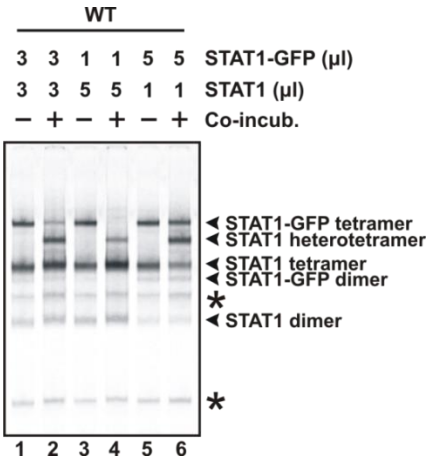

Figure 6: STAT1 hetero-tetramers consisting of two homodimers are formed on tandem GAS sites. *Extracts from U3A cells expressing either recombinant, untagged or GFP-tagged STAT1 were co-incubated at ratios of 1:1, 1:5 and 5:1 with [^{33}P]-2xGAS elements before loading on a non-denaturing EMSA gel. Lanes with odd numbers show the results for extracts that were incubated separately, while lanes with even numbers correspond to the co-incubated extracts. Asterisks indicate unspecific bands.*

3.1.3 The rate of protomer exchange is reduced through binding to DNA

To this point, the data demonstrated the presence of a STAT1/STAT1-GFP heterotetramer only with a 1:1 stoichiometry. This complex most probably consisted of two homo-dimers since no additional bands representing a 1:3 or 3:1 stoichiometry were observed. In order to validate the conditions under which complexes with a 1:3 and 3:1 stoichiometry were formed, extracts from IFNγ-treated U3A cells transfected with either variant were incubated separately in the presence of DNA (Figure 7, lane 1). Alternatively, lysates containing the two variants were mixed in the absence of [^{33}P]-2xGAS, which was only added immediately before the reactions were loaded onto the gel (Figure 7, lane 2). The two reactions were incubated for

45 min at room temperature, before the DNA-bound STAT1 complexes were electrophoretically separated by EMSA. When free exchange of STAT1 molecules was allowed in the absence of co-incubating DNA, this resulted in the occurrence of several additional bands not detected in the presence of the 2xGAS probe. This observation showed that not only dimers but also single tyrosine-phosphorylated protomers can interchange between different dimer pairs in solution, unless STAT1 is bound to high-affinity DNA-binding sites present in the incubation mix.

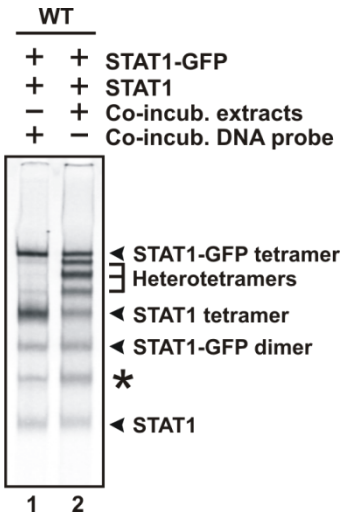

Figure 7: Untagged and GFP-tagged STAT1 form hetero-tetramers with 3:1 and 1:3 stoichiometry when unbound to DNA. *Co-incubation of extracts from reconstituted U3A cells expressing either untagged or GFP-tagged STAT1 at room temperature for 45 min before addition of [^{33}P]-2xGAS probe resulted in the appearance of the predicted bands with 3:1 and 1:3 stoichiometry (lane 2). No such bands were detected in the presence of binding to GAS elements. The asterisk indicates an unspecific band.*

The kinetics of the promoter exchange was then investigated. Protein extracts from reconstituted U3A cells containing either recombinant untagged or GFP-tagged STAT1 were co-incubated with the 2xGAS DNA probe for different durations of time (Figure 8). A comparison of lane 1 with lane 2 and 3 in Figure 8A shows that longer co-incubation of the STAT1 isoforms in the absence of DNA resulted in increased interchange of dimers and protomers of STAT1. This demonstrates that binding of STAT1 to DNA hinders the replacement of protomers within dimers.

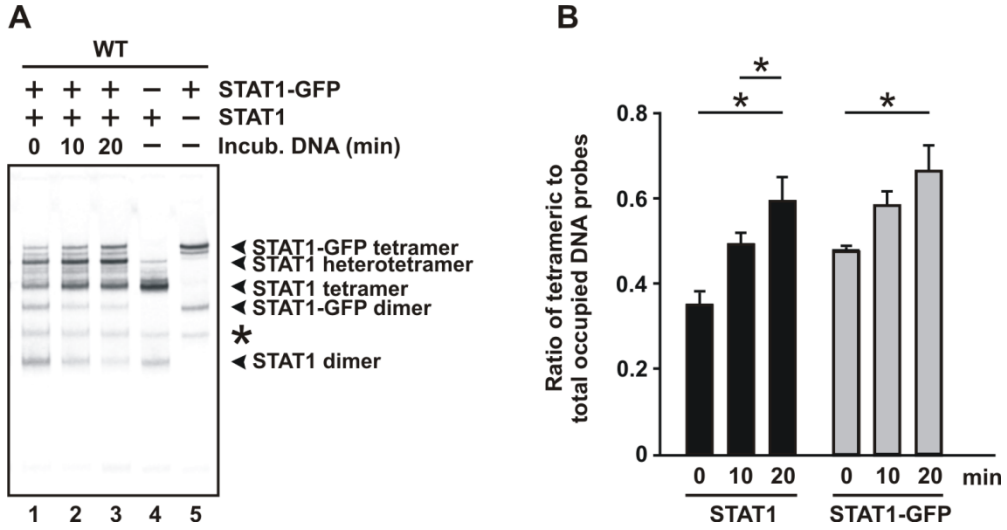

Figure 8: Binding of STAT1 to DNA hinders the exchange of protomers. *(A) [^{33}P]-labelled 2xGAS was incubated with mixed extracts from U3A cells expressing either untagged STAT1 or STAT1-GFP for the indicated durations of up to 20 min (lane 1-3). Lane 4 and 5 display the results of [^{33}P]-2xGAS incubation with only one of the STAT1 variants. The asterisk indicates an unspecific band. (B) Densitometry from three independent experiments showing the tetramer signal in relation to the combined signal of dimers and tetramers. Error bars represent the standard deviation. Asterisks indicate statistically significant differences.*

Furthermore, densitometric analysis of three independent experiments verified the impression that increasing incubation time of STAT1 with DNA favoured the formation of tetrameric complexes over the binding as a dimer. In summary, these data highlight the significance of DNA binding in the dissociation and re-association of dimers and the stabilization of tetrameric STAT1 complexes.

3.1.4 The exchange of STAT1 protomers is a process independent of intradimeric N-terminal interactions

To allow for inactivation of tyrosine-phosphorylated STAT1 dimers, a conformational change from a parallel to an antiparallel alignment is necessary (Zhong et al., 2005). A mechanistic model had been proposed by Mertens and colleagues that required intradimeric interactions between the N-termini of the partner protomers to break the phosphotyrosine-SH2 binding (Mertens et al., 2006). As a tool to study N-terminal interactions, the STAT1-F77A mutant was created. By exchange of the phenylalanine at position 77 to alanine, reciprocal N-domain-mediated binding between two dimers was critically weakened (Meyer et al., 2004). Further insights into the dynamics of protomer exchange were expected from studying the phenotype of the STAT1-F77A mutant. Since the STAT1-F77A mutant had been shown to display more efficient and prolonged phosphorylation as compared to the wildtype protein (Meyer et al.,

2004), protein extracts used in further experiments were tested by means of Western blotting technique to adjust for equal amounts of tyrosine-phosphorylated STAT1 (Figure 9B).

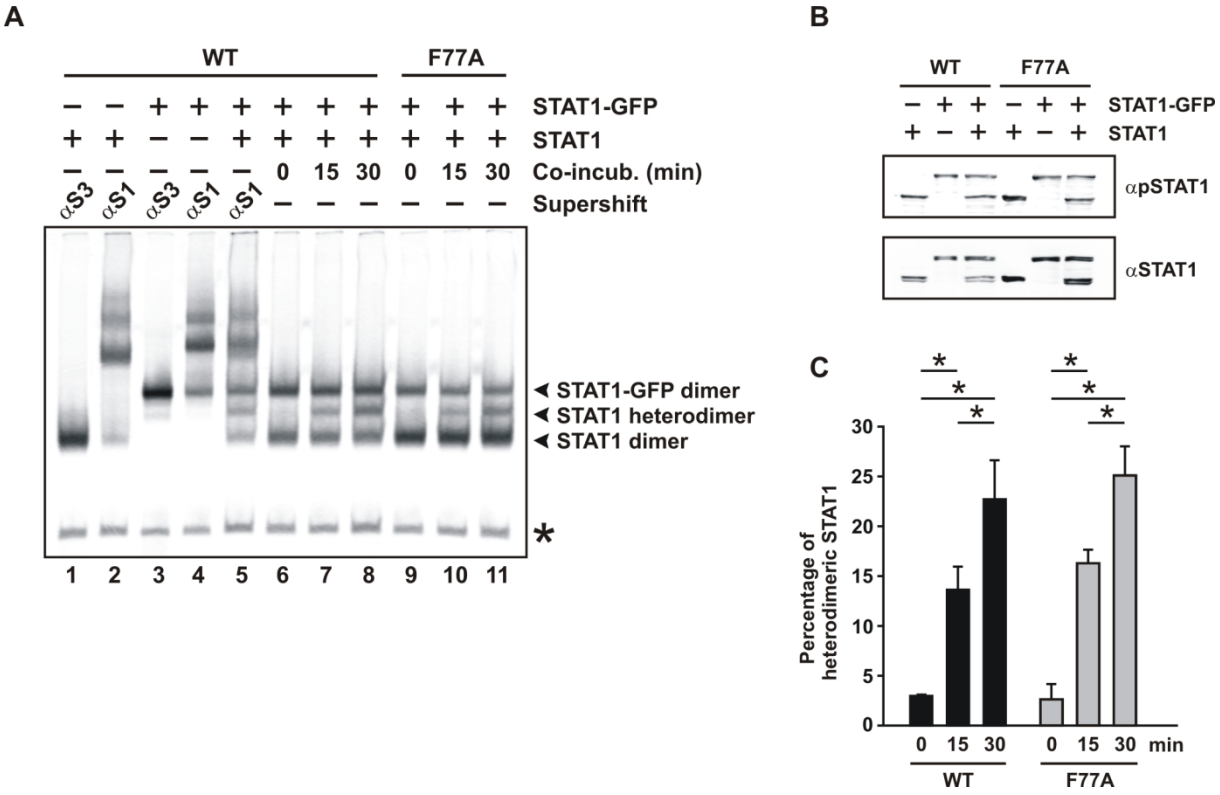

Figure 9: Protomer exchange kinetics of dimers does not differ between the wildtype STAT1 and the F77A mutant. *(A) Protein extracts of U3A cells that had been transfected with the native or GFP-tagged form of WT or F77A mutant STAT1 were co-incubated for the indicated durations. The probe used for binding STAT1 was [^{33}P]-M67 containing a single GAS site. The asterisk indicates an unspecific band. (B) No evidence of gross structural alterations in the STAT1-F77A mutant was detected as judged from Western blotting results. Lysates from IFNγ-pre-treated, reconstituted U3A cells expressing either the untagged form of STAT1α with a molecular weight of 91 kDa or the GFP-tagged variant with the molecular weight of 118 kDa were tested in isolation or as a mixture using a STAT1-phospho-tyrosine-specific antibody (top). The result from stripping-off bound immunoreactivity and exposure of the membrane with a pan-STAT1 antibody is shown at the bottom. (C) Densitometric analysis of three independent experiments performed as demonstrated in (A). Shown is the proportion of heterodimers among all dimers that were detected. Error bars represent the standard deviation. Asterisks indicate statistically significant differences.*

Protein extracts from transfected U3A cells expressing the untagged or the GFP-conjugated isoform of wildtype or F77A mutant STAT1 were co-incubated for 0, 15 or 30 min before addition of the M67 DNA probe (Figure 9A). Lanes 6-8 depict a representative result for wildtype STAT1. In line with the above mentioned observations, an increase in STAT1 hetero-dimers with increasing times of co-incubation before addition of the probe was detected. As can be seen from lane 9-11, the pattern of the F77A mutant did not differ from

the wildtype molecule. The readouts from three independently conducted EMSAs were quantified using densitometry analysis. The results shown in Figure 9C confirmed that there was no significant difference in the intradimeric protomer exchange kinetics between the wildtype protein and the F77A mutant when binding to a DNA probe carrying a single GAS motif was studied.

Subsequently, the differences in the DNA-association kinetics between the wildtype and the F77A mutant were tested by means of EMSA using the 2xGAS probe (Figure 10A). Lanes 7-9 show the results for the wildtype. Lane 7 corresponds to completely separate incubation of the wildtype and the GFP-tagged variant, lane 8 displays the co-incubation of the two isoforms in the presence of GAS, and lane 9 depicts co-incubation of the two STAT1 variants in the absence of GAS elements which were added immediately before loading onto the gel. Again, the results confirmed the conclusion from the previous experiments. Lanes 10-12 show the respective results for the STAT1-F77A mutant. The slight retardation in the migration of the tetramer band of native STAT1 carrying the F77A mutation probably results from a less compact form of the homo-tetramer due to its lack of tetramer stabilization through N-terminal interactions (Vinkemeier et al., 1996; Meyer et al., 2004).

As for the wildtype molecule, little to no signal was detectable for recombined isoforms other than the two homo-tetramers, upon incubation of the two STAT1 variants with the 2xGAS probe separately (Figure 10A, lane 10). Upon incubation of the two isoforms together with the DNA probe for the entire duration of the experiment, all five different compositions of the tetramer are observed (lane 11). When the protein extracts were mixed and co-incubated before addition of the DNA, again all five species appeared (lane 12). The main difference between the result of the incubation of the mixed protein extracts with and without the probe is the higher concentration of hetero-tetramers with 3:1 and 1:3 stoichiometry which corroborated the earlier observation that dimers within a tetramer are exchanged at a faster rate than protomers and that exchange rates for dimers and monomers dramatically drop as soon as they are bound to DNA.

In Figure 10B, the results from the corresponding densitometric analysis are displayed. The quantitation of the EMSA results showed the relative amount of GFP-tagged and untagged STAT1 isoforms in the tetramers formed under conditions of co-incubation with protein extracts and/or GAS elements. This analysis underlines the initial observation demonstrating that there is no difference in the protomer exchange kinetics between the STAT1 wildtype

protein and its F77A mutant. This finding supported the conclusion that reciprocal N-terminal interactions are dispensable for the exchange of protomers.

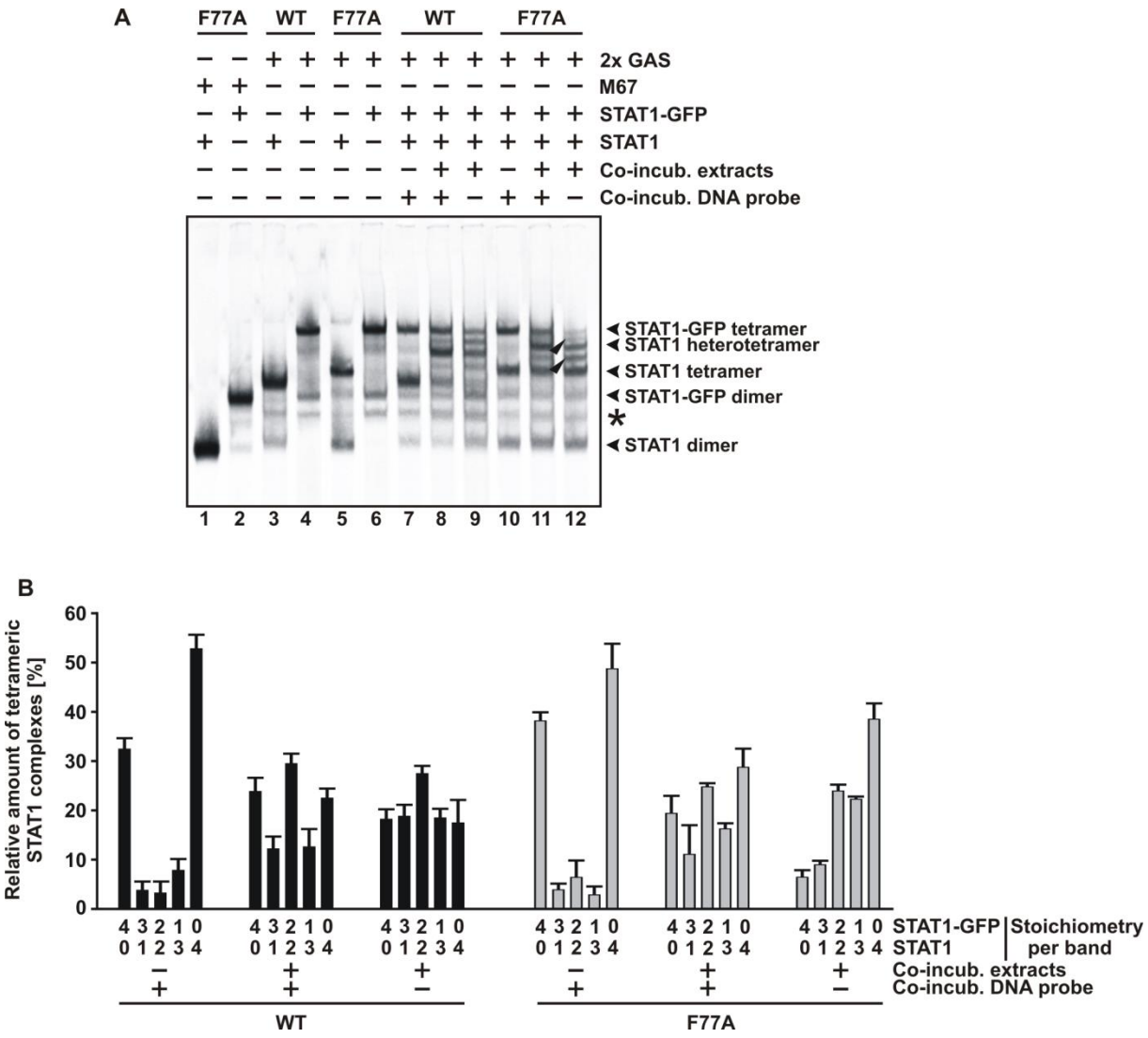

Figure 10: Amino-terminal interactions are dispensable for monomer exchange of STAT1. *(A) EMSA experiment comparing the intratetrameric and intradimeric subunit exchange kinetics of wildtype STAT1 (lane 7-9) with its F77A mutant (lane 10-12). The asterisk indicates an unspecific band. Unconjugated wildtype STAT1 homo-tetramers run slightly faster than STAT1-F77A homo-tetramers probably due to a more condensed structure facilitated through tetramer stabilization. (B) Densitometry analysis of the proportions of each variant at the indicated stoichiometric ratio from three independent gel runs. Error bars represent the standard deviation. Asterisks indicate statistically significant differences.*

3.2 Gene expression of ezrin is weakly induced by STAT1

3.2.1 Unique GAS motif in the promoter region of the human ezrin gene was identified

Ezrin, radixin and moesin constitute the ERM protein family, a class of cytoskeletal proteins with the main function of linking transmembrane proteins to the actin cortex. While recent studies have focused on the role of ERM proteins on leukocyte recruitment (e.g. Killock et al., 2009; Wang et al., 2014), less is known about the regulation of their gene expression.

An *in silico* search revealed the presence of a unique STAT-binding element in the promoter of the human ezrin (*EZR)* gene approximately 500 bases upstream of the first exon (Table 23). This motif consists of two GAS elements located in tandem orientation which are separated by only one base pair. Each element closely resembles the consensus STAT-binding site, termed GAS sequence (TTC[N]$_{3\text{-}4}$GAA), which is usually located in the vicinity of the transcriptional start site (Decker et al. 1997).

Table 23: GAS motifs surrounding the transcription-start site (TSS) in the promoter of the human EZR gene. *Gene sequence was obtained from www.ensembl.org.*

>chromosome:GRCh38:6:158765141:158820912:-1

TTCTAGAGTGAGCTCTCCCGCAGCAAATTCTACTGGCCCCCAAAGTATGTGTTTTGTGTGTCTTAAAA
ATTTGTTGAGAACCATTAGCAAAAAAACAAACAAAAAAACTTAA***TTC***CTA***GAA***T***TTC***AGA***GAA***ATCCC
ATGGAGCTTTTTGCCAGTCACGTCAAAAGAGGCCACAAACGTGCCA***CTTAACCAGA***GCTTCGGAAAGG
CGGCGGCTGGGCCGGCCACGTGCACCGAGACTCGGGGCCAGGTGCAGCCGCCCCAGGGCCGAGGCCTC
GGAACTGGCCCCCGGTCCCGGCCCCAAGCGGTCCAGCGATTCCCCCAAGCCGTCCGCCCCTCCAGATT
TATTTACGTTTTCCTGACTTCCCCCTGCCCGCTGTGGGACAAACAGCCTCCCCACTTGCATCTGCGAG
GGGAGTAGCGCGCACTTCCGCCAAGTTCCGCCCCCACCCAGCCCGAGGCCCGGCTGCCGCCATCTTGC
GGGGGGCGCACCTCACAGGTCGGGAGCTGGGCGGGAAGGGGCGTGGTCCCG**GGACCCGCCCCCGCCGGG**
GCTTTTGGGAGCGCGGGCAGCGAGCGCACTCGGCGGACGCAAGGGCGGCGGGGAGCACACGGAGCACT
GCAGGCGCCGGGTGAGGCGTGCGGCGGCCGGGGTC

Exon 1, IFNγ-activated site motif

Predicted TSS using the data base Berkeley Drosophila Genome Project (BDGP) neural network prediction tool (http://www.fruitfly.org/seq_tools/promoter.html)

Given that the IFNγ/STAT1 axis is a signalling pathway highly relevant to a plethora of immunological processes, STAT1 may be a candidate for regulating ezrin signalling in leukocytes. Although in the mouse genome a similar tandem GAS motif cannot be found in the *Ezr* gene promoter (Table 24), three optimal and two non-optimal GAS motifs were identified in a region spanning 1,200 base pairs upstream of the transcription start site to the

first intron. This finding warranted further research efforts to investigate the IFNγ/STAT1 signalling pathway as a putative mediator of *Ezr* gene transcription in mice.

Table 24: GAS motifs surrounding the TSS of the murine EZR gene sequence. *Gene sequence was obtained from www.ensembl.org.*

>chromosome:GRCm38:17:6737441:6785784:1

ACCTAGCACGGCACTAATTTCACGTGTGTA***TTC***ATT***GAA***GTCTACATCTGTGTAGATGTTGCTCCTTG
GATCCCTA***TTC***TAC***AAA***TTAGGATTACCGGGTCCCAAAGGAACTTTTCCCATTCTGGAATGGATATAC
TCAGCCCCGGAACGGAGTTGTGCACATGTCACATTCAATACATCTAATCCTCATTACAACTCACGGAA
CAGATGTCTTACGATGGGGCAATTTTGCAAATAAGAAAACTAAGGAATCAACCCTTCCAGTGCAGTAC
CCCAATAGAAATTCAGGAGCAGCTCGTATCTCAACCCTCACCCAACTTCAACCACCTGAAACTTTCAT
CCCCAGGTGGGGCTTTGAACCCGGCTTTGAGAACCAAGACTTTAATTATACCCCAACAGATTCCACCA
GTGCTACAGGAAAACATTGGACTATTCCGCGGGGCGGGGGAGGACTTTTAGAGTTAGTTTTTAGGCAG
ACTTCAGAGACCACTACCTGTGGAGCCTTTTGCTACAAATTAG***TTC***TTT***TAA***CTAAGGCATCCCGGGC
AAGGGTCTTCCACGCGCATGCCTGTTTCAGAGGCTGCCCAGGCCACGTGCACGGAGACCCGGGGCCGT
GACCAGGGTGAGACCCGGCAGCCCCACCCACGAACCTGCCCGGTGGCCGCCGCTCCAGCACGTGGGAG
TAGCATTTCGGCGACTCCGCTCCGTGCAGCGCGGGGCACTTGCACCTTCCCTCCGCGCTCGCCTGCTG
CAGCACCGGACTCCAAGGAGTCCTGAGCTAGGGCTCGCGGAAGGAGAGAGGTCCTGGGTCCCGTCCGC
TCTGGGTCCCGCGGAGCCGCGGCCATCTTGGCGGGCTCACCTCGCGGGTCGTGCGCTCGGGCTGGGAC
AGGGTGGGGCCCCGGGACCCCACCCCGCTGGGGATCGGGGGGGGGGGGACACGCACCGGAGGAGTGCT
CCGTGTGCCGTCACGTGCGCTCCAAGGAGGAGAGTGATGGATGGGGCGACCGCCTGTGCGCGGACTTG
GGAGTCCCCACGCGTGGGGGACAGTGGAGCTGAGCCTCCAGTGCAGCTCGAGCCGCTGCGTGACCCTC
CGTCCCGGGGTGGGGCACCCTTCCCGAAGCCAAGGCCGAGCGCGGGCTGCGCGGACGCGCGCCCCCCT
TCCGGCCGATCCCAGTTTGTGAAGAAAAGGGGCAAAAAGAAGTGTTAAAAGATCCCGGAATTGCGGTT
TGGCTC***TGGGGCAACG***GTTGCTACACGAAGTGAAACCTGCGGAGCGCTCGGGCGCGCGCCGCGCCC
CGCCCCGATCGGGCGTGACTCATCTTGGGACCGCCCGGCCGGT**TCTTATACTCGGGACTGCGGAGCGC**
GCGCAGGGCTTCCCTCCGCCTGCAGGTCCCGACGCGTCTCCGCCGTCGCCGTCGCCGTCGCCTCCGCC
GTACAGCCGAATAGCCGAGGACCCACGCAGAGCCACCAACCAGCCAAGATGCCCAAGCCAGTAAGTTG
TCCCTGTTTCGGAGCGGCTGTGCGCCAGGCCGGGTGTCCCCAGGGAATCACCTTGCACTGGCTGCTGG
GCAGC***TTC***TGTA***GAA***CCCAGTT***TTC***TGGT***GAA***GGGCCTCTTGTTACCTGTAGACGCCTTTGTGGCACT
CTCTAGTCCCCTTTGTGGGTGGTTCTTTTTCGGTTGCTAACGAACCCCCTACCAGGTTTCCGGACTGC
TTTAAAAGTGCTTAGTGCAACCTCCAAGTTTCTTAACTGGTGCAAGTAGCACTGAAGCTTTGGTGGCT
TCTCACACGACCGACACCTGTTCGCCCAGTTCCTTCGAGCGACCGAA

Exon 1, IFNγ-activated site motif, ***non-optimal IFNγ-activated site motif***

Predicted TSS using BDGP neural network prediction tool

3.2.2 STAT1 readily binds to the tandem GAS motif as a dimer but poorly as a tetramer

To evaluate whether the identified sequence was in fact an IFNγ-activated site, gel shift assays were applied using a radioactively labelled probe that contained the native sequence with the tandem GAS motif from the human *EZR* promoter region. Protein extracts from IFNγ-treated U3A cells expressing wildtype human STAT1 were incubated with this probe and tested for specific DNA-binding activity (Figure 11A). The autoradiograms showed a specific signal that was interpreted to represent binding of STAT1 to this probe as a dimer,

while tetrameric complexes were not detectable. The identity of the band was determined through a supershift reaction using an antibody recognizing STAT1 and, as a negative control, STAT3 (Figure 11A, lane 1 and 2).

Whether STAT1 preferentially bound to the first or the second GAS motif of the tandem sequence was then tested. In this study, four different mutant versions of the probe that were termed EZR M1 to EZR M4 were designed. The annealed oligonucleotide termed EZR M1 had an altered first GAS motif and would, therefore, not support STAT1 binding at that site, while for EZR M2 the second GAS motif was altered in the same way. The probe EZR M3 incorporated the mutated sites of both EZR M1 and EZR M2 and was expected not to bind STAT1, and in EZR M4, the GAA of the first and the TTC of the second motif were altered and, therefore, presented with two half-sites. As demonstrated in Figure 11A, lanes 4 to 7, it appeared that there was no preference towards the first or second motif of the tandem GAS element shown by similar signal intensity of the dimer band in lane 4 and 5. The complex formed was specific since no binding was detected for EZR M3 mutated at both sites (lane 6). EZR M4, however, still showed some, though reduced binding of STAT1 showing that either an intact half site could support the dimer binding or that the dimer could span a longer distance on the DNA with reduced binding affinity.

The tandem GAS element found in the *EZR* promoter region was different from previously reported tandem GAS motifs. For example, the gene *CCL2* was reported to have a one-and-a-half GAS motif that consisted of a full-length GAS motif and another half-site located at 10 bp distance from the GAS site. This sequence has been discussed to be better at facilitating tetramer stabilization and contributes to the stronger sensitivity of *CCL2* gene transcription in response to different phosphorylation levels of STAT1 (Hüntelmann et al. 2014).

In order to confirm that the GAS element found in the *EZR* promoter did not support tetramer binding, a probe was designed that spanned a larger sequence surrounding the GAS motif which was termed EZR long. This probe was tested with extracts of U3A cells expressing wildtype STAT1 or a mutant of STAT1 with point mutations in positions 92 and 96 which had been shown to provide significantly stronger stabilization of STAT1 tetramers (Staab et al., 2015). When testing this probe a prominent signal resembling binding as a tetramer was detected for the STAT1-DE92/96RR (Figure 11B, lane 4), while the corresponding signal for the wildtype molecule was hardly detectable (lane 2). In contrast, binding of dimeric STAT1 to the probe ERZ long was found for both STAT1 variants. Thus, it was assumed that the sequence found in the promoter region of the human *EZR* gene is

readily occupied by phospho-STAT1 dimers but represents only a weak target for tetramer binding.

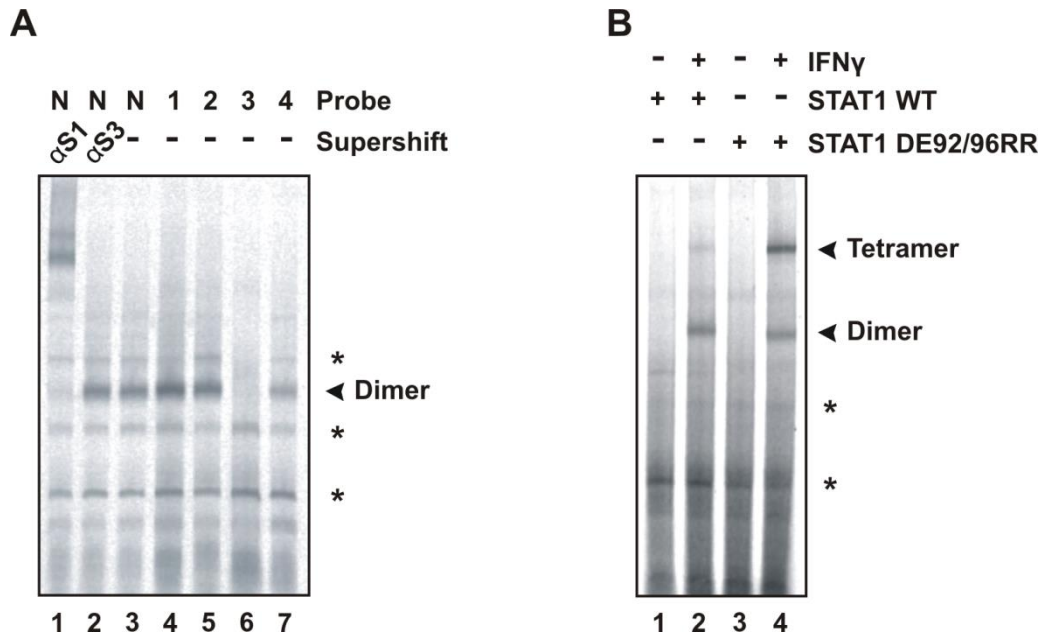

Figure 11: EMSA showing STAT1 binding to tandem GAS elements in the human EZR promoter. *(A) Native (N) and mutant versions (probes 1-4) of the tandem GAS motif found in the human EZR promoter were incubated with protein extracts of STAT1-expressing U3A cells treated with IFNγ and Na_3VO_4. Probes used were native EZR short (N) (5'-TTTTTAA**TTC**CTA**GAA**T**TTC**AGA**GAA**TC-3'), EZR M1 (1) (5'-TTTTTAATAGCTACTAT**TTC**AGA**GAA**TC-3'), EZR M2 (2) (5'-TTTTTAA**TTC**CTA **GAA**TTAGAGACTAATC-3'), EZR M3 (3) (5'-TTTTTAATAGCTACTATTAGAGACTAATC-3'), EZR M4 (4) (5'-TTTTTAA**TTC**CTAGTATTACAGA**GAA**ATC-3'). αS1 = STAT1-specific antibody, αS3 = STAT3-specific antibody. (B) Extracts from U3A cells reconstituted with either wildtype STAT1 or the DE92/96RR double mutant that had been pre-treated with IFNγ/Na_3VO_4 (lane 2 and 4) or left untreated (lane 1 and 3) were tested with the probe EZR long (5'-TTTTCAAACAAAAAAA CTTAA**TTC**CTA**GAA**T**TTC**AGA**GAA**ATCCCATGGAGCTTTTT-3'). Asterisks mark unspecific bands.*

3.2.3 STAT1 associates to the *EZR* promoter in Jurkat cells

After showing that tyrosine-phosphorylated STAT1 binds to the GAS elements in the promoter of the *EZR* gene, the next step was to evaluate whether this association was also present in living cells. To this end, we used extracts from Jurkat cells which are a well-studied cell line derived from a T cell leukaemia (Gillis and Watson, 1980). Analysis of STAT1 binding to the *EZR* promoter using the ChIP technique revealed that, after stimulation of cells with IFNγ, the respective DNA segment can be precipitated using an antibody targeted to STAT1 while under unstimulated conditions, no precipitation was observed (Figure 12). The

association of STAT1 to the *IRF1* promoter was included as a positive control. This result showed that STAT1 is recruited to the *EZR* promoter in IFNγ-treated Jurkat cells.

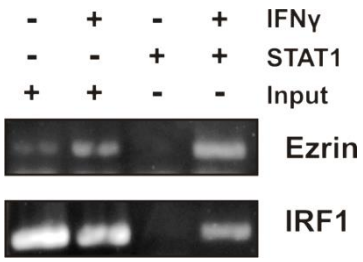

Figure 12: ChIP analysis of STAT1 association to the EZR promoter in IFNγ-treated Jurkat cells. *Shown is a representative result of a ChIP assay with an anti-STAT1 antibody used for the pulldown including the corresponding input (cross-linked and pre-cleared sample before pulldown). The experiment was performed in Jurkat cells treated with recombinant IFNγ for 45 min (+) and in untreated Jurkat cells (-). For evaluation, the precipitated fragments were amplified using conventional PCR and then visualized by means of agarose gel electrophoresis. IRF1 was analysed as a positive control.*

3.2.4 IFNγ-activated STAT1 induces *EZR* gene transcription

Since IFNγ-activated STAT1 is recruited to the promoter of the *EZR* gene, whether this process had an effect on gene transcription was of interest. As a measure for endogenous gene expression, quantitative PCR (qPCR) was used on reversely transcribed RNA isolates. Jurkat cells were chosen as the suitable system since, in this cell line, the ChIP experiments described above had identified the association of STAT1 to the *EZR* promoter. HL-60 cells, a myeloid progenitor leukaemia cell line (Collins et al., 1977), were used as a control to confirm the results obtained in Jurkat cells. The data showed that in Jurkat cells, *ezr* expression increased slightly after 6 h of incubation with IFNγ. This trend continued and was even more pronounced after 10 h incubation and led to a roughly three-fold induction (Figure 13A). Control experiments with known targets of IFNγ-induced STAT1 signalling, namely *irf1* and *stat1*, confirmed that the experimental conditions were suitable to induce STAT1-dependent gene transcription but also showed that the induction of the *EZR* gene was comparably mild (Figure 13B and 13C). Similar results were obtained from HL-60 cells. Expression of the *EZR* gene was mildly induced by IFNγ after 6 h and 10 h of incubation (Figure 13D). Control analysis of *irf1* and *stat1* was again in line with the results from Jurkat cells (Figure 13E and 13F).

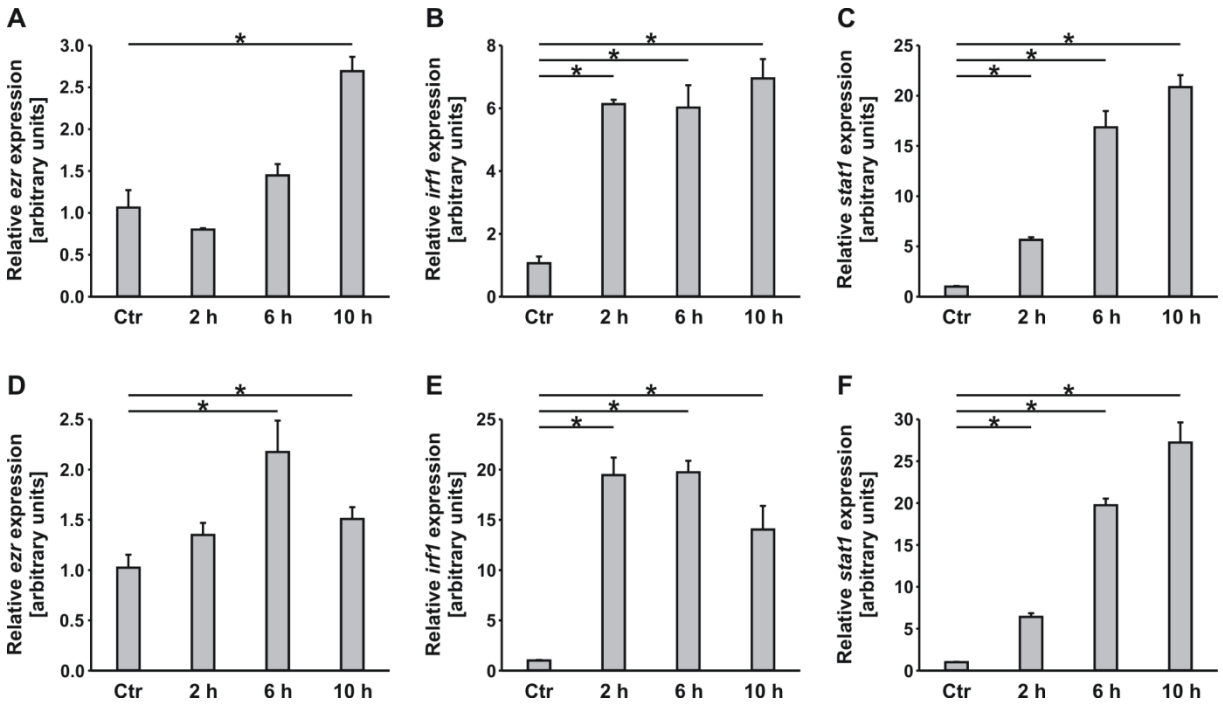

Figure 13: Real-time PCR results from Jurkat cells and HL-60 cells treated with IFNγ for 2 h, 6 h, and 10 h, respectively. *(A-C) Jurkat cells, (D-F) HL-60 cells. Expression of ezrin (A,D), irf1 (B,E) and stat1 (C,F). Evaluation was performed using the ΔΔCT method. Shown are representative results. Asterisks indicate statistically significant differences. Error bars represent standard error of the mean.*

In order to evaluate whether the observed gene induction was specific for IFNγ-activated STAT1 signalling, transcription of the *EZR* gene was analysed also in IFNα-treated cells (Figure 14A). It was shown that IFNα was less potent in inducing *EZR* gene transcription in Jurkat cells as compared to IFNγ. Analysis of *stat1*, *irf1* and *ifit1* – an IFNα target gene – confirmed adequate stimulation of Jurkat cells (Figure 14B-D).

These data support the hypothesis that *EZR* is a target gene of IFNγ-dependent STAT1 signalling. The relatively mild induction of the protein might be attributed to the fact that ezrin is a cytoskeletal protein of which only limited induction is needed. This contrasts to other STAT1-target genes with a much larger increase from baseline expression to cytokine-induced transcription.

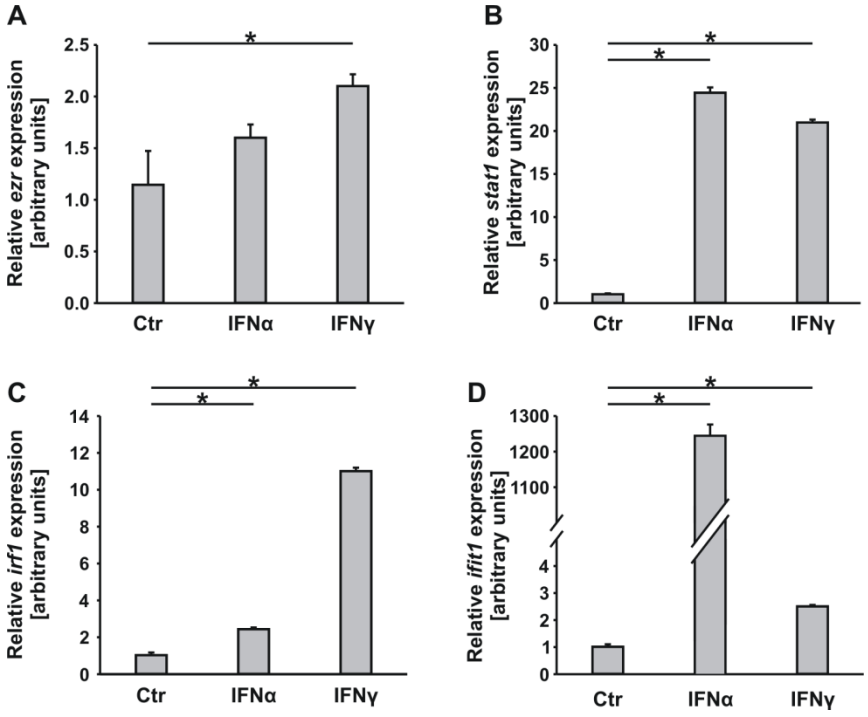

Figure 14: Real-time PCR results of Jurkat cells treated with IFNα and IFNγ showing induction of the EZR gene. *Expression levels for ezrin (A), stat1 (B), irf1 (C), and ifit1 (D) are shown in unstimulated controls (Ctr) as compared to cells stimulated for 6 h with either IFNα or IFNγ. Gene induction was analysed using the ΔΔCT method. Shown are representative results. Asterisks indicate statistically significant differences. Error bars represent standard error of the mean.*

3.2.5 No evidence of IFNγ-induced ezrin expression in leukaemia cell lines

Whether stimulation of leukaemia cell lines with IFNγ resulted in increased translation of ezrin was then tested. For this purpose, protein lysates were produced using a protocol of fractionated extraction from Jurkat cells and HL-60 cells pre-treated with IFNα or IFNγ, which were subsequently analysed by means of Western blotting. Stimulation with interferons had no impact on ezrin expression after 4 h, 8 h or 24 h of treatment, as shown by immunoblotting using an antibody directed against ezrin (Figure 15A and 15E). Quantitation from three experiments confirmed this finding (Figure 15B and 15F). Similar results were obtained using a pan-ERM antibody which detected both ezrin and moesin expression confirming that protein levels of ezrin were unchanged when related to the house-keeping enzyme GAPDH. In addition, no significant differences were seen for moesin expression (Figure 15C, 15D, 15G and 15H).

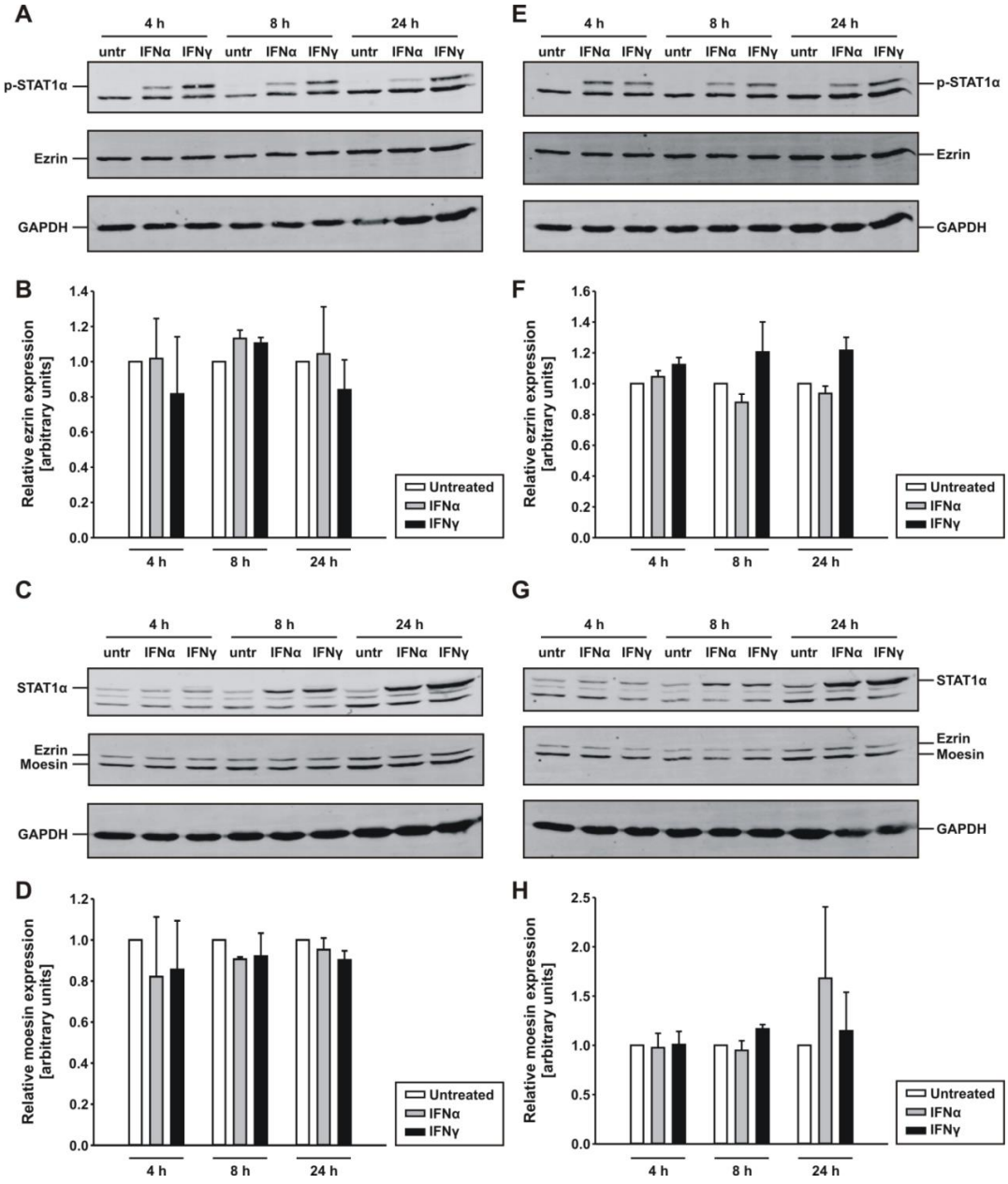

Figure 15: Expression of ezrin and moesin in Jurkat and HL-60 cells treated with IFNα or IFNγ. *(A) Expression of ezrin in relation to STAT1-phosphorylation levels after 4 h, 8 h and 24 h of IFNα or IFNγ treatment in HL-60 cells. (B) Densitometric quantitation of the ezrin signal in (A). (C) Expression of ERM proteins in relation to STAT1 expression after 4 h, 8 h and 24 h of IFNα and IFNγ treatment in HL-60 cells. Ezrin and moesin differ in their molecular weight (approximately by 5 kDa) and can, therefore, be distinguished, while radixin expression is absent in leukocytes. (D) Densitometric quantitation of the moesin signal in (C). (E) Expression of ezrin in relation to the STAT1-phosphorylation level after 4 h, 8 h and 24 h of IFNα or IFNγ treatment in Jurkat cells. (F) Densitometric quantitation of the ezrin signal in (E). (G) Expression of ERM proteins in relation to STAT1 expression after 4 h, 8 h and 24 h of IFNα and IFNγ treatment in Jurkat cells. (H) Densitometric quantitation of the moesin signal in (G). Shown are representative blots. Quantifications show the means of three independent experiments. Error bars represent standard error of the mean. All membranes were first exposed to an antibody against the respective ERM protein, and, subsequently, the same membrane was additionally developed for STAT immunoreactivity.*

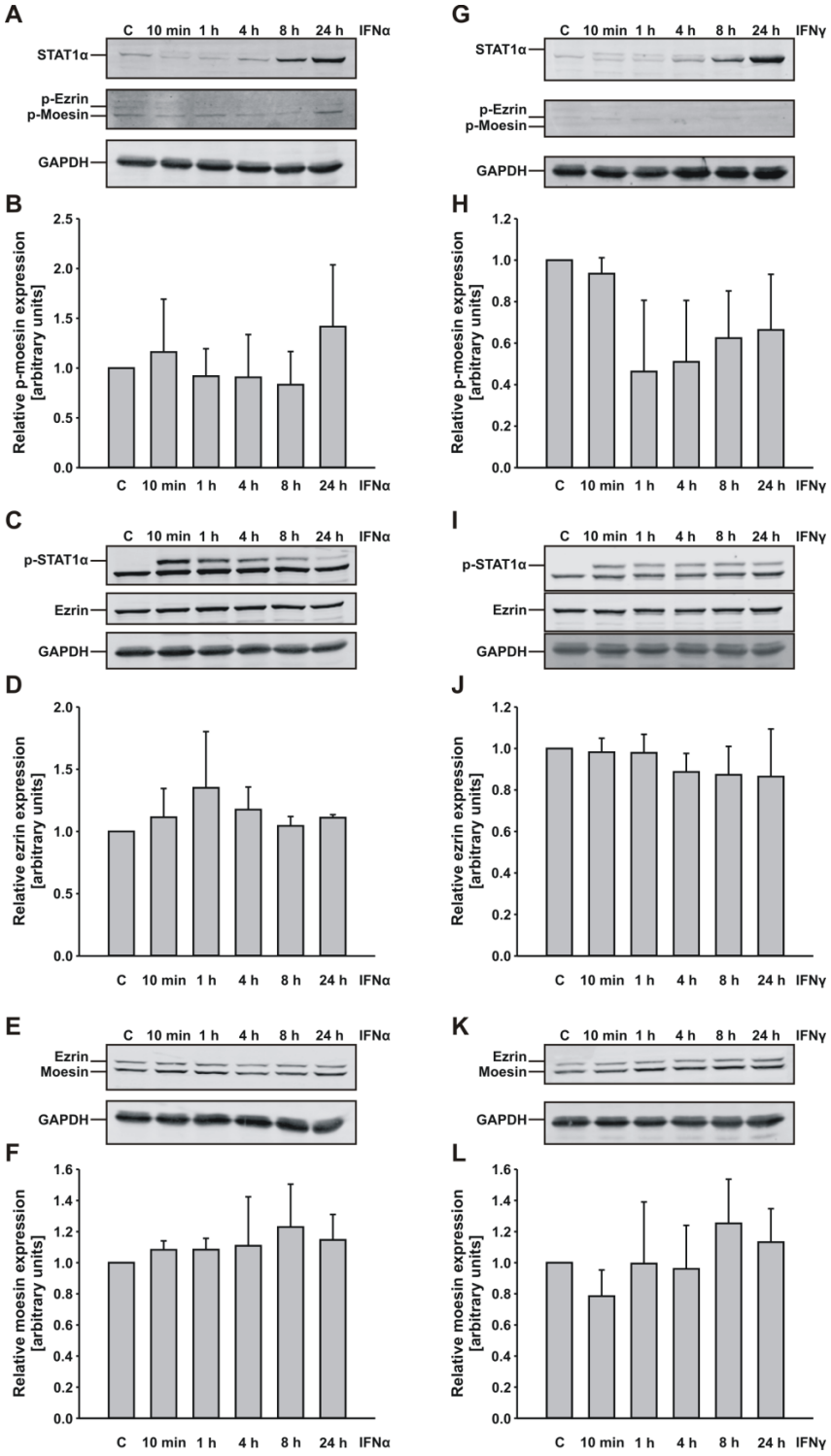

Figure 16: Expression and phosphorylation of ezrin and moesin in HL-60 cells treated with IFNα or IFNγ. *(A) Phosphorylation levels of ezrin and moesin in relation to STAT1 expression after 10 min, 1 h, 4 h, 8 h and 24 h of treatment with IFNα as compared with the untreated control. (B) Densitometric quantitation of the signal for phosphorylated moesin in (A). Due to low signal intensities, levels of phospho-ezrin were not quantified. (C) Expression of ezrin in relation to phosphorylated STAT1 after indicated times of treatment with IFNα. (D) Densitometric quantitation of the ezrin signal in (C). (E) Expression of ERM proteins after the indicated times of treatment with IFNα. (F) Densitometric quantitation of the moesin signal in (E). (G) Phosphorylation levels of ezrin and moesin in relation to STAT1 expression after 10 min, 1 h, 4 h, 8 h and 24 h of treatment with IFNγ*

as compared with the untreated control. (H) Densitometric quantitation of the signal for phosphorylated moesin in (G). (I) Expression of ezrin in relation to phosphorylated STAT1 in IFNγ-treated cells, as described above. (J) Densitometric quantitation of the ezrin signal in (I). (K) Expression of ERM proteins in cells treated with IFNγ. (L) Densitometric quantitation of the moesin signal in (K). Shown are representative blots. Quantitations show means of three independent experiments, and error bars represent standard error of the mean. The membranes in (A), (C), (G) and (I) were first exposed to an antibody against the respective ERM protein, and, subsequently, the same membrane was additionally developed for STAT immunoreactivity.

To test whether interferon signalling might have an effect on the phosphorylation levels of ezrin and/or moesin, an antibody targeted to all ERM proteins in their phosphorylated state was used. The respective Western blotting data (Figure 16A and 16G) including their densitometric analysis (Figure 16B and 16H) did not reveal significant differences in the phosphorylation level of moesin for any of the tested treatment durations ranging from 10 min to 24 h. Ezrin phosphorylation levels were barely detectable and, therefore, not quantified. The data obtained for ezrin and moesin (Figure 16C-F and 16I-L) confirmed the results demonstrated in Figure 15. In summary, the data showed that, despite being weakly activated on the transcriptional level in response to IFNγ signalling, ezrin production was not increased at the protein level in two widely used leukocyte-like cell lines.

3.2.6 *Ex vivo* analysis of STAT1-deficient and STAT1-F77A mutant mice does not show decreased ezrin protein expression

Since no ezrin induction on the protein level had been observed in IFNγ-treated cells, whether baseline ezrin expression was dependent on STAT1 signalling was tested. For this evaluation, bone marrows extracted from mice carrying a deletion of major parts of the STAT1 gene (referred to as STAT1-KO) and mice carrying a point mutation at position 77 which strongly impairs IFNγ signal transduction (referred to as STAT1-F77A) were compared to those of wildtype mice.

Figure 17A and 17C shows the baseline expression of ezrin and moesin in bone marrow of three individual animals of each genotype. The blot as well as the corresponding quantitation of ezrin and moesin expression (Figure 17B and 17D) showed no differences between the three genotypes.

To gain a deeper insight into the regulation of ezrin and moesin in murine bone marrow, the isolated cells were incubated with IFNα or IFNγ for 45 min and the whole cell proteins were isolated and analysed by means of Western blotting technique. Again, no significant differences between the three genotypes were detected for the expression of moesin (Figure

18A and 18B). Analysis of the phosphorylation levels of ezrin and moesin did not reveal a marked difference between the genotypes, neither did the treatment conditions (Figure 18C and 18D). Figure 18 E and F show the expression and quantitation of ezrin protein expression after stimulation again detecting no differences among the genotypes.

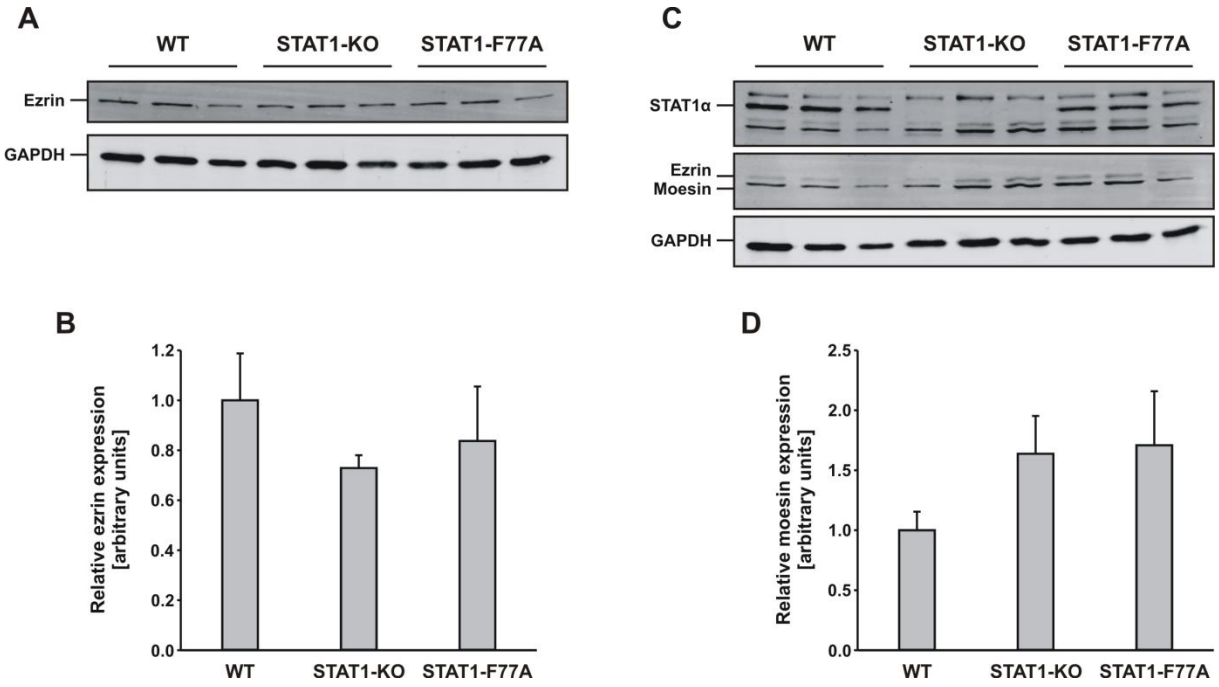

Figure 17: Ex vivo analysis of baseline expression of ezrin and moesin in bone marrow cells from wildtype, STAT1-deficient and STAT1-F77A mice. *(A) Expression of ezrin at baseline in protein extracts derived from bone marrow obtained from three individual mice of each genotype (B) Densitometric quantitation of the moesin signal in (A). (C) Expression of the ERM proteins in relation to STAT1 in protein extracts derived from murine bone marrow obtained from three individual animals of each genotype. (D) Densitometric quantitation of the moesin signal in (C). Error bars represent standard error of the mean. In (C), first, immunoreactivity for ERM protein was detected, and in a second step the same membrane was developed for STAT immunoreactivity.*

To test the hypothesis that in the absence of STAT1-dependent signalling, STAT3-dependent signalling becomes upregulated, STAT3 and p-STAT3 were detected in the bone marrow protein extracts of all three genotypes. Analysis of the phosphorylation level of STAT3 revealed an induction by IFNγ and to a limited extent also by IFNα. The induction, as well as, the baseline phosphorylation appeared to be slightly more pronounced in the F77A mutant but this effect remained below the level of significance (Figure 18G and 18H).

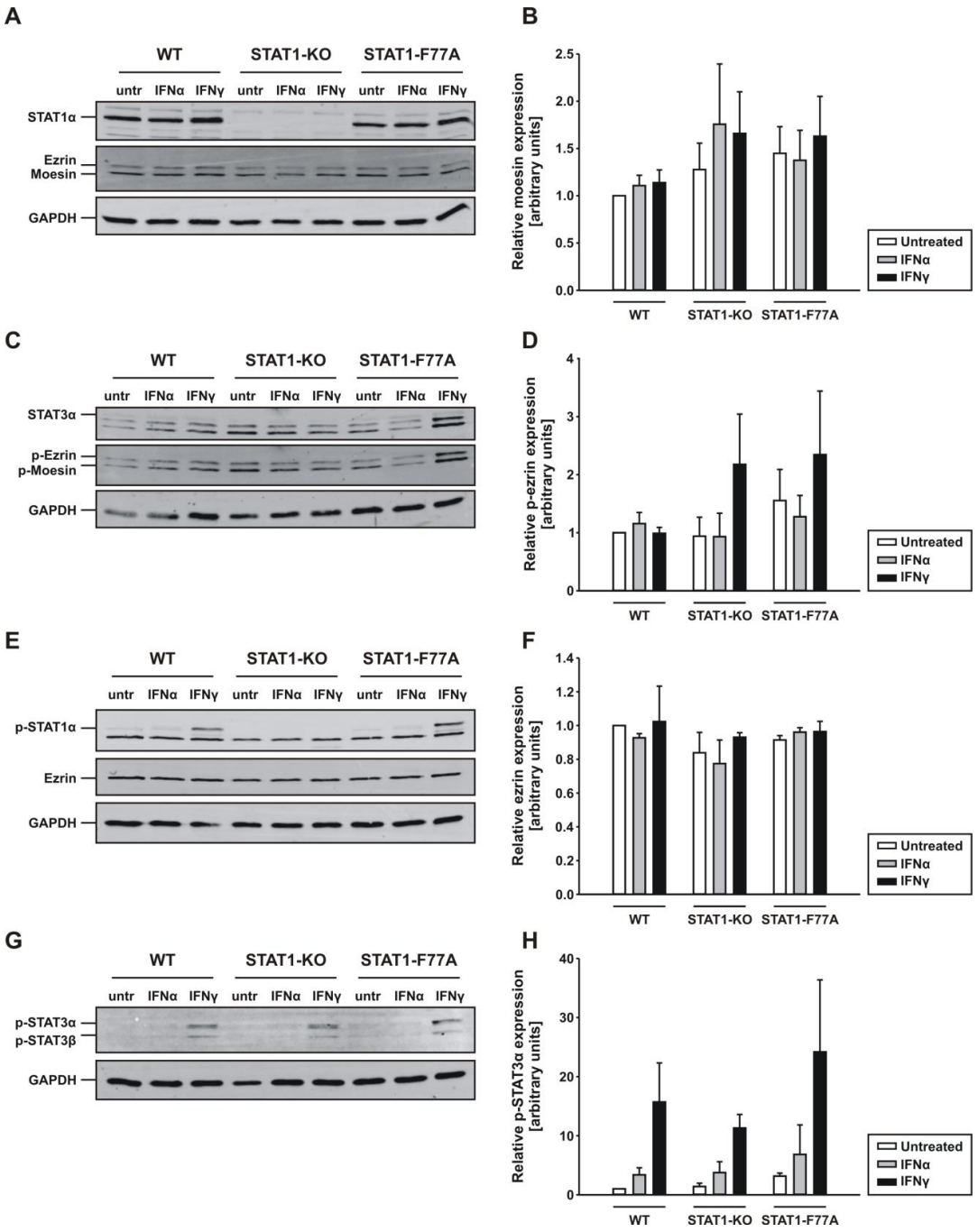

Figure 18: Phosphorylation levels of ezrin and moesin in bone marrow from wildtype, STAT1-deficient and STAT1-F77A knockin mice treated ex vivo with interferons. *(A) Expression of the ERM proteins in bone marrow cells treated for 0 min (untr) or 45 min with IFNα or IFNγ. (B) Densitometric quantitation of the moesin signal in (A). (C) Phosphorylation levels of ezrin and moesin bone marrow cells treated for 45 min with either IFNα or IFNγ. Signal for STAT3 was very weak. (D) Densitometric quantitation of the phospho-ezrin signal in (C). (E) Expression of ezrin in bone marrow cells treated for 45 min with IFNα or IFNγ. (F) Densitometric quantitation of the ezrin signal in (E). (G) Phosphorylation levels of STAT3 in bone marrow cells treated for 45 min with IFNα or IFNγ. (H) Densitometric quantitation of phospho-STAT3. Shown are representative blots. Quantitation shows means of three independent experiments. Error bars represent standard error of the mean. First, immunoreactivity for ERM protein was detected in (A), (C) and (E) and in a second step the same membrane was developed for STAT immunoreactivity.*

The data obtained from the two mouse models of impaired IFNγ/STAT1 signalling were in line with the results from Jurkat cells and HL-60 cells which did not show a significant change in ezrin expression upon cytokine stimulation. A mild but consistent and robust induction of *EZR* gene transcription by IFNγ signalling in both cell lines tested was shown. However, an increased production of ezrin at the protein level was neither detected in human cell lines nor in murine bone marrow cells.

3.3 Assessment of the role of IFNγ-dependent STAT1 signalling in myocardial infarction

Upon myocardial infarction, functional cardiac tissue is not only lost due to ischemia-related tissue necrosis but also by an accompanying inflammatory reaction (Bonaventura et al., 2016). Inhibiting the recruitment of inflammatory cells to the myocardium is hypothesized to be a promising approach to favour repair and reduce injury. With respect to the role of STAT1 in the context of cardiac ischemia, it was shown that STAT1 signalling favours apoptosis over autophagy, as demonstrated in an ischemia/reperfusion model using the Langendorff heart (McCormick et al., 2012). Since this model ignores the role of the immune reaction, the focus of this project was set on an *in vivo* model of myocardial infarction where cardiac function as well as the immune response can be monitored.

3.3.1 General characteristics of the study cohort and infarct survival

Mice carrying the STAT1-F77A mutation on a C57Bl/6N background as well as wildtype control mice were performed surgery on to induce myocardial infarction by ligating the left anterior descending artery. Table 25 summarizes the general characteristics of the study cohort. Mice were divided into a group that was sacrificed three days after surgery to analyse the hearts during the acute phase of inflammation and a second cohort that was kept for 4 weeks after surgery to acquire data on survival and cardiac remodelling. Echocardiography was performed before and 3 days, 1 week and 4 weeks after surgery to monitor cardiac function and remodelling. Additionally, samples were taken on day 3 for histological and biochemistry analyses to evaluate cardiac inflammation during the acute phase of myocardial infarction. Heterozygous mice were only included for the early analysis.

Table 25: Survival rates of mice after undergoing myocardial infarction surgery at day 3 post-myocardial infarction

	MI/Sham			**MI Survival/Death**		
	Total	♀	♂	**Total**	♀	♂
Total	125/23	59/11	66/12	117/8	56/3	61/5
WT	50/8	23/4	27/4	47/3	22/1	25/2
WT/F77A	28/7	14/3	14/4	25/3	13/1	12/2
F77A/F77A	47/8	22/4	25/4	45/2	21/1	24/1

All animals which survived the MI-surgery were observed for at least three days before being sacrificed in order to collect cardiac tissue for further analysis. Within the first 48 h after myocardial infarction, the mice lost a mean 9 % of their body weight but started to gain weight again and were only 5.2 % below their pre-surgery body weight on day 3. This observation was similar in wildtype, heterozygous and STAT1-F77A knockin mice and did not differ significantly between males and females. The overall survival rate of the surgery during the first three days was 88 % without significant differences among the genotypes. Females displayed a slightly higher survival rate (92.5 %) than males (84.8 %) which was in line with studies using different models of myocardial infarction, heart failure and atherosclerosis which describe beneficial effects of oestrogen (Piro et al. 2010).

In the cohort for the 4 week follow-up, only homozygous animals were included. The higher mortality of males as compared to females was confirmed. Data on the weight loss after surgery confirmed the observation that after an initial weight loss of about 10 % of the original body weight within the first day after surgery, mice started gaining weight again until reaching a weight gain of roughly 7 % of the pre-surgery weight at 4 weeks post-infarction. No significant differences between the genotypes were observed with respect to changes in body weight.

During the chronic follow-up, a high number of animals (in total 40 % of the study cohort) died or had to be euthanized. The mortality was non-significantly higher in the wildtype as compared with the STAT1-F77A knockin cohort (47.8 % 4-week-survival in the wildtype group as compared to 72.7 % 4-week-survival in the knockin group). The analysis of these data for males and females separately, showed that the effect disappeared for female animals while becoming significant in males for the 1-week as well as the 4-week time point. Figure

19 presents the Kaplan-Meier survival curves of the animals included in the study cohort up to 4-weeks after myocardial infarction. The data showed that while survival rates in females are in general high, a large proportion of male mice died between the 4th and 7th day after myocardial infarction. This drop in survival was significantly more pronounced in wildtype animals than in the STAT1-F77A knockin mice. Therefore, loss of the IFNγ-STAT1 axis was considered to be beneficial in male mice undergoing myocardial-infarction surgery.

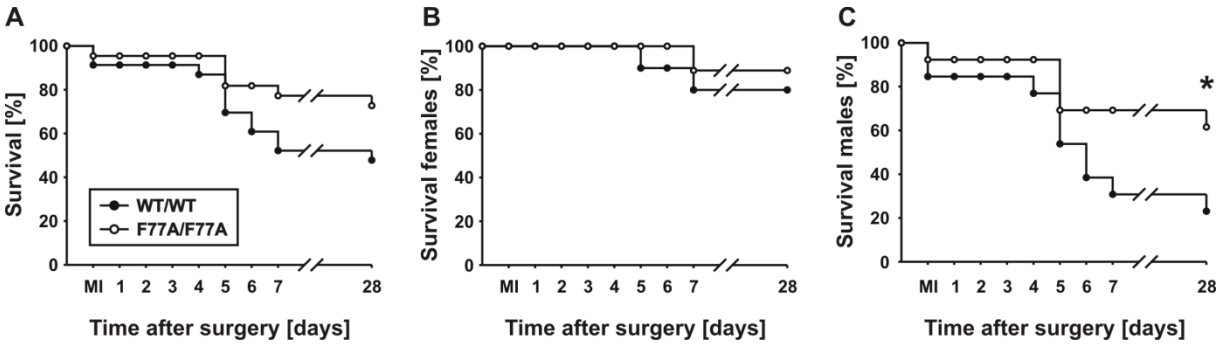

Figure 19: Kaplan-Meier survival analysis of mice subjected to experimental myocardial infarction. *Shown are the survival rates for all animals in the study group included in the 4-week analysis. Animals of both sexes (A) as well as exclusively female (B) and male (C) mice were evaluated. Asterisk indicates statistically a significant difference.*

3.3.2 H&E staining did not reveal differences in the size of the infarcted area

In order to assess the extent of inflammation of the ventricular wall during myocardial infarction, mice were sacrificed 3 days after MI surgery, and their explanted hearts were immediately fixed and embedded in paraffin. To allow for an estimation of the position of the sections used for staining, sections of 5 µm thickness were produced in a serial manner. Sections taken roughly 1.2 mm, 1.6 mm, 2.0 mm and 2.4 mm from the apex of the heart, corresponding to the entire region of the infarcted area, were subjected to H&E staining. Figure 20 shows representative sections of MI and sham-operated hearts of each genotype at ~1.6 mm from the cardiac apex. All samples except the sham-operated hearts showed pronounced accumulation of invading leukocytes after myocardial infarction, as can be concluded from the presence of numerous cells with a small cytoplasmic rim and haemalum-stained nuclei.

In order to quantify the extent of the inflamed area of the cardiac muscle, the angle for distribution of inflammatory foci over the entire circumference of the left ventricle was assessed (Figure 21A). Results showed that the size of the infarcted area did not differ

between wildtype, STAT1-F77A knockin and heterozygous mice, as judged from the measurement of the circumference affected by infiltrates.

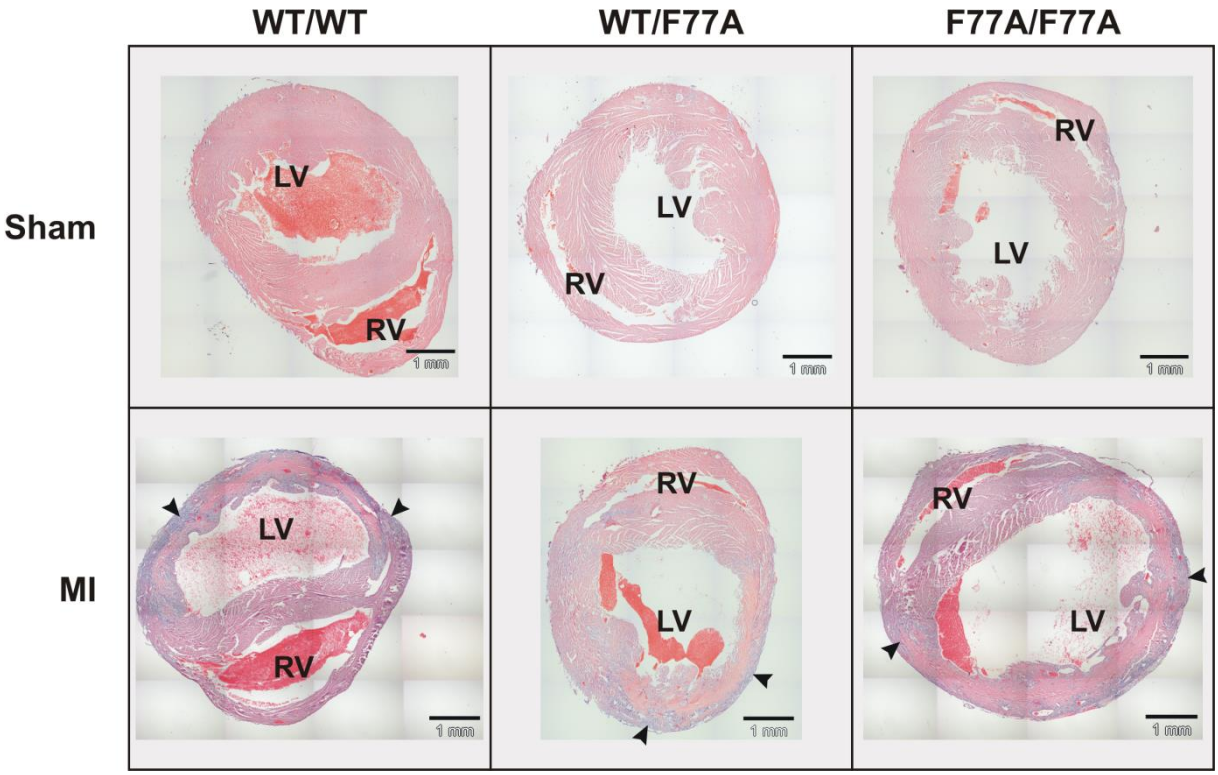

Figure 20: H&E staining of acute myocardial infarction. *Shown are representative slides of hearts 3 days after MI or sham operation of each genotype. Strong infiltration of the left ventricular myocardium is visible in all three genotypes after infarction but not in the hearts of sham-operated animals. Arrowheads mark representative areas of infiltration. LV: left ventricle, RV: right ventricle. Images are montages of 15 to 20 individual images.*

To take into account the severity of the inflammation and not only the distribution, a score between 0 (no inflammation) and 4 (very severe inflammation) was assigned to the H&E-stained MI samples at each of the aforementioned positions (Figure 21B). Again, there was no significant difference in the score assigned to the infarcted sections between the different genotypes. Figure 21C shows the results of the consecutive ranking of the extent of inflammation. There appeared to be a mild tendency of the STAT1-F77A samples towards a score at a slightly higher rank than the wildtype counterparts but the effect was below the level of significance and is not supported by the data of the heterozygous animals which received the lowest mean rank. These data showed that wildtype and STAT1-F77A knockin mice did not differ with respect to the severity and distribution of inflammatory foci in their hearts in the acute phase of inflammation, 3 days after myocardial infarction.

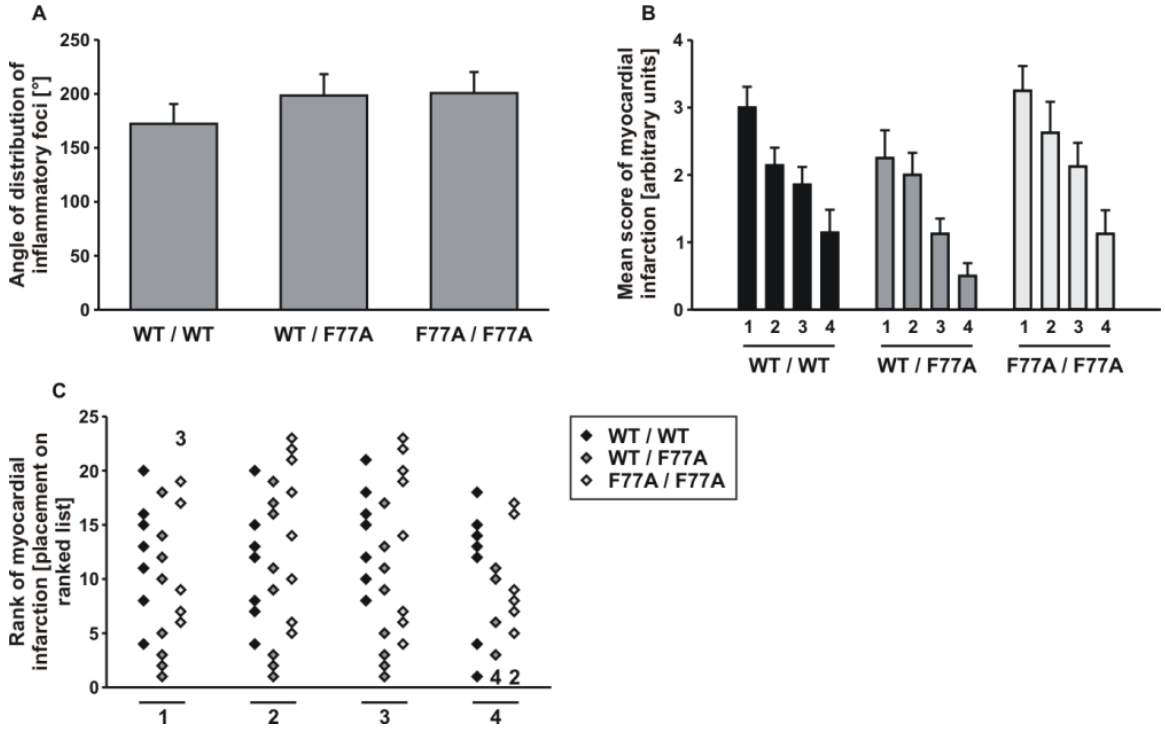

Figure 21: Evaluation of the extent of inflammation according to H&E staining of sections of paraffin-embedded cardiac tissue three days after myocardial infarction. *(A) The distribution of inflammatory infiltrates was assessed by determining the angle from the centre of the left ventricle in which areas of pronounced accumulation of small cells (assumed to be leukocytes) were located. The angle was determined for sections in the middle of the infarcted area. The mean was calculated for each genotype. Error bars represent standard error of the mean. (B) An arbitrary score was assigned to each infarcted heart in serial section near the apex (1, ~1.2 mm from apex), in the middle of the infarcted area (2, ~1.6 mm from the apex), in the upper part of the infarcted area (3, ~2 mm from the apex) and at the top part of the infarcted area (4, ~2.4 mm from the apex). The score "0" was assigned to sections without inflamed areas, "1" for small, restricted areas of inflammation of less than half the left ventricular wall, "2" for distribution of inflammatory foci over up to 90 % of the left ventricular wall, "3" for entire left ventricle with little or no involvement of septum and right ventricle and "4" for involvement of septum and right ventricle. Error bars represent standard error of the mean. (C) Scatter blot of the consecutive ranks assigned to each MI heart. Largest infarction was ranked highest. Each point corresponds to one heart at the respective position. Numbers indicate that several samples were assigned the same rank. For wildtype, 7 cases were analysed, and for heterozygous and knockin 8 animals were included.*

3.3.3 Mice carrying the STAT1-F77A mutant are protected from adverse cardiac remodelling

In the acute phase after myocardial infarction, immune cells are recruited to ischemic areas of the heart during a first inflammatory phase (reviewed in Bonaventura et al., 2016). This inflammatory reaction begins within the first hours after the insult and is resolved after a few days. It has been noted that the inflammatory environment extends beyond the ischemic tissue and may cause additional damage in the border zone. Shortly after the invasion of the tissue

by inflammatory cells, anti-inflammatory signalling starts to facilitate clearing of the inflammation. Following survival of myocardial infarction, patients often suffer from heart failure due to post-infarction left ventricular remodelling (reviewed in Galli and Lombardi, 2016). During this process, fibrotic scar formation of the previously hypoxic tissue is accompanied by an alteration in matrix composition as well as the absence of contracting cardiomyocytes in this area. As a consequence, the left ventricle is often dilated resulting in a permanently reduced ejection fraction.

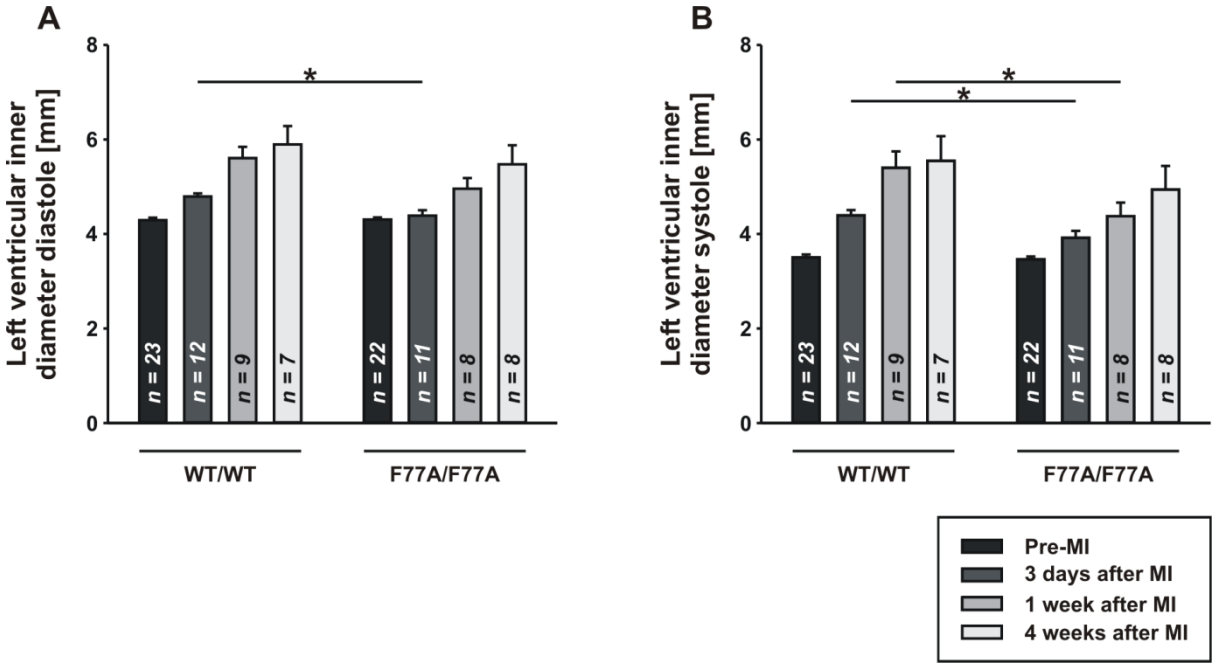

Figure 22: Increase in left ventricular diameter after myocardial infarction. *The diameter of the left ventricular lumen was measured in diastole (A) and systole (B) in wildtype and STAT1-F77A-expressing mice using echocardiographic images obtained in B mode. For all mice analysed, pre-infarction data were acquired. Mice were analysed either during the acute phase (analysis on day 3 after infarction) or kept for monitoring cardiac remodelling (analysis 1 week and 4 weeks after infarction). Shown are only the data acquired from female mice. The numbers of mice included in this experiment is indicated inside the columns. Asterisks indicate statistically significant differences. Error bars represent standard error of the mean.*

In order to evaluate the adaption of the cardiac tissue in the absence of IFNγ signalling, echocardiography was performed on mice, three days, one week and four weeks after ligation of the left anterior descending coronary artery and compared with the measurement obtained before surgery (mice of the day-3 cohort were analysed before and 3 days after surgery, mice of the 4-week cohort were analysed before and 1 week after and 4 weeks after surgery). Based on anatomical measurements of left ventricular dimensions, functional data were computed.

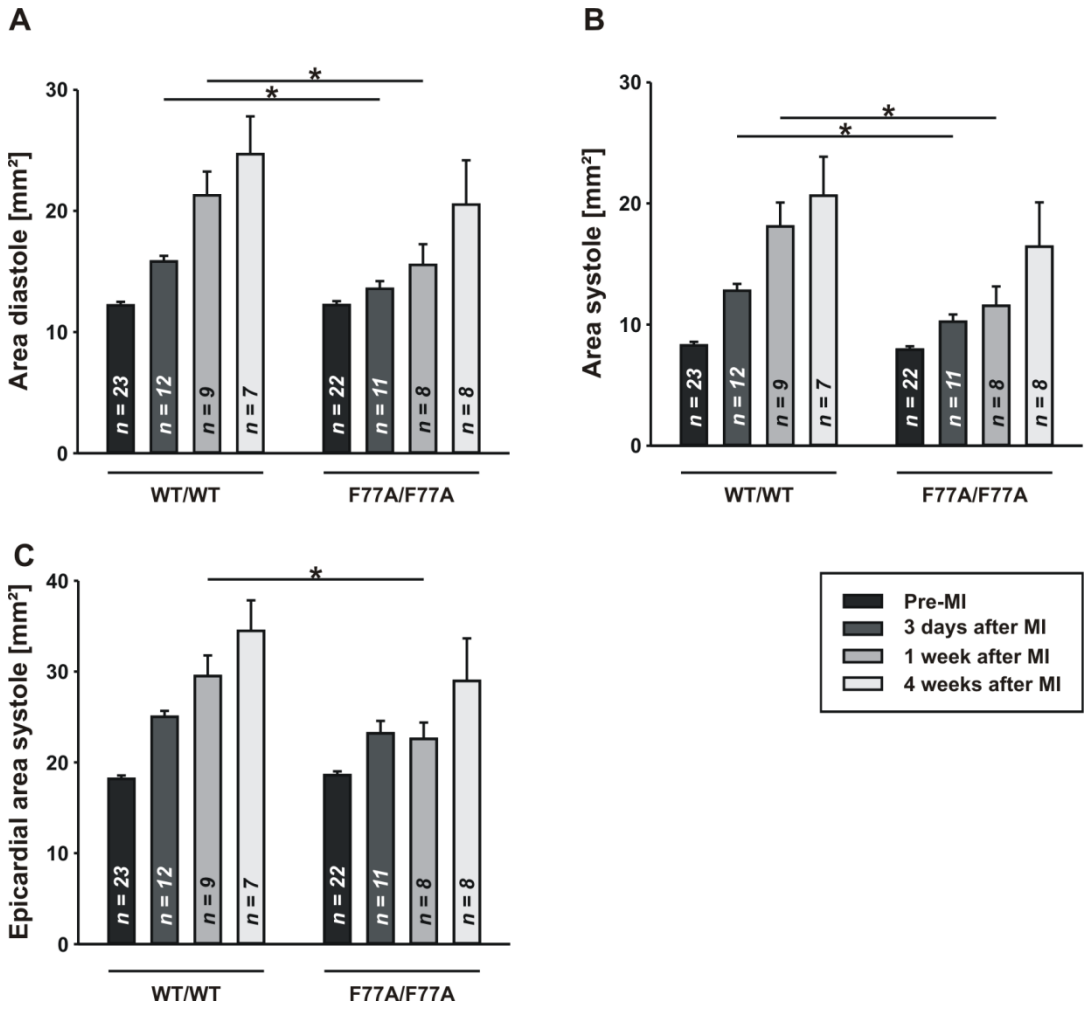

Figure 23: Increased left ventricular cross-sectional area due to myocardial infarction. *The cross-sectional area of the left ventricular lumen and the epicardial area were measured using echocardiographic images obtained in B mode. (A) Left ventricular cross-sectional area of the lumen in diastole. (B) Measurements obtained in systole. (C) End-systolic epicardial cross-sectional area. For all mice analysed, pre-infarction data were acquired. Mice were analysed either during the acute phase (analysis on day 3 after infarction) or kept for monitoring cardiac remodelling (analysis 1 week and 4 weeks after infarction). Shown are only the data acquired from female animals. The numbers of mice included are indicated inside the columns. Asterisks indicate statistically significant differences. Error bars represent standard error of the mean.*

Analysis of the entire cohort showed no differences in cardiac remodelling, shape or performance between the wildtype and the STAT1-F77A knockin mouse. Variance of all measurements was high. Separation of the data obtained from male and female mice and separate analysis of these produced a drop in variance. In females carrying the STAT1-F77A knockin allele, the increase in both diastolic and systolic left ventricular diameter was attenuated during short-term follow-up (Figure 22). Similar differences between female wildtype and knockin littermates were detected for the area of luminal and epicardial cross-

sections 3 days and 1 week following ligation of the coronary artery (Figure 23). In male mice, no difference was found among the genotypes (data not shown).

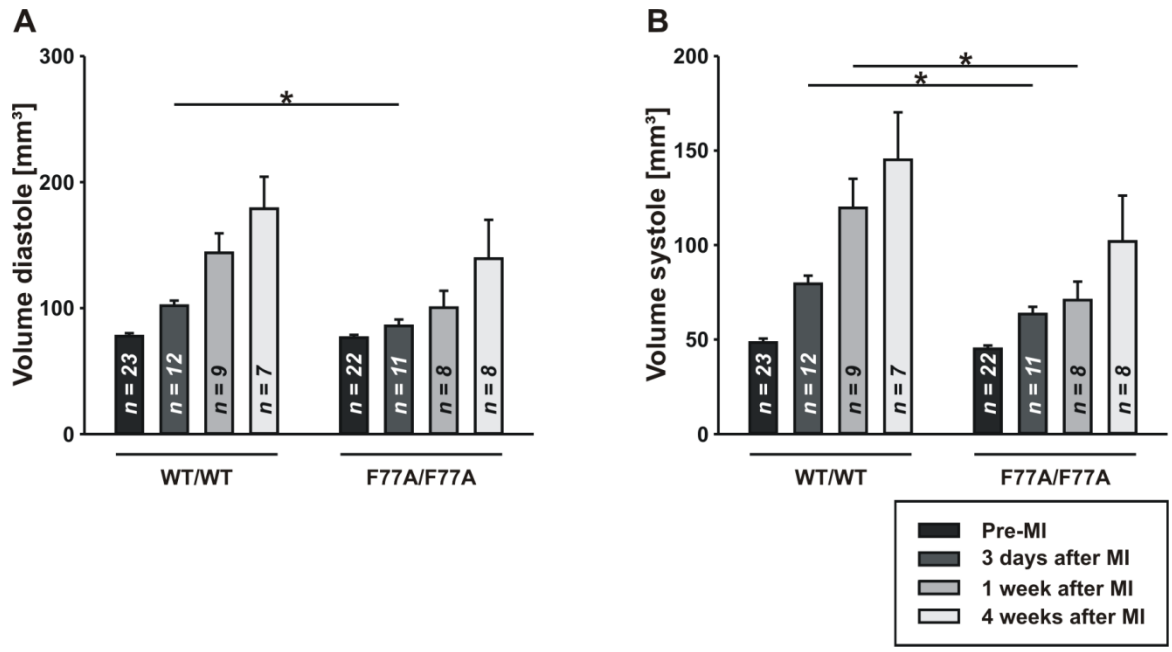

Figure 24: Increase in end-diastolic and end-systolic volume after myocardial infarction. *The end-systolic volume (A) and end-diastolic volume (B) were calculated from the echocardiographic data obtained in B mode. For all mice analysed, pre-infarction data were acquired. Mice were analysed either during the acute phase on day 3 after infarction or kept for monitoring cardiac remodelling at 1 week and 4 weeks following myocardial infarction. Shown are only the data acquired from female mice. Numbers of mice included are indicated inside the columns. Asterisks indicate statistically significant differences. Error bars represent standard error of the mean.*

Based on the anatomical measurements of left ventricular dimensions, end-diastolic and end-systolic volumes were computed (Figure 24). Following myocardial infarction, the left ventricle started to dilate massively, almost tripling its original volume by week 4 in the wildtype animals. In line with the above-mentioned data, enlargement of the left ventricle was reduced in the F77A knockin mice during the early phase on day 3 and week 1 and continued as a – however non-significant – trend up to week 4. Therefore, lack in IFNγ-responsiveness significantly ameliorated cardiac remodelling in females.

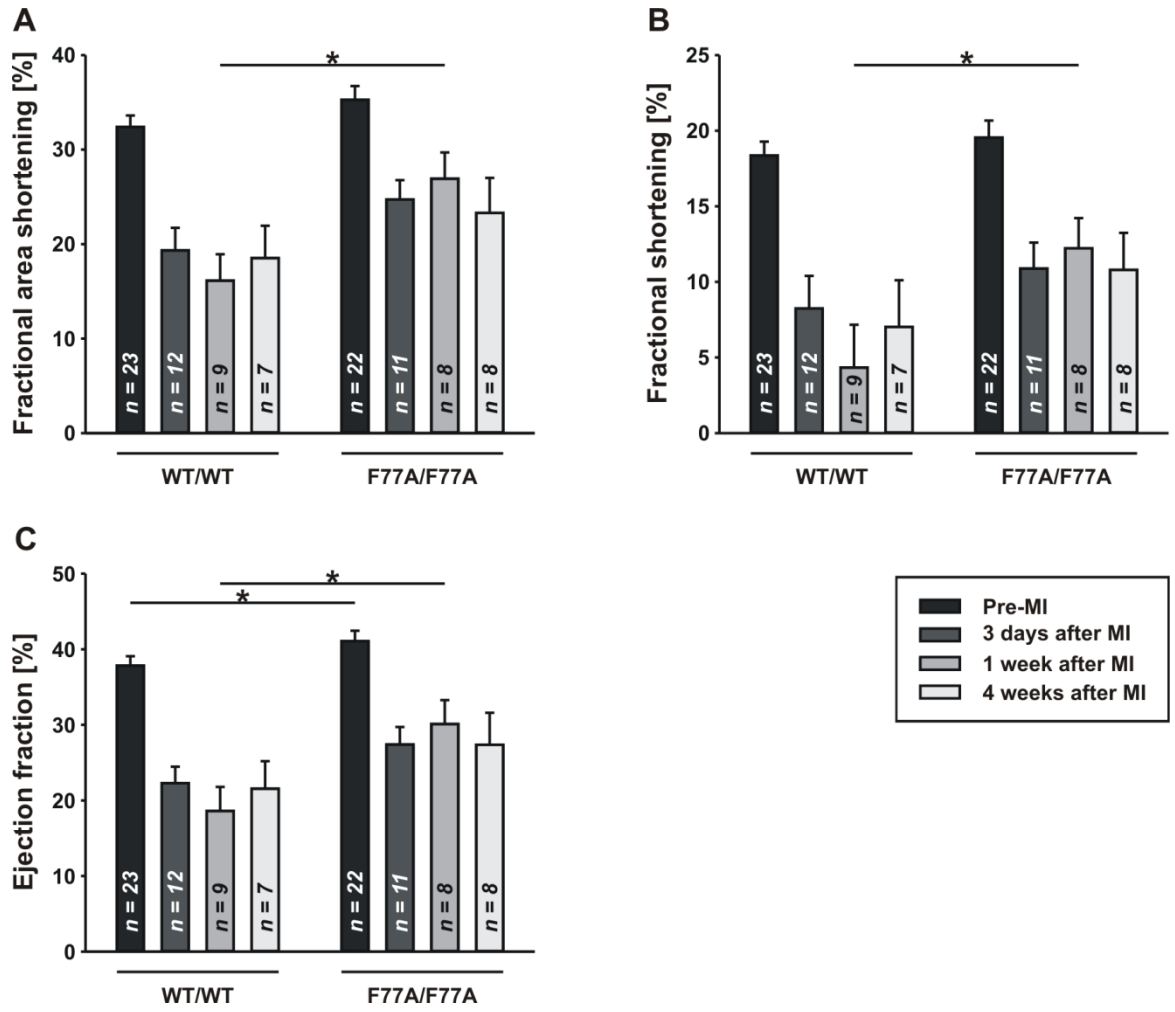

Figure 25: The reduced cardiac function after myocardial infarction is blunted in mice with impaired STAT1 tetramer stabilization. *Fractional area shortening (A), fractional shortening (B) and ejection fraction (C) were computed from the echocardiographic data obtained in B mode. For all mice analysed, pre-infarction data were acquired. Mice were analysed either during the acute phase on day 3 after infarction or kept for monitoring cardiac remodelling on week 1 and week 4 after coronary ligation. Shown are only the data acquired from female mice. The numbers of mice included are indicated inside the columns. Asterisks indicate statistically significant differences. Error bars represent standard error of the mean.*

In order to test the significance of these findings, fractional area shortening, fractional shortening and the ejection fraction were calculated (Figure 25). In response to the insult, cardiac function was markedly reduced as indicated by a pronounced and immediate drop in all three measurements. In STAT1-F77A female mice, cardiac function was ameliorated in comparison with the wildtype, 1 week after MI surgery. This trend was seen on a non-significant level on day 3 and week 4 after experimental infarction. Again, no significant differences were observed from the analysis of male mice. The lack of significant differences among the male cohorts might be attributed to the poor overall survival rates, as described above. Since only a few of the male mice survived, variance was high especially in the

wildtype group, suggesting that animals with the highest impact of the infarction were not included in our analysis. Overall, the data revealed that the IFNγ-irresponsive STAT1-F77A mutant mouse line displayed ameliorated cardiac dilation and blunted remodelling resulting in better cardiac performance. This finding suggested that the absence of a functional IFNγ/STAT1-dependent signal response was not only protective due to its direct non-transcriptional effect on apoptosis and autophagy (McCormick et al. 2012) but also due to other transcriptionally related mechanisms.

3.3.4 STAT1 expression is reduced in hearts of STAT1-F77A knockin mice compared with the wildtype on day 3 following myocardial infarction

Given the beneficial effects of the STAT1-F77A mutation in cardiac function during the acute phase of myocardial infarction, STAT1 regulation was then investigated at the molecular level. To this end, protein was extracted from the infarcted area of hearts that had been obtained and snap frozen 3 days after myocardial infarction. These lysates were compared with protein extracts isolated from unaffected areas of the basal parts of the ventricles and atria, as demonstrated by means of Western blotting. Figure 26A and 26B shows representative Western blots of protein samples from infarcted hearts of mice homo- and heterozygous for the STAT1-F77A mutation as compared with the wildtype. The phosphorylation levels of STAT1 and STAT3 as well as pan-STAT3 did not differ significantly between the three genotypes (Figure 26C, 26D and 26F). However, a significantly lower expression of STAT1 in the infarcted areas of the hearts of the STAT1-F77A knockin mice was detected. This observation is in line with the overall reduced expression of STAT1 in the non-infarcted areas (Figure 26E). The expression of STAT3 is favoured in the myocardium of STAT1-F77A mice, as demonstrated by the increased ratio of total STAT3 to STAT1 which is not reflected on the phosphorylation level (Figure 26G and 26H).

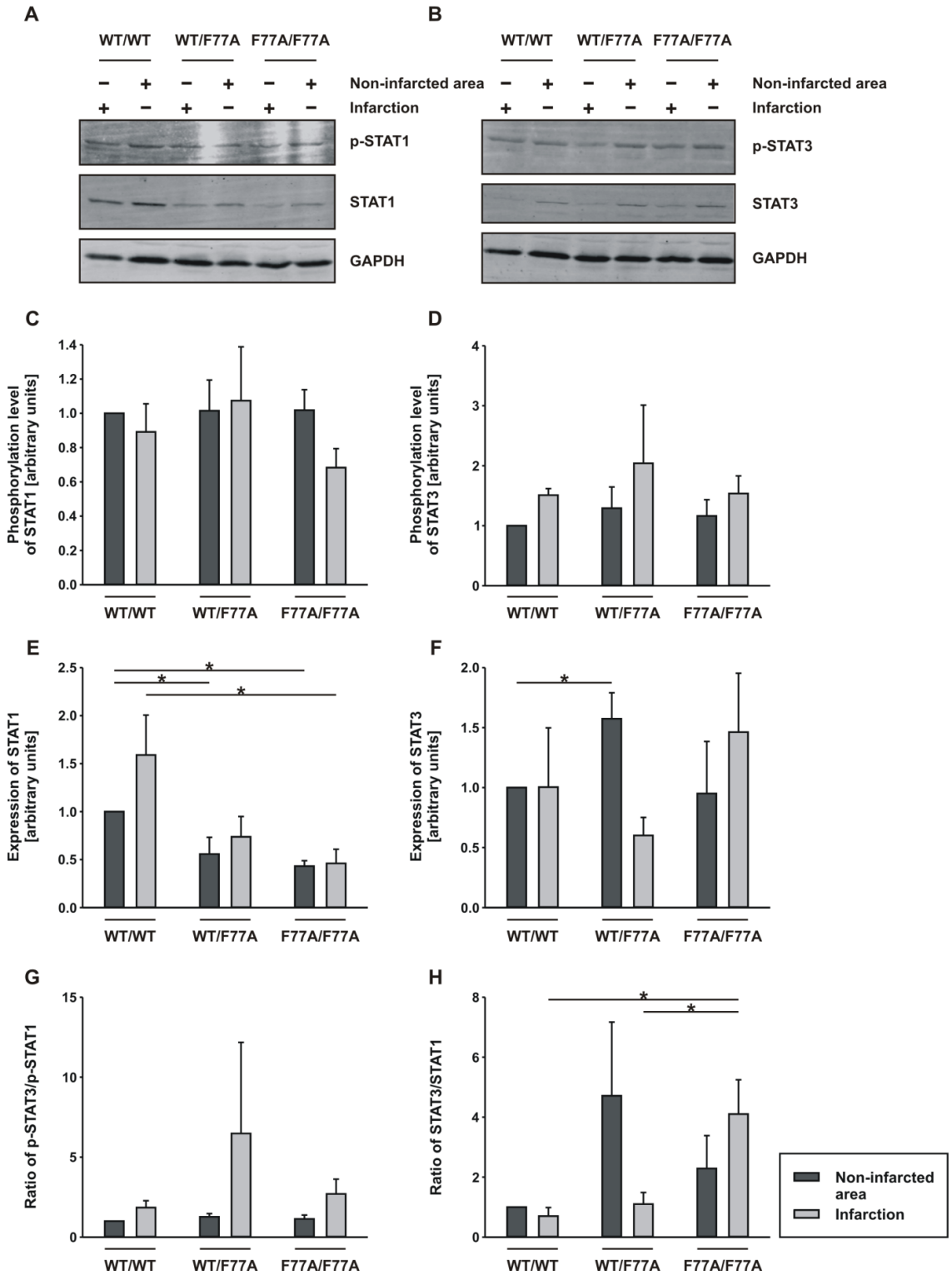

Figure 26: Expression and phosphorylation of STAT1 and STAT3 in heart tissue from STAT1-F77A knockin mice on day 3 after myocardial infarction. *(A) Representative Western blots of phosphorylated (p)-STAT1, STAT1 and GAPDH. (B) Representative western blots of p-STAT3, STAT3 and GAPDH. Densitometry analysis of phosphorylated STAT1 (C), phosphorylated STAT3 (D), and pan-STAT1 all normalized to GAPDH expression (E), as well as pan-STAT3 (F), phospho-STAT3 to phospho-STAT1 (G), and pan-STAT3 to pan-STAT1 (H). Data show means of four independent experiments. Only the α-form of STAT1 and STAT3 were evaluated. Asterisks indicate statistically significant differences. Error bars represent standard error of the mean.*

3.3.5 Immune histochemistry shows an accumulation of cells expressing tyrosine-phosphorylated STAT1 in the inflammatory infiltrate

After assessment of the expression and activation of STAT1 and STAT3 using Western blotting, immunohistochemical staining was performed. Slides (5 µm) of paraffin-embedded hearts obtained 3 days after myocardial infarction from wildtype C57BL/6N mice as well as mice heterozygous and homozygous for the STAT1-F77A allele were stained for tyrosine-phosphorylated STAT1. Figure 27A shows representative images taken from hearts of myocardial infarction- and sham-operated animals from each genotype three days after surgery. Following sham operation, no phospho-STAT1-positive cells were observed in the cardiac muscle. However, following myocardial infarction, cells scattered throughout the infarcted area stained positively for tyrosine-phosphorylated STAT1. There was a tendency for phospho-STAT1-positive cells to be distributed at a low density over the infarcted area and to form clusters with a higher density distributed randomly within the infarcted area. Outside the inflammatory infiltrate, only few cells that were stained for phospho-STAT1, indicating that there is an association of STAT1 activation with the acutely infarcted area.

The accumulation of cells which stained positively for p-STAT1 was quantified using a score, considering two factors: their distribution over the ventricular wall and septum and, in addition, the density of phospho-STAT1-positive cells within this area. A score of “4” indicates the widest distribution and highest density, while “0” represents the absence of positive immunoreactivity. Figure 27B and 28C show the results of these quantifications. Among the different genotypes, there was a marked difference in the distribution of the phospho-STAT1-positive cells, showing that, in the STAT1-F77A knockin mice, STAT1 phosphorylation was less restricted to confined areas. With respect to the density of p-STAT1-positive cells, there were no significant differences between the genotypes. This indicates that more cells staining positively for p-STAT1 were present in the infarcted area of cardiac sections obtained from STAT1-F77A knockin mice. These cells were distributed over a larger area of the myocardium but did not show stronger accumulation to confined regions when compared with the wildtype.

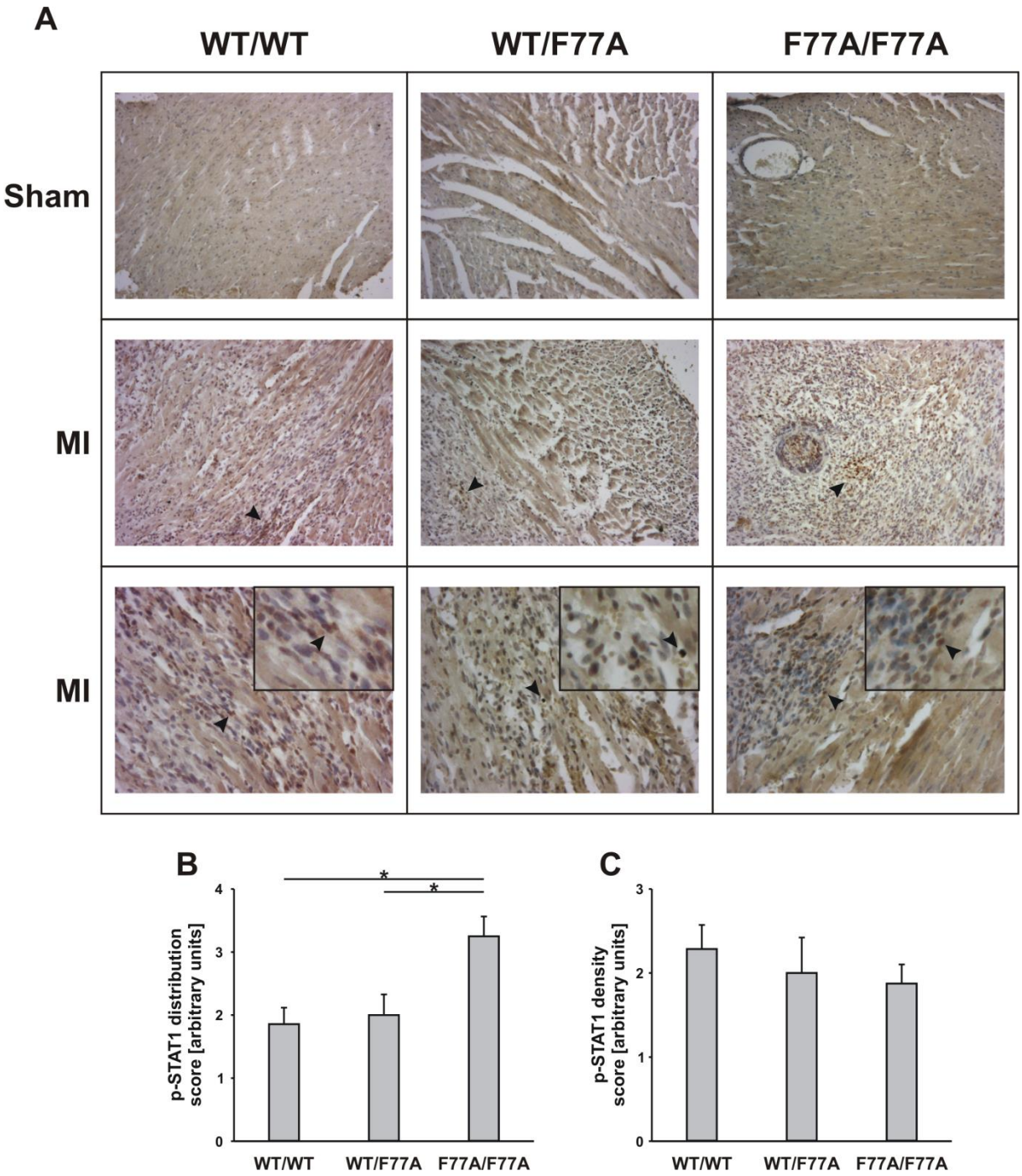

Figure 27: Staining of tyrosine-phosphorylated STAT1 in heart sections on day 3 after myocardial infarction or sham operation. *(A) Representative microscopic fields of view of the left ventricular wall of sham-operated animals (top) or the infarcted area of MI-operated animals (middle and bottom) of all three genotypes are shown. In the infarcted areas, p-STAT1-positive cells are accumulated in clusters (arrowheads) with moderate accumulation outside these areas. The bottom row shows a higher magnification of p-STAT1 areas with staining of p-STAT1-expressing cells. (B) Arbitrary quantification of the distribution of clusters of p-STAT1-positive cells over the ventricular wall and septum. (C) Arbitrary quantification of the density of p-STAT1-positive cells within the infarcted area. Asterisks indicate statistically significant differences. Error bars represent standard error of the mean.*

3.3.6 No evidence of altered recruitment of neutrophils, monocytes or T cells to areas of myocardial infarction was observed in STAT1-F77A mutant mice

A hallmark of ischemic injury of the cardiac muscle is an inflammatory reaction based on the recruitment of different immune cells. The main effectors in this context are neutrophil granulocytes, monocytes/macrophages, and T cells (Bonaventura et al. 2016). Whether the recruitment of one or all of these subsets was impaired in the absence of IFNγ signaling was considered. FACS analysis of the lymphatic organs was performed to quantify baseline populations of inflammatory cell types in wildtype and STAT1-F77A knockin mice. For this purpose, the populations of B cells, T cells, neutrophils and monocytes were analysed in blood, spleen, lymph nodes and thymus in 9-week-old females. The analysis revealed a mild increase in regulatory T cells in spleen and lymph nodes (Figure 28). None of the other cell types showed significant differences with respect to their population size.

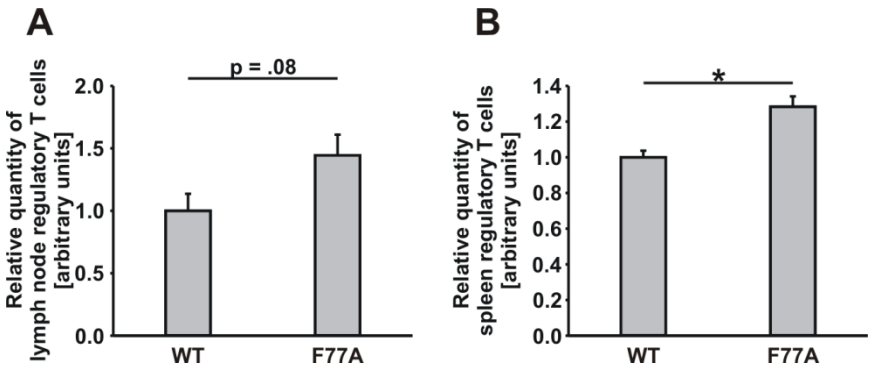

Figure 28: Analysis of the relative numbers of regulatory T cells in lymph node and spleen of the STAT1-F77A mouse line. *A: Analysis of regulatory T cell populations in lymph nodes (A) and spleen (B) of STAT1-F77A knockin mice as compared to wildtype controls. Asterisks indicate statistically significant differences. Error bars represent standard error of the mean.*

Figure 29 shows the typical expression patterns of two chemotactic cytokines in reconstituted U3A cells lacking endogenous STAT1 expression. The two STAT1-target genes *CCL2* and *CXCL10* display structurally different GAS elements in their promoter in which with the gene encoding *CCL2* has a one-and-a-half GAS motif, while *CXCL10* has one single GAS element. Both genes were induced less efficiently in the mutant despite almost normal expression levels at baseline. While *CCL2* showed a reduced induction approximately by a factor of 10, *CXCL10* induction had almost completely disappeared.

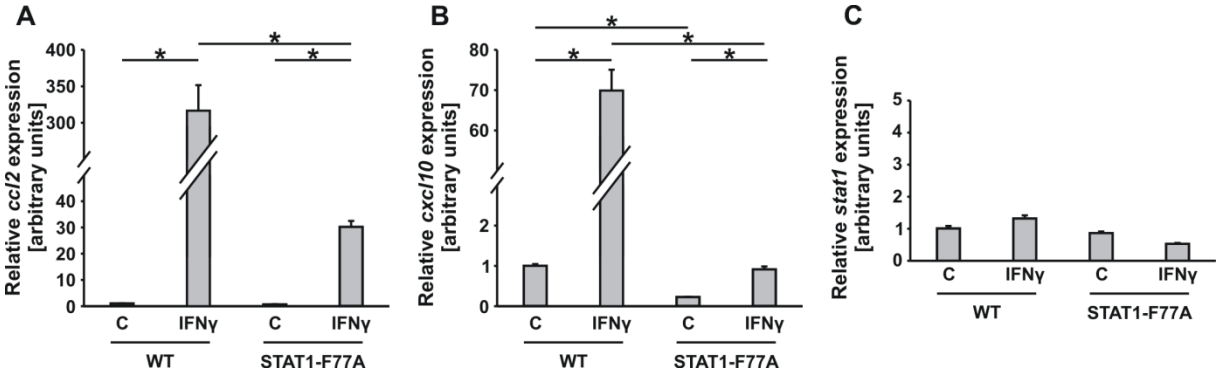

Figure 29: Reduced activation of two known IFNγ-target genes by STAT1-F77A in reconstituted U3A cells. *Shown are representative qPCRs of cDNA samples obtained from wildtype or STAT1-F77A expressing U3A cells. Untreated cells are compared with 6 h of IFNγ treatment for the induction of the ccl2 (A), cxcl10 (B) and, as control stat1 (C) transcript. Asterisks indicate statistically significant differences. Error bars represent standard error of the mean.*

Immunohistochemical staining using a horseradish-peroxidase-based method was utilised to identify different subsets of inflammatory cells during the acute phase of myocardial infarction. Staining for myeloperoxidase (MPO) was used as a marker for infiltrating neutrophils. The results identified neutrophils as the most prevalent cell type in the inflammatory infiltrates (Figure 30A). Quantification of the extent of myocardial infiltration by neutrophils revealed no significant differences in the overall area of infiltrates between the genotypes but a reduction in neutrophil density in animals carrying one but not two STAT1-F77A alleles (Figure 30B and 30C).

In order to assess the presence of monocytes and macrophages, CD68 expression was detected (Figure 31). Compared with the population of neutrophils at the site of inflammation, CD68-positive cells made up a markedly smaller proportion of the inflammatory infiltrate (Figure 31A). However, when quantifying the distribution and density of monocytes and macrophages, no difference was detected between the genotypes (Figure 31B and 31C).

As the last subset, the infiltration of T cells was assessed through staining for CD3. Analysis revealed that this subset constitutes the smallest portion among the three subsets (Figure 32A). Again, quantification revealed that the cells were distributed equally between the genotypes (Figure 32B and 32C). In summary, immunohistochemical staining for the most prominent leukocyte subsets of the inflammatory infiltrate in the acute phase after myocardial infarction identified a small, yet non-significant reduction in the portion of neutrophils in mice homozygous for the STAT1-F77A mutation as compared to wildtype animals. This trend was support by a significantly lower density of neutrophils in the heterozygous mice compared with the wildtype.

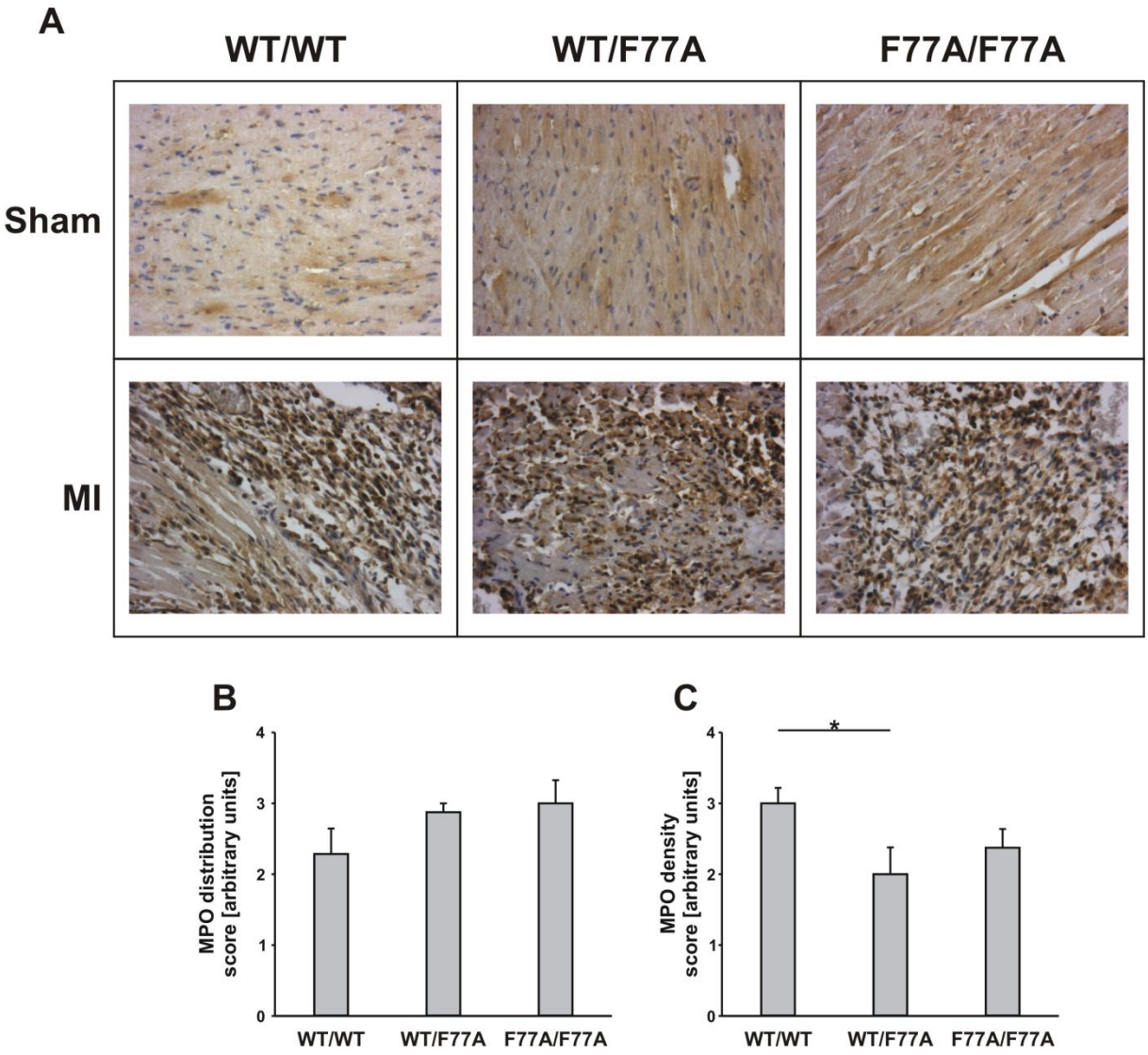

Figure 30: Staining of myeloperoxidase (MPO) on day 3 following myocardial infarction or sham operation. *(A) Shown are representative fields of view of the left ventricular wall of sham-operated animals (top) and MI-operated animals (bottom) of all three genotypes investigated. Arbitrary quantification of MPO-positive cells with respect to their distribution over the ventricular wall and septum (B) the density of MPO-positively stained cells (C). Asterisks indicate statistically significant differences. Error bars represent standard error of the mean.*

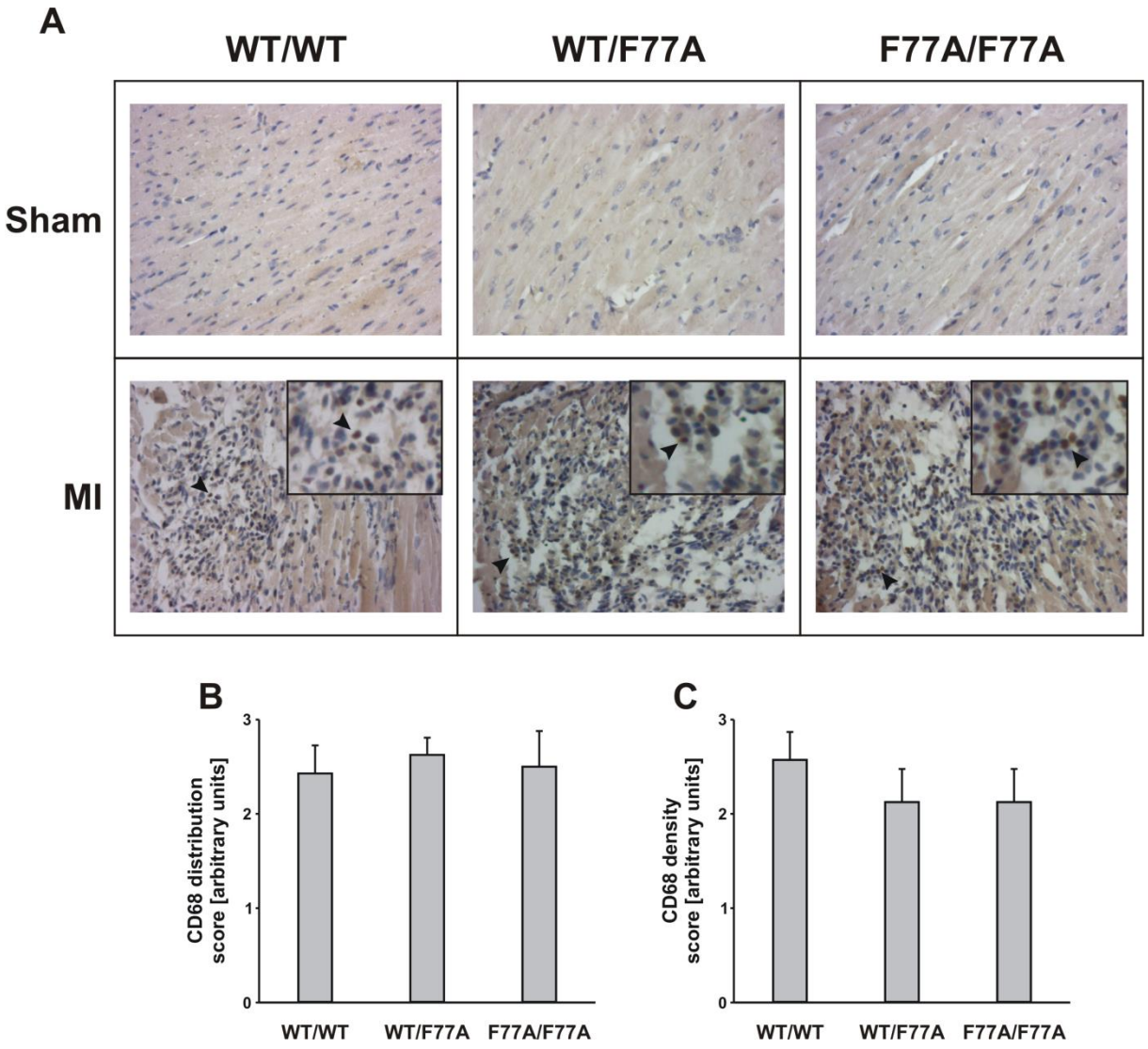

Figure 31: Staining of CD68 following ligation of the left ascending coronary artery or sham operation on day 3. *(A) Shown are representative fields of view of the left ventricular wall of sham-operated (top) or MI-operated animals (bottom) of all three genotypes investigated. Single CD68-positive cells were found in the inflammatory infiltrates (arrowheads) but not in the mock-operated ventricular wall. Arbitrary quantification of CD68-positive cells with respect to their distribution over the ventricular wall and septum (B) and the density of CD68-positively stained cells (C). Error bars represent standard error of the mean.*

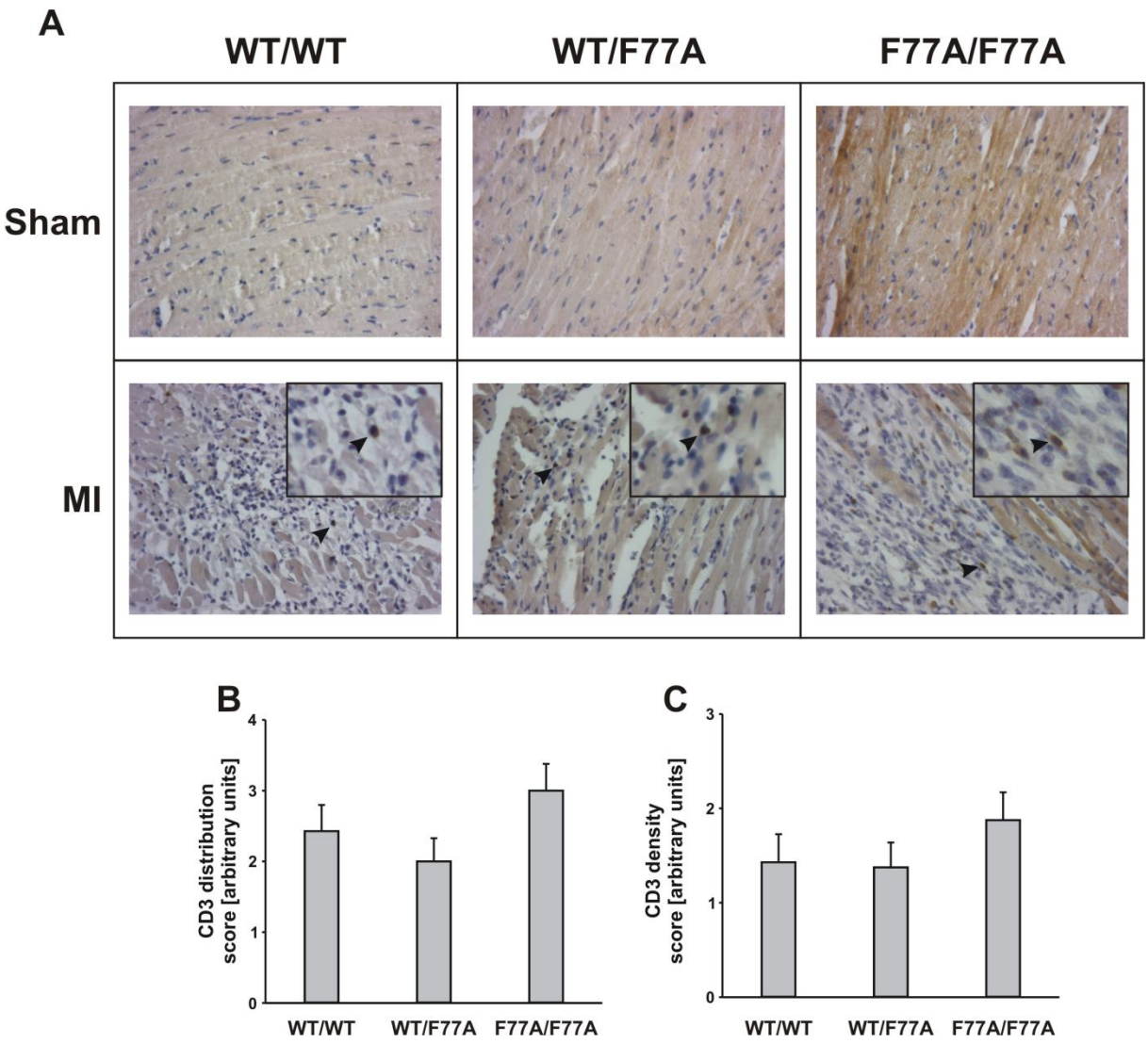

Figure 32: Expression of CD3 in infarcted heart tissue on day 3 follow-up. *(A) Representative fields of view of the left ventricular wall of sham-operated animals (top) and mice subjected to myocardial infarction (bottom) of all three genotypes are shown. CD3-positive cells were found in the inflammatory infiltrate (arrowheads) but not in the ventricular wall of sham-operated animals. Arbitrary quantification of the distribution of CD3-positive cells over the ventricular wall and septum (B) and the density of CD3-positive cells within the infarcted area (C).*

3.4 STAT1 deficiency delays onset of EAE upon challenge with lipopolysaccharide

A plethora of studies has been published that show that STAT1 and STAT3 are main factors in the determination of T cell fate (Ma et al. 2016). Defects in these pathways have been associated with dysfunction of the immune system including immunodeficiency and autoimmunity. Within the context of experimental autoimmune encephalomyelitis (EAE), lack of STAT1 expression was shown to result in exacerbated disease progression and a

higher rate of so-called atypical EAE (Bettelli et al. 2004; Peters et al. 2015). Studies on the impact of LPS on the onset and progression of EAE are rare and, depending on the exact time point of LPS application, a delay or exacerbation of the disease have been reported (Buenafe and Bourdette 2007; Park et al. 2015).

3.4.1 STAT1 knockout mice are protected upon LPS challenge

In this project, we aimed to discover the effect of a combination of MOG_{35-55} peptide-induced EAE and LPS-mediated activation of TLR4. Wildtype and STAT1-deficient mice both on a C57BL/6 genetic background were immunized following the standard protocol. Pertussis toxin was given at the time of immunization and 48 h later to increase the effectiveness of the challenge with the antigen. Half the mice cohort were given LPS i.p. (5 mg/kg body weight) 24 h after immunization. Following this protocol, the onset of EAE is expected between day 10 and day 12 after immunization.

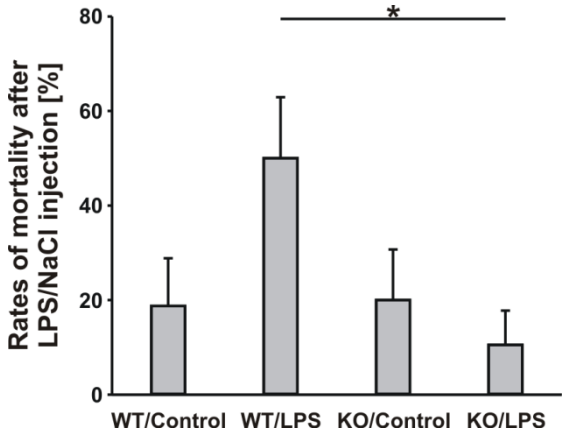

Figure 33: Survival before onset of EAE upon LPS challenge. *Shown is the percentage of animals surviving the period between immunization with MOG_{35-55} peptide and 10 days after immunization. Injection with LPS was performed i.p. on day 1 after immunization. Control animals were injected with an equal volume of 0.9 % NaCl solution. Asterisks indicate statistically significant differences. Error bars represent standard error of the mean.*

The mean weight at the time of LPS challenge was 21.4 g, and the mean age at MOG_{35-55} immunization was 11.3 weeks. Sixteen out of 66 animals, that had been immunized, died before the onset of EAE. Most of these animals belonged to the groups challenged with 5 mg/kg bodyweight LPS. This mortality was significantly higher in the wildtype than in the STAT1-deficient animals (Figure 33). The decreased sensitivity towards LPS challenge is in line with observations made for the STAT1-F77A mice in a previous study, also showing

decreased mortality in the knockin model compared with their wildtype littermates (Begitt et al. 2014).

3.4.2 Onset of clinical symptoms of EAE is delayed in STAT1 knockout mice injected with LPS

The mean onset of EAE was 10 to 12 days after immunization with MOG_{35-55} peptide and progressed usually as an ascending flaccid paresis of tail and limbs. Disease severity was rated using a scale from 0-10, where 0 corresponds to no symptoms, 7 to complete paresis of the hindlimbs, and 10 to death.

Figure 34 shows the mean onset and progression of EAE in STAT1-KO as compared to wildtype C57BL/6N mice that had been injected with LPS or with 0.9 % NaCl used as a control. In line with the literature, disease severity was mildly but not significantly increased in STAT1-deficient mice as compared to wildtype mice. Injection of LPS 24 h after immunization with MOG_{35-55} peptide resulted in a delay of disease onset by several days. This effect was even more pronounced in the group of STAT1-deficient mice injected with LPS (Figure 35). In terms of the disease severity, there were differences among the various treatment conditions: the NaCl-treated STAT1 knockout animals showed the most severe symptoms, while the LPS-treated wildtype animals presented with the mildest symptoms. The high variance is attributed to the high mortality rate upon LPS injection, which reduced the sample size of the cohort. In summary, the LPS-induced delay in the onset of EAE symptoms was equally pronounced in STAT1 knockout mice and wildtype animals.

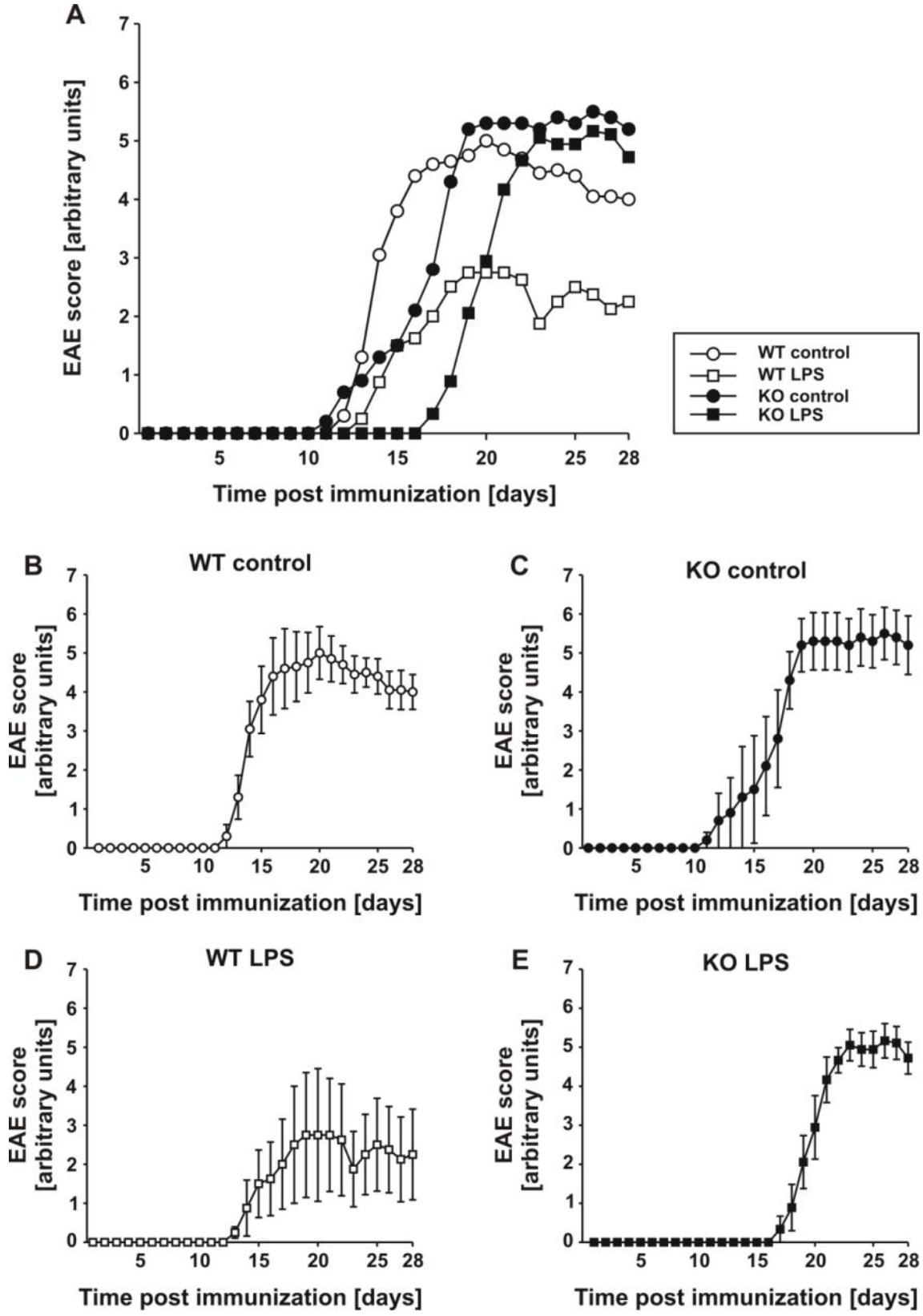

Figure 34: Clinical scores in STAT1-deficient and wildtype mice treated with and without LPS injection. *(A) Combined scores of all four experimental conditions. Clinical scores of EAE progression rated on a 10-point scale in wildtype mice injected with NaCl solution (B), in STAT1 knockout mice injected with NaCl solution (C), in wildtype mice injected with LPS (D), and in knockout mice injected with LPS (E). Error bars represent standard error of the mean.*

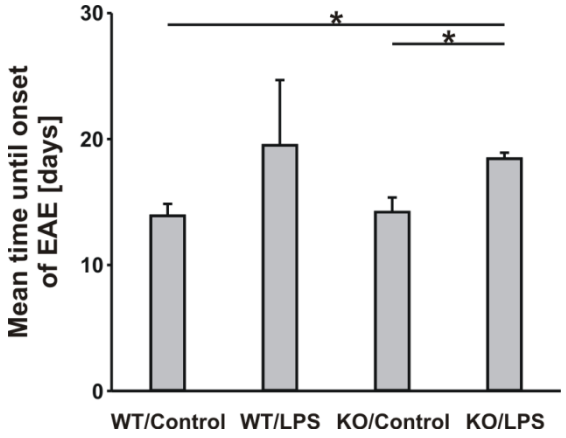

Figure 35: Mean date of EAE onset. *Comparison between the four groups of wildtype (WT) and STAT1 knockout (KO) mice challenged with and without LPS after immunization for the induction of EAE. Asterisks indicate statistically significant differences. Error bars represent standard error of the mean.*

3.4.3 Cells from STAT1 knockout mice show increased proliferation upon MOG_{35-55} peptide stimulation

EAE symptoms develop through the destruction of the myelin sheath of axons after invasion of the CNS by autoreactive immune cells. In order to provoke such a response, clonal expansion of antigen-specific $CD4^+$ T cells in the lymphatic organs is necessary (Rangachari and Kuchroo, 2013). To assess the proliferative capacity of immune cells derived from wildtype and STAT1-deficient mice, an *ex vivo* proliferation assay with MOG_{35-55} peptide was performed. Spleens and lymph nodes were extracted from mice of both genotypes which had been immunized with MOG_{35-55} peptide and then challenged with LPS or left untreated on day 10 and day 17 after immunization. Single cell suspensions produced from spleen and lymph nodes were incubated with either MOG_{35-55} peptide as a specific stimulus or concanavalin A as an unspecific stimulus for two days before addition of [^{3}H]-labelled thymidine for 16 h to evaluate proliferation through the readout of incorporated radioactivity.

Figure 36A shows the results of this proliferation assay for spleen-derived cells obtained 10 days after immunization. For the cell isolates from wildtype animals, there were only minor differences between LPS-challenged and unchallenged cells. When comparing cells from wildtype carriers with cells derived from STAT1 knockout animals and treated under the same conditions, a markedly higher proliferation rate in response to MOG_{35-55} peptide as well as concanavalin A was observed in the unchallenged cells. In contrast, cells obtained after LPS treatment displayed a markedly reduced response to MOG_{35-55} peptide, while the

concanavalin A response remained strong. Similar results were obtained for cell isolates derived from the lymph nodes (Figure 36B), although these differences did not reach statistical significance.

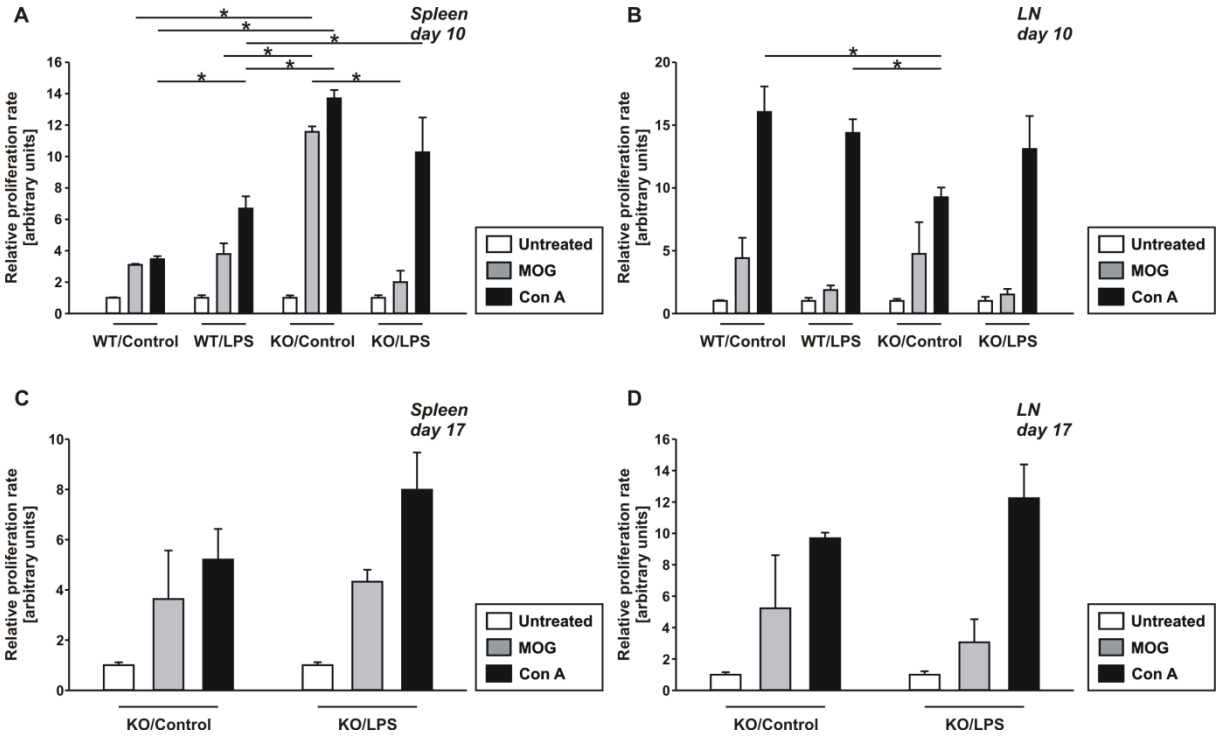

Figure 36: Relative proliferation rates of cells derived from lymphatic organs challenged with MOG_{35-55} peptide or concanavalin A. *Spleen (A) and lymph node (LN) cells (B) extracted on day 10, as well as spleen cells (C) and lymph node (D) cells extracted on day 17 were stimulated with MOG_{35-55} peptide, concanavalin A (Con A) or left untreated. Proliferation was measured by incorporation of [^{3}H]-labelled thymidine for 16 h. Asterisks indicate statistically significant differences. Error bars represent standard error of the mean.*

Although LPS markedly delayed the onset of EAE in both wildtype and knockout mice, the reduced proliferation capacity in response to a specific antigen was more pronounced in the KO animals, while, in the wildtype animals, it remained at a similar level to that in the group of the untreated controls. The KO mice which had not been injected with LPS showed enhanced proliferation in response to the specific as well as the unspecific stimulus. Given the considerable differences between the cells derived from STAT1-deficient mice with and without LPS injection, a second proliferation assay was performed using cells obtained 17 days after MOG_{35-55} immunization. This time point was chosen since LPS delayed the onset of disease symptoms by about 1 week. Figure 36C shows the respective data of cells derived from the spleen. No significant differences were observed among the two conditions. These findings were supported by the lack of significant differences in the data obtained for the

lymph node derived cells (Figure 36D). This indicates that the impact of LPS stimulation on lymphocyte proliferation was transient and in line with the *in vivo* observation that LPS injection delayed but did not reduce the severity in EAE in STAT1-deficient mice.

3.4.4 STAT1 knockout cells produce increased amounts of IL-17A and IFNγ

A major mediator of the development of EAE is the population of $CD4^+$ T cells which can develop towards different cell fates such as Th1, Th2, Th17 and regulatory T cells in response to signalling peptides (Bonelli et al., 2014). For the model of EAE in mice, Th1 cells and Th17 cells have been identified as the major actors in disease progression (Rangachari and Kuchroo, 2013). In order to identify whether the proliferative expansion of cells shown in Figure 36 was attributed to Th1 or Th17 cells, the secretion of marker cytokines of both cell lineages was quantified in the culture supernatant using ELISA technique. Figure 37 shows the results for the secretion of IL-17A, the marker cytokine of Th17 cells. Only low amounts of IL-17A were detected in the supernatants of cultured cells from spleen and lymph nodes of wildtype animals on day 10 (Figure 37A and 37B). The STAT1 knockout cells obtained from mice which had been immunized but not treated with LPS produced significantly higher amounts of IL-17A under MOG_{35-55} peptide or concanavalin A stimulation than cells from wildtype mice. This suggested stronger proliferation of Th17 cells and was in line with the more severe progression of EAE in this group. Cells derived from STAT1-deficient mice following injection with LPS secreted only low amounts of IL-17A in response to MOG_{35-55} peptide and concanavalin A.

ELISA analysis was repeated for cells derived from spleen and lymph nodes of STAT1-KO animals sacrificed on day 17 after immunization (Figure 37C and 37D). In line with the observations made in the proliferation assays described above (Figure 36C and 36D), the differences between the LPS-treated and non-treated conditions disappeared at this later time point.

ELISA analysis was subsequently performed under similar experimental conditions to identify IFNγ concentration in the *ex vivo* culture supernatant as a readout of Th1 proliferation (Figure 38). In the cells derived from untreated wildtype spleen, there was a marked secretion of IFNγ in response to MOG_{35-55} peptide stimulation that exceeded the response to concanavalin A supporting the notion that Th1 cells are the main actors of EAE in this context (Figure 38A). In the cells derived from the LPS treated animals, the secretion of IFNγ appeared to be lower although this effect was non-significant. Interestingly, there was a strong

secretion of IFNγ in the cells derived from STAT1 knockout animals treated with MOG_{35-55} peptide – the condition that showed the highest proliferation and also highest secretion of IL-17A. Again, this effect was reversed in the cells derived from animals that had been injected with LPS. Data of the cells derived from lymph nodes confirmed these observations, although secreted levels of IFNγ were much lower in the supernatants of these cultured cells and in some cases below the level of detection (Figure 38 B).

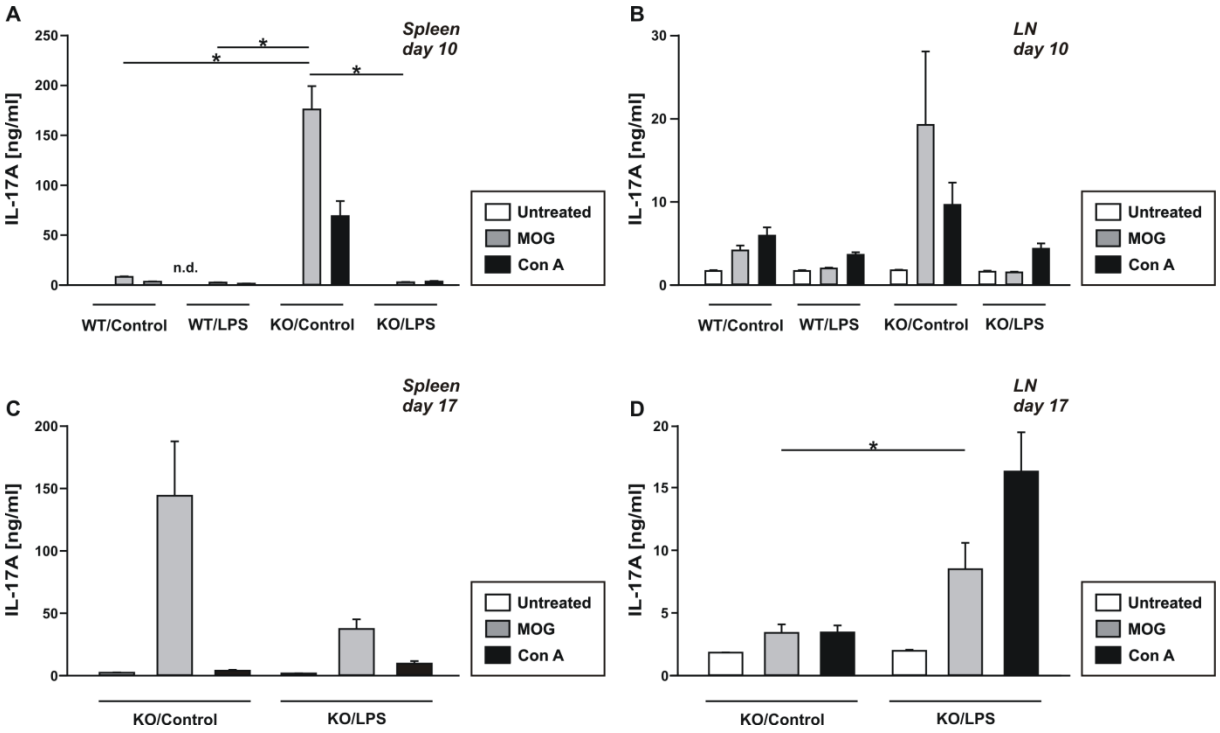

Figure 37: IL-17A concentrations in the supernatants of spleen and lymph node cells from MOG_{35-55}-immunised mice in the presence or absence of LPS challenge. *Spleen cells (A, C) and lymph node cells (B, D) obtained on day 10 (A, B) or day 17 (C, D) after MOG_{35-55} immunization of mice in the absence or presence of LPS injection were stimulated ex vivo with MOG_{35-55} peptide, concanavalin A (Con A) or left untreated. Production of IL-17A was measured using ELISA technique. n.d. marks measurements below the detection level. Asterisks indicate statistically significant differences. Error bars represent standard error of the mean.*

The results of the later time point on day 17 post-immunization were in line with the previous observation that at this point, the differences between the STAT1-deficient animals injected with LPS or saline disappeared (Figure 38 C and D). In summary, the secreted cytokine patterns supported the observations made from the proliferation assays and the clinical scoring for disease progression.

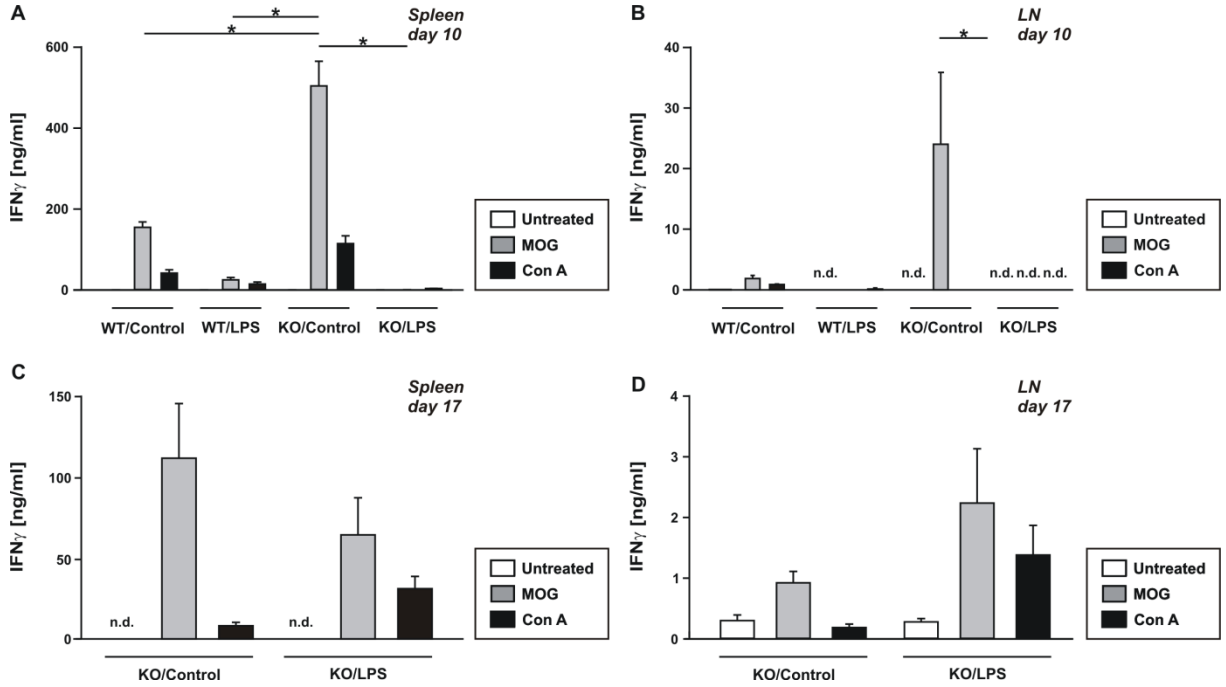

Figure 38: Dysregulated IFNγ production in the supernatants of primary cells from lymphatic organs of STAT1 knockout animal cells immunized with MOG_{35-55} peptide in the presence or absence of LPS co-stimulation. *Spleen cells (A, C) and lymph node cells (B, D) obtained on day 10 (A, B) or day 17 (C, D) after MOG_{35-55} immunization of mice in the absence (controls) or presence of LPS challenge. IFNγ concentrations in the supernatants of primary cells were detected using ELISA technique. n.d. marks measurements below the detection level. Asterisks indicate statistically significant differences. Error bars represent standard error of the mean.*

4 Discussion

Since the 1990s, STAT1 regulation has been under investigation as to its function in immunological processes (Shuai et al., 1992; Larner et al., 1993). Numerous studies have highlighted the essential role of the STAT1 transcription factor in defending viral, bacterial and parasite pathogens, and mutations in this protein have been shown to affect susceptibility to a catalogue of pathogens in mammals (Zhang et al., 2008). From crystallographic data, it is known that STAT1 can form a DNA-bound parallel dimer conformation as well as an anti-parallel conformation not bound to DNA (Chen et al., 1998; Mao et al., 2005). Reciprocal interactions between N-terminal domain dimers are required for stabilization of tetrameric complexes. To characterize the physiological consequences of impaired tetramer stability in an organismic context, a genetic knockin mouse line carrying the STAT1-F77A mutant allele has been described (Begitt et al., 2014). The phenotype of this mouse line shows decreased stabilization of tetramers, loss of cooperative DNA binding and an overall failure to induce IFNγ-regulated target genes. In this project, the impact of abolished STAT1 cooperative DNA binding was studied in a murine model of ischemic injury and the impact of a complete loss of STAT1-dependent signalling was analysed in the context of autoimmunity. Both pathological conditions are characterized by a pronounced inflammatory reaction which induces loss of functional tissue. The role of STAT1 in the regulation of rearrangements of the actin cytoskeleton in leukocytes through the ERM proteins will be discussed as a possible mechanism of leukocyte recruitment. The results underscore the fact that the STAT1-F77A mutant is a valuable tool for the understanding of STAT1 signal transduction and, in particular, for the study of the molecular mechanisms of the conformational transition from the parallel to the anti-parallel conformation.

The proposed mechanism of STAT1-dimer conformational shift, which is in line with data from the Vinkemeier laboratory (Wenta et al., 2008), relies on the constant dissociation and re-association of protomers as opposed to the hypothesis of N-terminal interactions facilitating the conversion between the two conformational states of the STAT1 dimer (Mertens et al., 2006). An experimental set-up using EMSA was established to study the recombination between full-length untagged STAT1 and the GFP-tagged fusion protein thereof. The assay proved helpful in identifying inter-molecular interactions since it allowed for the identification of the two STAT1 variants based on an electrophoretic separation due to their different molecular weights (Figure 3). Both STAT1 variants demonstrated similar affinity and binding kinetics when interacting with consensus GAS elements, indicating that

the carboxy-terminal fusion to GFP neither augments nor impairs the dissociation of tyrosine-phosphorylated STAT1 dimers from their target sequence on DNA (Figure 4). Co-incubation experiments with untagged and GFP-tagged STAT1 showed that the two variants were able to form functional heterotetramers in the presence of specific GAS binding sites – a prerequisite to render them helpful in the study of the kinetics of the exchange of protomers (Figure 5 and Figure 7).

However, incubation of STAT1 dimers with DNA was shown to significantly slow down the kinetics of the protomer exchange which led to the notion that DNA binding protects from monomer exchange (Figure 9). Regarding the tetramer, the exchange of dimers was observed in the absence of DNA binding (Figure 7). It is worthy of note that reciprocal amino-terminal interactions facilitated by the critical phenylalanine residue in position 77 are dispensable for the dissociation into promoters, as shown by the fact that a STAT1 mutant carrying a mutation to alanine in this critical residue also showed dissociation (Figure 9 and Figure 10). Therefore, in contrast to its pivotal role in tetramer stabilization and cooperative DNA binding, no indication was found that the phenylalanine in position 77 was needed for the transition between the STAT1 conformational states or the exchange of protomers.

The data on the kinetics of the protomer exchange (Figure 9) when compared with the DNA binding kinetics (Figure 4) show that while the association and release from DNA occurs rather rapidly the *in vitro* half-life of phosphorylated STAT1 dimers at room temperature exceeds 10 min. The structure of the phosphorylated STAT1 dimer was shown to be relatively stable even in the absence of DNA. High-affinity binding to its known target sequence further decelerates the exchange kinetics of STAT1 monomers. Furthermore, the results show that reciprocal interactions of the amino-termini of two adjacent monomers are not necessary for the formation of new dimer combinations.

As an alternative model for the reciprocal amino-terminal interactions facilitating the transition between the two conformational states of the STAT1 dimer (Mertens et al., 2006), a different mechanism had been proposed (Wenta et al., 2008). From the literature, it seems well established that the phosphorylation status of the critical tyrosine residue 701 is important for dimer orientation. While phosphorylated STAT1 preferentially acquires the parallel conformation, the absence of tyrosine phosphorylation stabilizes the more condensed anti-parallel conformation. Wenta and colleagues estimated a half-life of 20-40 min for each STAT1 dimer conformation which is of the same order of magnitude identified for the half-life of the protomer exchange kinetics measured in this project. This supports the hypothesis

that conformational change might be achieved by dissociation and re-association in different conformational states.

The acquired data cannot exclude the possibility that the phosphorylated STAT1 dimer is constantly oscillating between the two different conformational states at a rate much faster than the kinetics identified for the exchange of protomers and that this oscillation might be supported by amino-terminal interactions. However, this putative oscillation cannot be the rate limiting step in the dimer dissociation kinetics nor the main determinant of dimer stability.

The physiological significance of these observations remains to be evaluated. It is assumed that the anti-parallel STAT1 dimer is the substrate for the inactivating STAT1-specific phosphatase, since binding of STAT1 to DNA hinders dephosphorylation (Meyer et al., 2003; Mertens et al., 2006). The conformational change from the parallel to the anti-parallel state is a prerequisite for STAT1 inactivation. Mutant isoforms of STAT1 such as F77A which are discussed to specifically hinder the alignment in the anti-parallel orientation have been found to be associated with prolonged tyrosine phosphorylation (Zhong et al., 2005; Mertens et al., 2006).

A study using single-molecule microscopy has shown that phosphorylated STAT1 associates to the DNA in a way that alternates short binding events of up to 5 sec with distinct saltatory movements (Speil et al., 2011). This process was interpreted as a series of intermitting events of retardation and immobilization by putative STAT1-binding sites. These data support the observation from this study that DNA-dimer interactions of STAT1 are less stable and characterised by a shorter half-life than intradimer interactions. Therefore, the dimer dissociation kinetics could be the rate limiting step in the STAT1 activation cycle.

The findings support the hypothesis that constant dissociation and re-association of phospho-STAT1 dimers occurs. However, the kinetics of the protomer exchange appears to be relatively slow in comparison with the fast release of dimers from DNA suggesting that the dissociation kinetics is the rate limiting step in the STAT1-mediated transcriptional response within the nucleus. The results from this thesis clearly demonstrate that high-affinity binding to DNA hinders monomer exchange and that intradimeric interactions between the N-termini are dispensable for the protomer exchange.

The focus of this project was then directed towards the regulation of the expression of the *EZR* gene and whether STAT1 is playing a role in this context. Several reports have identified

components of the JAK/STAT pathway as mediators in actin cytoskeleton rearrangements during inflammatory processes and one way to induce stimulus-dependent cytoskeletal alterations is by ezrin signalling. Up to now, the focus of most of these studies had been on immediate changes, mostly via Rho kinase signalling. In macrophages, IFNγ was shown to increase the fraction of filamentous actin and Rac1-GTP which enhances the phagocytosis of bacteria (Frausto-Del-Río et al., 2012). Another study demonstrated that acquisition of an M1 or M2 type by macrophages is linked to the reorganization of the cytoskeleton. *In vitro* differentiation experiments have revealed that M1 macrophages, as induced by IFNγ and LPS, are round and flat in shape, while M2 macrophages, as induced by IL-4 and IL-13, are elongated and show a more polarized phenotype. When being grown on a surface that strongly favours an elongated cell shape, the M2 lineage was favoured even in the presence of LPS and IFNγ stimuli showing that cell shape and cytoskeletal structure help determine macrophage cell fate (McWhorter et al., 2013). In T cells, signalling induced by CXCL12 and CCL21 triggers dephosphorylation of ERM proteins and increases motility of the cells. Surprisingly, knockdown of JAK1 and JAK2 inhibited ERM phosphorylation and impaired chemokine-induced migration suggesting that JAK/STAT signalling can influence ERM metabolism (Pérez-Rivero et al., 2013).

Unlike the moesin and radixin gene, the gene encoding ezrin carries a GAS motif near the transcription start site (Table 23 and Table 24). In humans, this GAS motif possesses a unique structure since two optimal STAT1-binding sites are located approximately 500 bp upstream of the transcription start site in tandem orientation, separated by only 1 bp. With these characteristics, the GAS motif of the *EZR* gene markedly differs from the one-and-a-half GAS site of the *CCL2* gene which has been suspected of being more sensitive to changes in STAT1 phosphorylation levels and could therefore be affected to a higher degree than most STAT1-target genes by just minor increases in STAT1 phosphorylation (Hüntelmann et al., 2014).

The EMSA experiments performed in this project using the motif from the human *EZR* gene support the conclusion that this sequence can only be occupied by a single STAT1 homodimer (Figure 11). No preference for either of the two GAS elements aligned in tandem orientation was observed. This finding suggests that the putative GAS elements in the promoter of the human *EZR* gene are a target sequence for STAT1 homodimers which can only bind one dimer specifically most probably for steric reasons. Since most STAT1-target genes contain only one GAS motif in the vicinity of the TSS (Decker et al., 1997), the role of the putative STAT1 target sequence of the *EZR* gene was studied in the context of living cells.

ChIP experiments in Jurkat cells revealed that STAT1 binds to the *EZR* promoter in these cells (Figure 12). Since this human cell line was derived from a T cell leukaemia (Gillis and Watson, 1980), the binding of STAT1 to the *EZR* promoter not only suggests a role in gene regulation but might also indicate that this is of relevance in T cell function. However, since ezrin expression and activation have been found in connection with carcinogenesis (Leiphrakpam et al., 2014), induction of the *EZR* promoter might also be due to the transformed nature of this cell line.

Real-time PCR of reversely transcribed RNA extracted from Jurkat as well as HL-60 cells consistently revealed a significant increase in *ezr* mRNA expression by the factor 2.5 in response to IFNγ treatment (Figure 13 and Figure 14). This effect was less pronounced in response to stimulation with IFNα. Both interferons induce the phosphorylation of the STAT1 homodimer but in response to IFNα, a fraction of the STAT1 monomers becomes also sequestered into ISGF-3 (Horvath, 2000). Since no ISRE-binding site has been identified for the *EZR* promoter, the reduced induction below the level of significance in response to IFNα is in line with the hypothesis that *EZR* is an exclusive target gene of IFNγ-mediated STAT1 signalling. The observation that the induction of *ezrin* transcription is relatively mild might be attributed to the fact that ezrin is a cytoskeletal protein which only needs induction by a low magnitude and is moderately expressed at baseline. In contrast, most other IFNγ-regulated genes are cytokines, transcription factors and effectors of immune response which are close to silent at baseline and induced at high magnitudes to protect the tissue from infections by pathogenic agents.

Surprisingly, the induction of ezrin expression was not observed on the protein level, neither in leukaemia-derived tumour cell lines nor in bone marrow lysates obtained from wildtype mice, STAT1-deficient mice and mice which expressed the STAT1-F77A mutant (Figure 15, Figure 16, Figure 17, and Figure 18). This suggests that STAT1-induced changes in the protein expression of ezrin are below the detection level or that a different mechanism counteracts the weak induction of *ezr* mRNA production. A candidate for this effect would be the protease calpain. In response to extracellular stimuli, calpain actively cleaves ezrin in a Ca^{2+}-dependent manner (Yao et al., 1993). Calpain inhibition resulted in massive overexpression of ezrin and mild overexpression of radixin and moesin in NIH-3T3 cells. By overexpressing these ERM proteins, calpain inhibition led to an impairment in the cytoskeletal rearrangements necessary in cell spreading (Potter et al., 1998). Studies in the myeloid leukaemia-derived cell lines THP-1 and U937 have shown that IFNγ upregulates

mRNA and intracellular protein levels of calpain expression (Deshpande et al., 1995). Therefore, increase in calpain expression may be a possible mechanism to counterbalance STAT1-induced *ezrin* transcription.

Besides the regulation of *ezrin* on the transcriptional level, whether IFNα- or IFNγ-induced signalling could evoke phosphorylation of ERM proteins was evaluated. Threonine phosphorylation of the ERM proteins has been shown to regulate their activation status. The Rho kinases, a family of small GTPases, were described to phosphorylate ezrin at Thr567, radixin at Thr564, and moesin at Thr558. Phosphorylation of this conserved residue reduces head-to-tail associations of the amino-terminal and the carboxy-terminal domains (Matsui et al., 1998). Interactions of ERM proteins and small GTPases have been implicated in a variety of ERM-dependent mechanisms including polarization, adhesion, migration and T cell homing (Okamoto et al., 1999; Menager et al., 1999; Denker and Barber, 2002; Cernuda-Morollón et al., 2010; Ishihara et al. 2015). IFNγ-activated signalling mediates internalization of tight-junction proteins in a RhoA/ROCK-dependent manner, thereby impairing epithelial barrier integrity (Youakim and Ahdieh, 1999; Utech et al., 2005). Therefore, phosphorylation of ERM protein in response to interferon treatment was monitored.

In HL-60 cells, ERM phosphorylation levels were comparatively low and showed no induction by interferon treatment over different durations of time ranging from 10 min to 24 h (Figure 16). In protein lysates obtained from murine bone marrow, phosphorylation of ezrin and moesin was readily detectable. Treatment of single cell suspensions derived from murine bone marrow with IFNα or IFNγ for 45 min, produced no significant changes in phosphorylation levels of ERM proteins (Figure 18). Therefore, the observations do not support the hypothesis that interferon-induced signalling directly affects ERM phosphorylation.

The STAT1-F77A mutant included in these experiments was linked to poor induction of IFNγ-mediated gene expression due to a lack in tetramer stabilization which is pivotal for cooperative DNA binding of STAT1 (Meyer et al., 2004; Begitt et al., 2014). This mutation has impact on the susceptibility towards infectious disease, as the STAT1-F77A mouse is protected from vesicular stomatitis virus but showed higher mortality upon infection with *Listeria monocytogenes*. These data are in line with the notion that most genes which are upregulated as a response to viral infection are mediated by type I interferons via the ISGF-3 and that lack in binding cooperativity has little impact on ISGF-3 association to ISRE-binding sites (Meyer et al., 2004; Begitt et al., 2014). The phenotype of the STAT1-F77A mouse has

so far only been studied in infectious diseases. Here, for this project, its phenotype in the context of myocardial infarction was evaluated.

Over the last two decades, STAT proteins have been attributed a role in myocardial infarction and ischemia/reperfusion injury (Fuchs et al., 2003; Hilfiker-Kleiner et al., 2004; Boengler et al., 2008; Fischer and Hilfiker-Kleiner, 2007; Fischer and Hilfiker-Kleiner, 2008; Hilfiker-Kleiner et al., 2010; McCormick et al., 2012; Knight et al., 2012). Ischemia has been shown to promote apoptosis in an IFNγ/STAT1-dependent manner by inducing the expression of caspase 1 in cultured neonatal cardiomyocytes as well as in the murine heart using the Langendorff perfusion method (Stephanou et al., 2000). For the promotion of apoptosis in cardiomyocytes, the most important role was attributed to the STAT1 C-terminal domain since expression of a truncated mutant lacking the last 60 amino acids resulted in decreased rates of apoptosis. This effect was not found to be directly regulated via STAT1 transcriptional activity, because lack of the DNA-binding domain did not impair the pro-apoptotic actions of a STAT1 mutant (Stephanou et al., 2002). STAT1 and STAT3 have both been shown to become phosphorylated in response to ischemic injury to the myocardium. Different antioxidant agents which are known to be cardioprotective were shown to inhibit STAT1 activation (McCormick et al., 2006; Scarabelli et al., 2009). Given the function of STAT3 in mitochondrial respiration (Wegrzyn et al., 2009; Carbognin et al., 2016) STAT3 is known to have cardioprotective effects under pressure overload as well as during ischemia/reperfusion injury (Fuchs et al., 2003; Hilfiker-Kleiner et al., 2004; Boengler et al., 2008; Fischer and Hilfiker-Kleiner, 2007; Fischer and Hilfiker-Kleiner, 2008; Heusch et al., 2011). A lack of STAT3 expression in cardiomyocytes resulted in impaired cell survival upon inflammatory stimuli and the spontaneous development of fibrosis and cardiac dysfunction during the process of aging (Jacoby et al., 2003). These effects are partially attributed to its transcriptional pro-survival and anti-ROS actions. In recent years, some non-canonical interactions of STAT3 with the NF-κB signalling pathway and with complex I of the mitochondrial electron-transport chain have been identified. These interactions have been shown to further reduce damage to cardiomyocytes by limiting damage by reactive oxygen species (ROS) (Zouein et al., 2015). Therefore, the current notion is that, in cardiomyocytes, STAT1 increases the cell damage by promoting apoptosis while STAT3 mediates pro-survival signalling.

The human heart consists of approximately four to five billion cardiomyocytes (Frangogiannis, 2012; Bonaventura et al., 2016), a cell type which has a very limited

regenerative capacity. Upon myocardial infarction, functional cardiomyocytes are lost due to necrotic cell death as well as apoptosis. Tissue inflammation has been a main feature of ischemic injury of the heart and induces a pro-apoptotic environment often with damaging effects to the post-infarction myocardium. If a substantial amount of cardiomyocytes is lost, only defective healing marked by collagen deposition and scar formation but no functional healing by cardiomyocyte proliferation occurs (Scarabelli and Gottlieb, 2004; Frangogiannis, 2012; Bonaventura et al., 2016). Post-infarction cardiac repair is orchestrated in three phases. The first phase is characterised by massive invasion of the cardiac muscle by inflammatory cells. This leads to the clearance of the infarcted tissue of cell debris and dead cells and initiates reparative signalling pathways. During the second, proliferative phase, vascular cells and myofibroblasts are recruited by growth factors mainly secreted by macrophages. As a result, the structural integrity of the heart becomes restored by the synthesis of extracellular matrix proteins. During the third and final phase, many of the effector cells become quiescent or undergo apoptosis to avoid excess extracellular matrix deposition. The newly formed collagen is crosslinked to ensure structural integrity therefore completing the scar (Frangogiannis, 2012; Bonaventura et al., 2016).

Upon necrosis of the myocardium, damage-associated molecular patterns induce an activation of the innate immune system (Kono and Rock, 2008). The induction of damage-associated signalling was shown for several factors released during tissue necrosis, such as high mobility group box 1 (HMGB1), galectin-9 and heat-shock proteins. These factors induced maturation of dendritic cells, cytokine production, differentiation of Th1 cells and induction of receptor of advanced glycation end products (RAGE) signalling (Basu, 2000; Scaffidi et al., 2002; Dai et al., 2005). This pro-inflammatory environment leads to the recruitment of immune cells to the ischemic heart. The main effectors of this inflammatory response were identified as being neutrophil granulocytes, monocytes/macrophages, lymphocytes, mast cells, myofibroblasts, platelets and vascular cells (Bonaventura et al., 2016). Platelets are the first cells to become activated and localize to the infarcted area. Upon binding to adhesion or matrix proteins, they become activated and release a variety of chemotactic factors (Gawaz 2004). Binding of neutrophils with cardiomyocytes induced the intracellular generation of reactive oxygen species in both interaction partners (Entman et al., 1992). Adhesion molecules have received some attention in the context of the recruitment of inflammatory cells to the myocardium. Neutralizing antibodies against CD11a, CD11c, CD18, ICAM-1 and P-selectin were shown to reduce the infiltrate as well as the infarction size (Yamazaki et al., 1993; Tojo et al., 1996). However, first clinical trials translating the

promising findings from cell-adhesion inhibition in animal models into humans by administration of neutralizing antibodies against integrins to patients during the first hours after myocardial infarction did not result in detectable beneficial effects (Christia and Frangogiannis, 2013).

Since the role of STAT1 upon myocardial ischemia has mainly be assessed in *ex vivo* models, in this project an *in vivo* model was applied to evaluate how STAT1-dependent signalling is involved in myocardial infarction and post-infarction remodelling. Ligation of the left anterior descending artery was performed on mice carrying the F77A knockin mutation in the *Stat1* gene. During the first 96 h after the induction of myocardial infarction, no differences between wildtype and knockin mice were observed with respect to weight loss or sickness behaviour. Mortality during the first 4 days after infarction was below 10 %. However, between day 4 and day 7, survival of wildtype mice dropped from 87 % to 52 %, while survival rates of the STAT1-F77A knockin mice decreased from 95 % to 77 % (Figure 19). In the study cohort, this effect was almost completely attributed to the male sex, while mortality rates of female mice were equally low in the two genotypes. In the male mice, the carriers of the STAT1-F77A mutant were protected from death during the follow-up period after myocardial infarction. The timing of the marked drop in survival, which is usually more pronounced in males than in females, is due to left ventricular rupture or heart failure - a phenomenon that has been reported in several studies to occur between the 2nd and 7th day after infarction (Scherrer-Crosbie et al., 2001; Gao et al., 2005; Xiang et al., 2009; Sauvé et al., 2010). A mouse model of ischemia/reperfusion injury in mice deficient for the IFNγ-induced gene *Ccl2* resulted in attenuated and delayed cardiac remodelling which was caused by reduced recruitment of macrophages and myofibroblasts (Dewald et al., 2005). Diminished recruitment of macrophages to sites of inflammation was also described for a genetic knockout model of the gene encoding the CCL2 receptor (Kurihara et al., 1997). Since the STAT1-F77A mutant does not induce transcription of the *CCL2* gene as efficiently as the wildtype (Figure 29), a reduced recruitment of macrophages to the infarcted hearts of the knockin mouse was expected. Another cytokine, which is usually induced via IFNγ-dependent STAT1 signalling, is CXCL10. In the STAT1-F77A knockin model, *cxcl10* is only induced by IFNα, while IFNγ fails to induce gene transcription (Begitt et al. 2014, Figure 29). Ischemia/reperfusion injury of the heart in the CXCL10-deficient mouse was characterized by increased numbers of neutrophils in the early acute phase 24-72 h post-infarction and enhanced density of macrophages in the late acute phase 3-7 days after the infarction. This was accompanied by an increased recruitment of myofibroblasts and an early dilative

remodelling leading to poor cardiac function (Bujak et al., 2009). Since both cytokines are less inducible in the STAT1-F77A knockin mouse model and one has proven beneficial while the other mediates adverse effects during post-infarction remodelling, the outcome of myocardial infarction in the STAT1-F77A mouse was difficult to predict. However, since both cytokines mediate the recruitment of different cellular subsets to the inflamed region, an overall reduced recruitment of immune cells resulting in attenuated post-infarction remodelling was expected.

Ligation of the left anterior descending artery was rapidly followed by massive infiltration of the myocardium with several leukocytes subsets. The extent of this infiltration did not differ among the wildtype and the homozygous STAT1-F77A knockin mouse line (Figure 20, Figure 21, Figure 27, and Figure 30-32) In the STAT1-F77A knockin mouse line, a higher number of cells staining positively for activated STAT1 was observed. This observation is in line with the *in vitro* data showing that the STAT1-F77A mutant displays prolonged and increased rates of phosphorylation compared with the wildtype molecule (Meyer et al., 2004). Cells stained positively for tyrosine-phosphorylated STAT1 were found at similar densities in the hearts of wildtype and knockin mice during the acute phase of myocardial infarction, although, in the transgenic mouse line, these cells were distributed over a larger area. The cells recruited during the acute phase are mainly neutrophils, monocytes/macrophages, and T cells, as demonstrated by means of immunohistochemistry. Massive infiltration of the myocardium with neutrophils was detected during the acute phase as well as a moderate infiltration with macrophages and T cells (Figure 30, Figure 31, and Figure 32). Neutrophil infiltration was pronounced in all genotypes and was significantly reduced in heterozygous mice, but not in homozygous mice carrying the STAT1-F77A mutation as compared to their wildtype littermates.

Protein lysates of the hearts revealed increased expression levels of STAT1 and STAT3 in the infarcted areas compared with lysates obtained from non-infarcted areas (Figure 26). While phosphorylation levels of STAT1 appeared to be fairly equal among the genotypes, there was a higher expression of STAT1 in the infarcted myocardium of wildtype mice as compared with the hetero- and homozygous STAT1-F77A knockin mice. Since the STAT1-F77A mutant fails to activate STAT1-driven IFNγ target genes, STAT3-mediated signalling may be preferred in this mouse line. Corroborating this hypothesis, it was found that the ratio of STAT3 to STAT1 expression is increased in homozygous STAT1-F77A mice as compared

to wildtype and heterozygous animals, while the corresponding ratios of their phosphorylated forms were similar among the three genotypes.

Clinical studies in humans after myocardial infarction have identified ejection fraction, end-systolic volume and end-diastolic volume to be valid and strong predictors of post-infarction survival. Elevated end-systolic volume proved to be the most accurate predictor for post-infarction death from cardiac dysfunction-related causes (White et al., 1987). To some extent, post-infarction cardiac remodelling and scar formation can be seen as beneficial since it helps to restore and maintain cardiac output. Continued maladaptive cardiac remodelling, however, was linked to the progression of heart failure (Cohn et al., 2000).

When analysing for the effects of the STAT1-F77A knockin on post-infarction cardiac remodelling by means of echocardiography, the transgenic mouse line showed attenuated cardiac dilation in females (Figure 22-25). Analysis of the heterozygous genotype before and three days after myocardial infarction did not contradict the observed effect but was not identified clearly as showing a gene-dose effect or mimicking the results of the wildtype or the mutant (data not shown). The striking difference among the sexes was unexpected but could be attributed to the reduction in cohort size due to the high mortality rate during the first week after surgery. It is possible that, preferentially those animals of the study cohort which had the most severely affected heart function died. Corroborating the data from the pure anatomical measurements including the end-systolic and end-diastolic volume, hearts of STAT1-F77A mice showed an ameliorated cardiac performance during the course of cardiac remodelling (Figure 25). After MI injury, fractional area shortening, fractional shortening and ejection fraction were reduced in both wildtype and homozygous mutant mice. However, the drop was less pronounced in the IFNγ-irresponsive STAT1-F77A mutant.

All findings were most pronounced at week 1 after MI injury and had partially faded to being non-significant when the data obtained 4 weeks after the insult were analysed. Since only few female mice died during the follow-up, this result might indicate that the functional effect is transient. In the CCL2 knockout mouse, cardiac remodelling was delayed which resulted in a more favourable outcome with regard to cardiac performance (Dewald et al., 2005). Since *CCL2* induction by the STAT1-F77A mutant is impaired, the observed effect could be attributed to a similar one mediated by fewer macrophages and a lower recruitment of myofibroblasts. However, this hypothesis must remain controversial since no reduction in macrophage recruitment was observed for the knockin mice in the early phase after myocardial injury. The reduced numbers of neutrophils in the myocardial infiltrates in

heterozygous mice suggest that these animals may be protected from neutrophil-induced ROS generation (Entman et al., 1992). This favours higher rates of cardiomyocyte survival and improved cardiac function as a permanent effect. Although the exact mechanism remains to be identified, the data clearly show beneficial effects of impaired IFNγ-dependent signalling during the early phase after MI injury.

Cellular effects in myocardial infarction are the consequence of hypoxia-induced organ damage and are mainly mediated by processes of innate immunity including the recruitment of neutrophils and macrophages and the induction of extracellular matrix deposition (Bonaventura et al., 2016). In contrast, autoimmunity is a process resulting from the recognition of self-antigens by B or T lymphocytes. STAT1 and STAT3 and their downstream signalling effectors, have been attributed some functions during the development of several autoimmune diseases including multiple sclerosis (MS) and systemic lupus erythematosus (Feng et al., 2002; Ding et al., 2016). Therefore, the study was aimed at evaluating the clinical consequences of interactions between the innate immunity as activated by LPS challenge and factors of the adaptive immunity as induced by experimental autoimmune encephalomyelitis.

In this study, mice were injected with 5 mg/kg body weight LPS during the induction phase of EAE. This injection resulted in the development of severe symptoms of systemic inflammation and was accompanied by weight loss and general signs of fatigue. Interestingly, mortality was particularly high in the group of LPS-injected wildtype mice which express all components of intact IFNγ-dependent signalling (Figure 33). The results showed that the STAT1 genotype is a strong predictor of mortality in the sense that the STAT1 knockout mice are protected upon LPS treatment. This is in line with a report that mice deficient for STAT1, STAT4 or TYK2 are protected from LPS-induced sepsis-related death (Kamezaki et al., 2004).

Lipopolysaccharide is a bacterial substance that induces signalling via the toll-like receptor 4. The toll-like receptors (TLRs) are a class of pattern recognition receptors and part of the innate immune system which poses a first line defence mechanism in the recognition of characteristic structures displayed by microbial pathogens (Kawai and Akira, 2010). Although most studies on TLR4 have focused on its role in innate immunity, LPS-dependent TLR4 signalling was identified as promoter of the development of Th17 cells but not Th1 or Th2 cells (Park et al., 2015).

Besides the direct effect of LPS in acute inflammation, mice injected with it displayed their first symptoms of EAE later than mice not co-treated with it (Figure 35). Wildtype mice that had received an LPS injection prior to disease development showed a higher variability in their disease onset with a mean delay of approximately one week. This effect is in line with a report of a delay of 5 days in EAE onset in mice in response to LPS treatment three days prior to EAE induction (Buenafe and Bourdette, 2007). In this study, the delay in onset was attributed to the induction of TNFα, TGFβ, IFNβ and SOCS3 in response to the TLR4 stimulus. This delay could also be reported for the STAT1-deficient mice but with a more consistent delay in disease onset of 1 week. The knockout mice developed slightly more pronounced disease symptoms regardless of whether they had been treated with LPS or not (Figure 34). However, this exacerbated disease progression was not as pronounced as had been reported earlier by the laboratory group of Bettelli (Bettelli et al., 2004). Most studies indicate protective and beneficial effects due to LPS treatment (e.g. Raziuddin and Morrison, 1982; Buenafe and Bourdette, 2007; Ellestad et al., 2009; Li et al., 2010), whereas there are some which name detrimental effects of LPS (e.g. Nogai et al., 2005). However, the protocols used in these studies vary widely with respect to the dose as well as the time point of LPS administration. In general, gavage of LPS to mice prior to the induction of EAE delayed or attenuated disease development.

One proposed mechanism of LPS action was the induction of IL-10 production by dendritic cells which has proven to be inhibitory to disease progression (Zhou et al., 2014). An earlier study showed that mice which produce transgenic IL-10 under the control of the *H2* promoter are protected from EAE induction (Cua et al., 1999). However, this notion might be problematic since LPS-induced IL-10 production is, at least in part, considered to result from type I interferon signalling (Iyer et al., 2010). High IL-10 production has been reported for the STAT1 knockout as well as the T-bet-STAT1 double knockout mice (Bettelli et al., 2004).

Experimental autoimmune encephalomyelitis is an inducible model of a neurodegenerative disease mimicking the main features of multiple sclerosis (MS). Most commonly, EAE is induced in rodent models such as mouse and rat but also protocols for EAE induction in non-human primates are utilised (Hart et al., 2015). Multiple sclerosis is among the most common causes of neurological disability in young adults with higher prevalence in females than in males. Owing to demyelination and axon loss, patients develop physical and mental disability. Approximately 2 million people are estimated to be affected by this disease worldwide,

roughly half of whom live in Europe (Kingwell et al., 2013; Grigoriadis and van Pesch, 2015). According to disease progression, MS is categorized as the relapsing-remitting MS, which can develop into the secondary progressive form, or the primary progressive form of MS. Patients suffering from relapsing-remitting MS alternate between periods of severe disease symptoms and periods of almost complete recovery. In some cases, the disease course develops into the secondary progressive form with no recovery. Patients suffering from the primary progressive form do not go into remission (Kieseier and Hartung, 2003).

On the immunological level, MS is a disease mediated by dysfunction of parts of the innate, as well as, the adaptive immune system. Infiltration of the CNS, mainly the white matter by Th1 and Th17 cells, is a characteristic feature of the disease. Release of inflammatory cytokines activates macrophages and microglia which leads to the production of reactive oxygen and nitrogen species. In this pro-inflammatory environment, axons are demyelinated and degenerate leading to neurological disease symptoms (Grigoriadis and van Pesch, 2015). In the model of MOG_{35-55} peptide-induced EAE, dendritic cells pick up the peptide, migrate to the lymph nodes and cross-present the antigen to naïve T cells (Slavin et al., 2001). Symptoms are caused by the demyelination of axons of CNS neurons evoked by invasion of the CNS by autoreactive T cells, and the onset of disease is preceded by the activation and proliferation of T cells in the lymphatic organs (Soulika et al., 2009).

Several studies in mice have reported that impairment of the IFNγ-STAT1 axis, including genetic knockout of the genes encoding for STAT1, IFNγ or the ligand-binding chain of IFNGR, do not ameliorate EAE development and progression but rather augments disease severity, susceptibility and mortality (Ferber et al., 1996; Krakowski and Owens, 1996; Willenborg et al., 1996; Bettelli et al., 2004). Differences in numbers and function of regulatory T cells have been suggested as an underlying mechanism for the EAE progression in these transgenic models. In 129Sv mice, reduced numbers of regulatory T cells, as defined by the co-expression of CD4 and CD25, have been reported in STAT1-deficient mice as compared to a wildtype background (Nishibori et al., 2004). Furthermore, STAT1-deficient regulatory T cells were reported to lack the ability to inhibit growth. This observation contradicts our analysis of decreased numbers of regulatory T cells in the IFNγ-irresponsive STAT1 knockin mouse line, as shown in Figure 28. Some studies have reported that FoxP3-positive induced regulatory T (iTreg) cells are less frequent in STAT1- and in IRF1-deficient mice and that IFNγ-signalling is either a suppressor or inducer of Treg development (Wang et al., 2006; Fragale et al., 2008; Chang et al., 2009). The results from the experiments with the

STAT1-F77A knockin mouse line support studies showing that defective IFNγ signaling is linked to increased iTreg differentiation.

A different mechanism to explain the protective effect of IFNγ-dependent signalling in EAE was the induction of iNOS which leads to increased levels of reactive nitrogen species (Willenborg et al., 1999). The inhibitory effect of increased NO production resulting from IFNγ- or concanavalin A-induced signalling has been repeatedly reported (Albina et al., 1991; Krenger et al., 1996; Zettl et al., 1997). This mechanism was identified as specific for Th1 activation: IFNγ which was released from Th1 cells inhibited exacerbated Th1 activation resulting from NO production by APCs (van der Veen et al., 2000). Deficiency in iNOS expression was shown to hinder remission during the course of EAE. Overall, lack of iNOS was shown to augment EAE progression in mice (Fenyk-Melody et al., 1998; Sahrbacher et al., 1998). Furthermore, IFNγ-dependent signalling has been seen to regulate activation-induced cell death in T lymphocytes (Refaeli et al., 2002).

In an adoptive transfer model of EAE, Th1 recipient mice displayed a chemokine profile of high CXCL9, CXCL10 and CXCL11 expression, while Th17 recipients secreted CXCL1 and CXCL2. Although the cytokine profiles were distinct, clinical disease progression was similar in Th1- and Th17-mediated disease (Kroenke et al., 2008). In IFNγ knockout mice, the recruitment of inflammatory cells to the CNS is mainly mediated by CXCL2 and CCL1, not by CCL5 and CCL2 as in the wildtype (Tran et al., 2000). In an experimental autoimmune uveitis model, a similar pattern of recruitment of immune cells via the Th2 and Th17 cytokines CCL1, CXCL2, CCL11, CCL17 and CCL22 instead of the Th1-dependent cytokines CCL5, CXCL9, and CXCL10 was observed for the IFNγ knockout mouse (Su et al., 2007). Here, the differential expression of cytokines led to an increased recruitment of neutrophil and eosinophil granulocytes and a reduced recruitment of lymphocytes and monocytes.

In vitro proliferation assays using cell isolates derived from spleen and lymph nodes of MOG_{35-55} peptide-immunized mice shortly before the predicted onset of initial disease symptoms demonstrated a striking difference among the cells of wildtype and STAT1-deficient mice (Figure 36). While MOG_{35-55} peptide and concanavalin A both readily induced proliferation in cells from wildtype lymph nodes, cells derived from STAT1 knockout mice showed an even stronger increase in proliferation in response to either stimulus. This observation is in line with the notion that disease symptoms were augmented by the STAT1 knockout genotype as indicated by the severity of clinical symptoms. In support of these

findings, T cells from STAT1 knockout mice have been reported to be hyperproliferative (Bettelli et al., 2004). Increased proliferation of activated $CD4^+$ T cells characterised by high expression of CD44 and low expression of CD62L has been previously reported for IFNγ-deficient mice (Chu et al., 2000). In this model, the effect was, in part, attributed to failure of APCs to induce apoptosis.

Pre-treatment of mice with LPS showed little effect on the proliferation of cells of the wildtype genotype (Figure 36). However, the analysis of the impact of LPS on proliferation in the knockout genotype, revealed that the proliferation rate in response to MOG_{35-55} peptide was critically impaired while the response to concanavalin A appeared to be unchanged. These findings indicate that LPS has little effect on the induction of proliferation of T cells in spleen and lymph nodes of wildtype animals, whereas it impairs proliferation in cells from STAT1 knockout mice. MHC class II molecules are under transcriptional control of STAT1. A study using early life exposure of mice to LPS showed a protective effect of this treatment on EAE severity which was mainly attributed to reduced expression of MHC class II molecules on antigen presenting cells (Ellestad et al., 2009). Since it had been shown that STAT1 signalling in APCs limits T cell proliferation, the observations can be explained by an impaired antigen presentation after LPS treatment with an overall impaired effect on growth inhibition in the STAT1 knockout (van der Veen et al., 2000).

Reports on the mechanisms underlying the onset and progression of EAE have attributed major roles to $CD4^+$ lymphocytes and, in particular, Th1 and Th17 cells (Rangachari and Kuchroo, 2013; Bonelli et al., 2014). Th1 and Th17 cells are characterised by the secretion of marker cytokines which are IFNγ in the case of Th1 cells and IL-17A in Th17 cells (Mosmann et al., 1986; Park et al., 2005). Assessment of the release of these cytokines in supernatants of *ex vivo* cultures of spleen and lymph node cells led to the notion that cells from immunized STAT1-deficient mice readily released large amounts of both cytokines in response to MOG_{35-55} peptide encounter (Figure 37 and Figure 38). This observation was surprising since IFNγ-dependent signalling is mainly transduced via the transcription factor STAT1, and the gene encoding T-bet, *TBX21*, is a known STAT1-target gene and the master-regulator of Th1 differentiation (Lighvani et al., 2001; Afkarian et al., 2002; Villarino et al., 2010). The expectation in this context was that the Th17 lineage would be preferred in the absence of IFNγ/STAT1-dependent signal transduction (Harrington et al., 2005). Furthermore, it has been reported that lack of STAT1-mediated signalling usually pushes a STAT3-dependent reaction with STAT3 as a regulator of RORγt, the main inducer of Th17

maturation. Disturbances of the balance between STAT1- and STAT3-dependent signal pathways have been linked to altered lineage decision as a response to typical Th1 or Th17 inducing cytokines (Qing and Stark, 2004; Yang et al., 2007; Peters et al., 2015; Wan et al., 2015). However, although T-bet is regulated by IFNγ-dependent STAT1 signalling, it can be upregulated in T cell subsets in the absence of IFNγ signalling and even in the combined knockdown of IFNγ and IL-12. In the context of T cell fate, IFNγ-producing and IL-17A-producing T cells developed as well as T cells expressing both cytokines (Yeh et al., 2011). A study on Th17 cells showed that commitment towards this lineage was not permanent. Upon treatment of Th17 cells with Th1- or Th2-inducing factors, the production of Th1 and Th2 marker cytokines could still be induced (Stritesky et al., 2008). IL-23 has been identified as an agent which pushes the development of IL-17A and IFNγ double positive cells from Th17 cells. Knockout of STAT1, STAT4 or TBX21 did not reduce the size of this T cell population (Duhen et al., 2013). Similar to its effect in leukocyte proliferation, LPS treatment abrogated the release of IL-17A and IFNγ by the cultured cells. This effect was similar in the two genotypes and in line with the observation of delayed onset of disease symptoms after treatment with LPS. Therefore, the strong induction of cytokine production in the STAT1 knockout can, in part, be explained by the strong proliferation. Additionally, Th17 cells that acquire the double positive phenotype of IL-17A and IFNγ-producing cells can also contribute to the high secretion of both cytokines.

In summary, this project underscores the protomer exchange kinetics as a critical step in the STAT1 activation/inactivation cycle and describes this process as an alternative mechanism for the conformational change between the parallel and anti-parallel dimer conformation. Furthermore, it was shown that DNA binding of STAT1 not only hinders dephosphorylation but also the exchange of STAT1 protomers. The gene encoding the cytoskeletal protein ezrin was identified as a STAT1-regulated target gene since binding of tyrosine-phosphorylated STAT1 to the *EZR* promoter induced a weak transcriptional response. This effect could not be found at the level of protein expression which might indicate a counteracting mechanism. The phenotype of the STAT1-F77A mutant was further characterised by showing that this mutant was proficient in facilitating normal monomer exchange kinetics. Moreover, this mutant, similar to the complete functional knockout of STAT1, displayed no reduced expression levels of ezrin or moesin, supporting the notion that STAT1 is dispensable for the baseline expression of the two ERM proteins. In the context of inflammation following myocardial infarction, STAT1-F77A knockin males showed significantly higher rates of survival, while females were partially protected from cardiac

dilation and had a less impaired cardiac function when compared with their wildtype littermates. Analysis of the inflammatory infiltrate revealed a minor increase in cells expressing activated STAT1, while slightly fewer neutrophil granulocytes were recruited during the acute phase in heterozygous STAT1-F77A knockin mice. Analysis of the role of STAT1 in autoimmunity using EAE as the model of choice, revealed hyperproliferation and increased production of Th1 and Th17 marker cytokines in the STAT1 knockout context. These findings emphasize the role of STAT1 in non-infectious inflammatory diseases.

5 References

Abroun S, Saki N, Ahmadvand M, Asghari F, Salari F, Rahim F. STATs: An old story, yet mesmerizing. *Cell J* 2015;17(3):395–411.

Afkarian M, Sedy JR, Yang J, Jacobson NG, Cereb N, Yang SY, Murphy TL, Murphy KM. T-bet is a STAT1-induced regulator of IL-12R expression in naïve CD4+ T cells. *Nat Immunol* 2002;3(6):549–57.

Albina JE, Abate JA, Henry WL Jr. Nitric oxide production is required for murine resident peritoneal macrophages to suppress mitogen-stimulated T cell proliferation. Role of IFN-gamma in the induction of the nitric oxide-synthesizing pathway. *J Immunol* 1991;147(1):144–8.

Alexander WS. Suppressors of cytokine signalling (SOCS) in the immune system. *Nat Rev Immunol* 2002;2(6):410–6.

Alonzi T, Maritano D, Gorgoni B, Rizzuto G, Libert C, Poli V. Essential role of STAT3 in the control of the acute-phase response as revealed by inducible gene inactivation in the liver. *Mol Cell Biol* 2001;21(5):1621–32.

Bach EA, Aguet M, Schreiber RD. The IFN gamma receptor: a paradigm for cytokine receptor signaling. *Annu Rev Immunol* 1997;15:563–91.

Baden HA, Sarma SP, Kapust RB, Byrd RA, Waugh DS. The amino-terminal domain of human STAT4. Overproduction, purification, and biophysical characterization. *J Biol Chem* 1998;273(27):17109–14.

Bagawath-Singh S, Staaf E, Stoppelenburg AJ, Spielmann T, Kambayashi T, Widengren J, Johansson S. Cytokines induce faster membrane diffusion of MHC class I and the Ly49A receptor in a subpopulation of natural killer cells. *Front Immunol* 2016;7:16.

Barreiro O, Yanez-Mo M, Serrador JM, Montoya MC, Vicente-Manzanares M, Tejedor R, Futhmayr H, Sanchez-Madrid F. Dynamic interaction of VCAM-1 and ICAM-1 with moesin and ezrin in a novel endothelial docking structure for adherent leukocytes. *J Cell Biol* 2002;157(7):1233–45.

Basu S, Binder RJ, Suto R, Anderson KM, Srivastava PK. Necrotic but not apoptotic cell death releases heat shock proteins, which deliver a partial maturation signal to dendritic cells and activate the NF-kappaB pathway. *Int Immunol* 2000;12(11):1539–46.

Becker S, Groner B, Müller CW. Three-dimensional structure of the Stat3beta homodimer bound to DNA. *Nature* 1998;394(6689):145–51.

Begitt A, Droescher M, Meyer T, Schmid CD, Baker M, Antunes F, Knobeloch KP, Owen MR, Naumann R, Decker T, Vinkemeier U. STAT1-cooperative DNA binding distinguishes type 1 from type 2 interferon signaling. *Nat immunol* 2014;15(2):168–76.

Begitt A, Meyer T, van Rossum M, Vinkemeier U. Nucleocytoplasmic translocation of Stat1 is regulated by a leucine-rich export signal in the coiled-coil domain. *Proc Natl Acad Sci U S A* 2000;97(19):10418–23.

Bettelli E, Carrier Y, Gao W, Korn T, Strom TB, Oukka M, Weiner HL, Kuchroo VK. Reciprocal developmental pathways for the generation of pathogenic effector TH17 and regulatory T cells. *Nature* 2006;441(7090):235–8.

Bettelli E, Sullivan B, Szabo SJ, Sobel RA, Glimcher LH, Kuchroo VK. Loss of T-bet, but not STAT1, prevents the development of experimental autoimmune encephalomyelitis. *J Exp Med* 2004;200(1):79–87.

Boengler K, Hilfiker-Kleiner D, Drexler H, Heusch G, Schulz R. The myocardial JAK/STAT pathway: from protection to failure. *Pharmacol Ther* 2008;120(2):172–85.

Bonaventura A, Montecucco F, Dallegri F. Cellular recruitment in myocardial ischaemia/reperfusion injury. *Eur J Clin Invest* 2016;46(6):590–601.

Bonelli M, Shih H, Hirahara K, Singelton K, Laurence A, Poholek A, Hand T, Mikami Y, Vahedi G, Kanno Y, O'Shea JJ. Helper T cell plasticity: impact of extrinsic and intrinsic signals on transcriptomes and epigenomes. *Curr Top Microbiol Immunol* 2014;381:279–326.

van Boxel-Dezaire AH, Zula JA, Xu Y, Ransohoff RM, Jacobberger JW, Stark GR. Major differences in the responses of primary human leukocyte subsets to IFN-beta. *J Immunol* 2010;185(10):5888–99.

Bradford MM. A rapid and sensitive method for the quantitation of microgram quantities of protein utilizing the principle of protein-dye binding. *Anal Biochem* 1976;72:248–54.

Bretscher A, Edwards K, Fehon RG. ERM proteins and merlin: integrators at the cell cortex. *Nat Rev Mol Cell Biol* 2002;3(8):586–99.

Buenafe AC, Bourdette DN. Lipopolysaccharide pretreatment modulates the disease course in experimental autoimmune encephalomyelitis. *J Neuroimmunol* 2007;182(1-2):32–40.

Bujak M, Dobaczewski M, Gonzalez-Quesada C, Xia Y, Leucker T, Zymek P, Veeranna V, Tager AM, Luster AD, Frangogiannis NG. Induction of the CXC chemokine interferon-gamma-inducible protein 10 regulates the reparative response following myocardial infarction. *Circ Res* 2009;105(10):973–83.

Carbognin E, Betto RM, Soriano ME, Smith AG, Martello G. Stat3 promotes mitochondrial transcription and oxidative respiration during maintenance and induction of naïve pluripotency. *EMBO J* 2016;35(6):618–34

Caretto D, Katzman SD, Villarino AV, Gallo E, Abbas AK. Cutting edge: the Th1 response inhibits the generation of peripheral regulatory T cells. *J Immunol* 2010;184(1):30–4.

Cernuda-Morollón E, Millán J, Shipman M, Marelli-Berg FM, Ridley AJ. Rac activation by the T-cell receptor inhibits T cell migration. *PloS One* 2010;5(8):e12393.

Cetin B, Gonul II, Buyukberber S, Afsar B, Gumusay O, Algın E, Turan N, Ozet A, Benekli M, Coskun U. The impact of immunohistochemical staining with ezrin-carbonic anhydrase IX and neuropilin-2 on prognosis in patients with metastatic renal cell cancer receiving tyrosine kinase inhibitors. *Tumour Biol* 2015;36(11):8471–8.

Chang JH, Kim YJ, Han SH, Kang CY. IFN-gamma-STAT1 signal regulates the differentiation of inducible Treg: potential role for ROS-mediated apoptosis. *Eur J Immunol* 2009;39(5):1241–51.

Chauhan AK, Moore TL. T cell activation by terminal complex of complement and immune complexes. *J Biol Chem* 2011;286(44):38627–37.

Cheeran MC, Mutnal MB, Hu S, Armien A, Lokensgard JR. Reduced lymphocyte infiltration during cytomegalovirus brain infection of interleukin-10-deficient mice. *J Neurovirol* 2009;15(4):334–42.

Chen EJ, Shaffer MH, Williamson EK, Huang Y, Burkhardt JK. Ezrin and moesin are required for efficient T cell adhesion and homing to lymphoid organs. *PloS One* 2013;8(2):e52368.

Chen W, Jin W, Hardegen N, Lei KJ, Li L, Marinos N, McGrady G, Wahl SM. Conversion of peripheral CD4+CD25- naive T cells to CD4+CD25+ regulatory T cells by TGF-beta induction of transcription factor Foxp3. *J Exp Med* 2003a;198(12):1875–86.

Chen X, Bhandari R, Vinkemeier U, van Den Akker F, Darnell JE Jr, Kuriyan J. A reinterpretation of the dimerization interface of the N-terminal domains of STATs. *Protein Sci* 2003b;12(2):361–5.

Chen X, Vinkemeier U, Zhao Y, Jeruzalmi D, Darnell JE Jr, Kuriyan J. Crystal structure of a tyrosine phosphorylated STAT-1 dimer bound to DNA. *Cell* 1998;93(5):827–39.

Cheon H, Stark GR. Unphosphorylated STAT1 prolongs the expression of interferon-induced immune regulatory genes. *Proc Natl Acad Sci U S A* 2009;106(23):9373–8.

Christia P, Frangogiannis NG. Targeting inflammatory pathways in myocardial infarction. *Eur J Clin Invest* 2013;43(9):986–95.

Chu CQ, Wittmer S, Dalton DK. Failure to suppress the expansion of the activated CD4 T cell population in interferon gamma-deficient mice leads to exacerbation of experimental autoimmune encephalomyelitis. *J Exp Med* 2000;192(1):123–8.

Cohen SN, Chang AC, Hsu L. Nonchromosomal antibiotic resistance in bacteria: genetic transformation of Escherichia coli by R-factor DNA. *Proc Natl Acad Sci U S A* 1972;69(8):2110–4.

Cohn JN, Ferrari R, Sharpe N. Cardiac remodeling—concepts and clinical implications: A consensus paper from an international forum on cardiac remodeling. *J Am Coll Cardiol* 2000;35(3):569–82.

Collins SJ, Gallo RC, Gallagher RE. Continuous growth and differentiation of human myeloid leukaemic cells in suspension culture. *Nature* 1977;270(5635):347–9.

Copeland NG, Gilbert DJ, Schindler C, Zhong Z, Wen Z, Darnell JE Jr, Mui AL, Miyajima A, Quelle FW, Ihle JN, Jenkins NA. Distribution of the mammalian Stat gene family in mouse chromosomes. *Genomics* 1995(29):225–8.

Cross AK, Woodroofe MN. Chemokines induce migration and changes in actin polymerization in adult rat brain microglia and a human fetal microglial cell line in vitro. *J Neurosci Res* 1999;55(1):17–23.

Cua DJ, Groux H, Hinton DR, Stohlman SA, Coffman RL. Transgenic interleukin 10 prevents induction of experimental autoimmune encephalomyelitis. *J Exp Med* 1999;189(6):1005–10.

Cypowyj S, Picard C, Maródi L, Casanova J, Puel A. Immunity to infection in IL-17-deficient mice and humans. *Eur J Immunol* 2012;42(9):2246–54.

Dai S, Nakagawa R, Itoh A, Murakami H, Kashio Y, Abe H, Katoh S, Kontani K, Kihara M, Zhang SL, Hata T, Nakamura T, Yamauchi A, Hirashima M. Galectin-9 induces maturation of human monocyte-derived dendritic cells. *J Immunol* 2005;175(5):2974–81.

Darnell JE Jr. STATs and gene regulation. *Science* 1997;277(5332):1630–5.

Darnell JE Jr, Kerr IM, Stark GR. Jak-STAT pathways and transcriptional activation in response to IFNs and other extracellular signaling proteins. *Science* 1994;264(5164):1415–21.

Decker T, Kovarik P. Serine phosphorylation of STATs. *Oncogene* 2000;19(21):2628–37.

Decker T, Kovarik P, Meinke A. GAS elements: a few nucleotides with a major impact on cytokine-induced gene expression. *J Interferon Cytokine Res* 1997;17(3):121–34.

Denker SP, Barber DL. Cell migration requires both ion translocation and cytoskeletal anchoring by the Na-H exchanger NHE1. *J Cell Biol* 2002;159(6):1087–96.

Deshpande RV, Goust JM, Chakrabarti AK, Barbosa E, Hogan EL, Banik NL. Calpain expression in lymphoid cells. Increased mRNA and protein levels after cell activation. *J Biol Chem* 1995;270(6):2497–505.

Devaux P, Priniski L, Cattaneo R. The measles virus phosphoprotein interacts with the linker domain of STAT1. *Virology* 2013;444(1-2):250–6.

Dewald O, Zymek P, Winkelmann K, Koerting A, Ren G, Abou-Khamis T, Michael LH, Rollins BJ, Entmann ML, Frangogiannis NG. CCL2/monocyte chemoattractant protein-1 regulates inflammatory responses critical to healing myocardial infarcts. *Circ Res* 2005;96(8):881–9.

Ding C, Chen X, Dascani P, Hu X, Bolli R, Zhang H, Mcleish KR, Yan J. STAT3 signaling in B cells is critical for germinal center maintenance and contributes to the pathogenesis of murine models of lupus. *J Immunol* 2016;196(11):4477–86.

Doi Y, Itoh M, Yonemura S, Ishihara S, Takano H, Noda T, Tsukita S. Normal development of mice and unimpaired cell adhesion/cell motility/actin-based cytoskeleton without compensatory up-regulation of ezrin or radixin in moesin gene knockout. *J Biol Chem* 1999;274(4):2315–21.

Duhen R, Glatigny S, Arbelaez CA, Blair TC, Oukka M, Bettelli E. Cutting edge: the pathogenicity of IFN-gamma-producing Th17 cells is independent of T-bet. *J Immunol* 2013;190(9):4478–82.

Durbin JE, Hackenmiller R, Simon MC, Levy DE. Targeted disruption of the mouse Stat1 gene results in compromised innate immunity to viral disease. *Cell* 1996;84(3):443–50.

Ellestad KK, Tsutsui S, Noorbakhsh F, Warren KG, Yong VW, Pittman QJ, Power C. Early life exposure to lipopolysaccharide suppresses experimental autoimmune encephalomyelitis by promoting tolerogenic dendritic cells and regulatory T cells. *J Immunol* 2009;183(1):298–309.

Elzagheid A, Korkeila E, Bendardaf R, Buhmeida A, Heikkilä S, Vaheri A, Syrjänen K, Pyrhönen S, Carpén O. Intense cytoplasmic ezrin immunoreactivity predicts poor survival in colorectal cancer. *Hum Pathol* 2008;39(12):1737–43.

Endo K, Kondo S, Shackleford J, Horikawa T, Kitagawa N, Yoshizaki T, Furukawa M, Zen Y, Pagano JS. Phosphorylated ezrin is associated with EBV latent membrane protein 1 in nasopharyngeal carcinoma and induces cell migration. *Oncogene* 2009;28(14):1725–35.

Entman ML, Youker K, Shoji T, Kukielka G, Shappell SB, Taylor AA, Smith CW. Neutrophil induced oxidative injury of cardiac myocytes. A compartmented system requiring CD11b/CD18-ICAM-1 adherence. *J Clin Invest* 1992;90(4):1335–45.

Fagerlund R, Mélen K, Kinnunen L, Julkunen I. Arginine/lysine-rich nuclear localization signals mediate interactions between dimeric STATs and importin alpha 5. *J Biol Chem* 2002;277(33):30072–8.

Fehon RG, McClatchey AI, Bretscher A. Organizing the cell cortex: the role of ERM proteins. *Nat Rev Mol Cell Biol* 2010;11(4):276–87.

Feng X, Petraglia AL, Chen M, Byskosh PV, Boos MD, Reder AT. Low expression of interferon-stimulated genes in active multiple sclerosis is linked to subnormal phosphorylation of STAT1. *J Neuroimmunol* 2002;129(1-2):205–15.

Fenyk-Melody JE, Garrison AE, Brunnert SR, Weidner JR, Shen F, Shelton BA, Mudgett JS. Experimental autoimmune encephalomyelitis is exacerbated in mice lacking the NOS2 gene. *J Immunol* 1998;160(6):2940–6.

Ferber IA, Brocke S, Taylor-Edwards C, Ridgway W, Dinisco C, Steinman L, Dalton D, Fathman CG. Mice with a disrupted IFN-gamma gene are susceptible to the induction of experimental autoimmune encephalomyelitis (EAE). *J Immunol* 1996;156(1):5–7.

Fischer P, Hilfiker-Kleiner D. Role of gp130-mediated signalling pathways in the heart and its impact on potential therapeutic aspects. *Br J Pharmacol* 2008;153 Suppl 1:S414–27.

Fischer P, Hilfiker-Kleiner D. Survival pathways in hypertrophy and heart failure: the gp130-STAT axis. *Basic Res Cardiol* 2007;102(5):393–411.

Flaishon L, Lantner F, Hershkoviz R, Levo Y, Shachar I. Low levels of IFN-gamma down-regulate the integrin-dependent adhesion of B cells by activating a pathway that interferes with cytoskeleton rearrangement. *J Biol Chem* 2001;276(50):46701–6.

Fontenot JD, Rasmussen JP, Gavin MA, Rudensky AY. A function for interleukin 2 in Foxp3-expressing regulatory T cells. *Nat Immunol* 2005;6(11):1142–51.

Fragale A, Gabriele L, Stellacci E, Borghi P, Perrotti E, Ilari R, Lanciotti A, Remoli AL, Venditti M, Belardelli F, Battistini A. IFN regulatory factor-1 negatively regulates CD4+ CD25+ regulatory T cell differentiation by repressing Foxp3 expression. *J Immunol* 2008;181(3):1673–82.

Frangogiannis NG. Regulation of the inflammatory response in cardiac repair. *Circ Res* 2012;110(1):159–73.

Frausto-Del-Río D, Soto-Cruz I, Garay-Canales C, Ambriz X, Soldevila G, Carretero-Ortega J, Vázquez-Prado J, Ortega E. Interferon gamma induces actin polymerization, Rac1 activation and down regulates phagocytosis in human monocytic cells. *Cytokine* 2012;57(1):158–68.

Frisullo G, Angelucci F, Caggiula M, Nociti V, Iorio R, Patanella AK, Sancricca C, Mirabella M, Tonali PA, Batocchi AP. pSTAT1, pSTAT3, and T-bet expression in peripheral blood mononuclear cells from relapsing-remitting multiple sclerosis patients correlates with disease activity. *J Neurosci Res* 2006;84(5):1027–36.

Fu XY. A transcription factor with SH2 and SH3 domains is directly activated by an interferon α-induced cytoplasmic protein tyrosine kinase(s). *Cell* 1992;70(2):323–35.

Fuchs M, Hilfiker A, Kaminski K, Hilfiker-Kleiner D, Guener Z, Klein G, Podewski E Schieffer B, Rose-John S, Drexler H. Role of interleukin-6 for LV remodeling and survival after experimental myocardial infarction. *FASEB J* 2003;17(14):2118–20.

Furutani Y, Matsuno H, Kawasaki M, Sasaki T, Mori K, Yoshihara Y. Interaction between telencephalin and ERM family proteins mediates dendritic filopodia formation. *J Neurosci* 2007;27(33):8866–76.

Galli A, Lombardi F. Postinfarct left ventricular remodelling: a prevailing cause of heart failure. *Cardiol Res Pract* 2016;2016:2579832.

Gao XM, Xu Q, Kiriazis H, Dart AM, Du XJ. Mouse model of post-infarct ventricular rupture: time course, strain- and gender-dependency, tensile strength, and histopathology. *Cardiovasc Res* 2005;65(2):469–77.

Gawaz M. Role of platelets in coronary thrombosis and reperfusion of ischemic myocardium. *Cardiovasc Res* 2004;61(3):498–511.

Gillis S, Watson J. Biochemical and biological characterization of lymphocyte regulatory molecules. V. Identification of an interleukin 2-producing human leukemia T cell line. *J Exp Med* 1980;152(6):1709–19.

Grigoriadis N, van Pesch V. A basic overview of multiple sclerosis immunopathology. *Eur J Neurol* 2015;22 Suppl 2:3–13.

Gutzmer R, Lisewski M, Zwirner J, Mommert S, Diesel C, Wittmann M, Kapp A, Werfel T. Human monocyte-derived dendritic cells are chemoattracted to C3a after up-regulation of the C3a receptor with interferons. *Immunology* 2004;111(4):435–43.

Hamada K, Shimizu T, Matsui T, Tsukita S, Hakoshima T. Structural basis of the membrane-targeting and unmasking mechanisms of the radixin FERM domain. *EMBO J* 2000;19(17):4449–62.

Harada T, Kyttaris V, Li Y, Juang YT, Wang Y, Tsokos GC. Increased expression of STAT3 in SLE T cells contributes to enhanced chemokine-mediated cell migration. *Autoimmunity* 2007;40(1):1–8.

Harrington LE, Hatton RD, Mangan PR, Turner H, Murphy TL, Murphy KM, Weaver CT. Interleukin 17-producing CD4+ effector T cells develop via a lineage distinct from the T helper type 1 and 2 lineages. *Nat Immunol* 2005;6(11):1123–32.

Hart BA 't, van Kooyk Y, Geurts JJ, Gran B. The primate autoimmune encephalomyelitis model; a bridge between mouse and man. *Ann Clin Transl Neurol* 2015;2(5):581–93.

Heusch G, Musiolik J, Gedik N, Skyschally A. Mitochondrial STAT3 activation and cardioprotection by ischemic postconditioning in pigs with regional myocardial ischemia/reperfusion. *Circ Res* 2011;109(11):1302-8.

Hilfiker-Kleiner D, Hilfiker A, Fuchs M, Kaminski K, Schaefer A, Schieffer B, Hillmer A, Schmiedl A, Ding Z, Podewski E, Podeswki E, Poli V, Schneier MD, Schulz R, Park JK, Wollert KC, Drexler H. Signal transducer and activator of transcription 3 is required for myocardial capillary growth, control of interstitial matrix deposition, and heart protection from ischemic injury. *Circ Res* 2004;95(2):187–95.

Hilfiker-Kleiner D, Shukla P, Klein G, Schaefer A, Stapel B, Hoch M, Müller W, Scherr M, Theilmeier G, Ernst M, Hilfiker A, Drexler H. Continuous glycoprotein-130-mediated signal transducer and activator of transcription-3 activation promotes inflammation, left ventricular rupture, and adverse outcome in subacute myocardial infaction. *Circulation* 2010;122(2):14–55.

Hoeve J ten, Jesus Ibarra-Sanchez M de, Fu Y, Zhu W, Tremblay M, David M, Shuai K. Identification of a nuclear Stat1 protein tyrosine phosphatase. *Mol Cell Biol* 2002;22(16):5662–8.

Horvath CM. STAT proteins and transcriptional responses to extracellular signals. *Trends Biochem Sci* 2000;25(10):496–502.

Hu X, Herrero C, Li W, Antoniv TT, Falck-Pedersen E, Koch AE, Woods JM, Haines GK, Ivashkiv LB. Sensitization of IFN-gamma Jak-STAT signaling during macrophage activation. *Nat Immunol* 2002;3(9):859–66.

Hu X, Ivashkiv LB. Cross-regulation of signaling pathways by interferon-gamma: implications for immune responses and autoimmune diseases. *Immunity* 2009;31(4):539–50.

Hüntelmann B, Staab J, Herrmann-Lingen C, Meyer T. A conserved motif in the linker domain of STAT1 transcription factor is required for both recognition and release from high-affinity DNA-binding sites. *PloS One* 2014;9(5):e97633.

Ishihara S, Nishikimi A, Umemoto E, Miyasaka M, Saegusa M, Katagiri K. Dual functions of Rap1 are crucial for T-cell homeostasis and prevention of spontaneous colitis. *Nat Commun* 2015;6:8982.

Ivanov II, McKenzie BS, Zhou L, Tadokoro CE, Lepelley A, Lafaille JJ, Cua DJ, Littman DR. The orphan nuclear receptor RORgammat directs the differentiation program of proinflammatory IL-17+ T helper cells. *Cell* 2006;126(6):1121–33.

Ivetic A, Ridley AJ. Ezrin/radixin/moesin proteins and Rho GTPase signalling in leucocytes. *Immunology* 2004;112(2):165–76.

Iyer SS, Ghaffari AA, Cheng G. Lipopolysaccharide-mediated IL-10 transcriptional regulation requires sequential induction of type I IFNs and IL-27 in macrophages. *J Immunol* 2010;185(11):6599–607.

Jacoby JJ, Kalinowski A, Liu M, Zhang SS, Gao Q, Chai G, Ji L, Iwamoto Y, Li E, Schneider M, Russell KS, Fu XY. Cardiomyocyte-restricted knockout of STAT3 results in higher sensitivity to inflammation, cardiac fibrosis, and heart failure with advanced age. *Proc Natl Acad Sci U S A* 2003;100(22):12929–34.

John S, Vinkemeier U, Soldaini E, Darnell JE Jr, Leonard WJ. The significance of tetramerization in promoter recruitment by Stat5. *Mol Cell Biol* 1999;19(3):1910–8.

Jouanguy E, Zhang S, Chapgier A, Sancho-Shimizu V, Puel A, Picard C, Boisson-Dupuis S, Abel L, Casanova JL. Human primary immunodeficiencies of type I interferons. *Biochimie* 2007;89(6-7):878–83.

Kamezaki K, Shimoda K, Numata A, Matsuda T, Nakayama KI, Harada M. The role of Tyk2, Stat1 and Stat4 in LPS-induced endotoxin signals. *Int Immunol* 2004;16(8):1173–9.

Kaplan MH, Schindler U, Smiley ST, Grusby MJ. Stat6 is required for mediating responses to IL-4 and for development of Th2 cells. *Immunity* 1996a;4(3):313–9.

Kaplan MH, Sun YL, Hoey T, Grusby MJ. Impaired IL-12 responses and enhanced development of Th2 cells in Stat4-deficient mice. *Nature* 1996b;382(6587):174–7.

Kaptein A, Paillard V, Saunders M. Dominant negative Stat3 mutant inhibits interleukin-6-induced Jak-STAT signal transduction. *J Biol Chem* 1996;271(11):5961–4.

Kawai T, Akira S. The role of pattern-recognition receptors in innate immunity: update on Toll-like receptors. *Nat Immunol* 2010;11(5):373–84.

Kawata T, Shevchenko A, Fukuzawa M, Jermyn KA, Totty NF, Zhukovskaya NV, Sterling AE, Mann M, Williams JG. SH2 signaling in a lower eukaryote: a STAT protein that regulates stalk cell differentiation in dictyostelium. *Cell* 1997;89(6):909–16.

Kieseier BC, Hartung HP. Current disease-modifying therapies in multiple sclerosis. *Semin Neurol* 2003;23(2):133–46.

Kikuchi S, Hata M, Fukumoto K, Yamane Y, Matsui T, Tamura A, Yonemura S, Yamagishi H, Keppler D, Tsukita S, Tsukita S. Radixin deficiency causes conjugated hyperbilirubinemia with loss of Mrp2 from bile canalicular membranes. *Nat Genet* 2002;31(3):320–5.

Killock DJ, Parsons M, Zarrouk M, Ameer-Beg SM, Ridley AJ, Haskard DO, Zvelebil M, Ivetic A. In vitro and in vivo characterization of molecular interactions between calmodulin, ezrin/radixin/moesin, and L-selectin. *J Biol Chem* 2009;284(13):8833–45.

Kingwell E, Marriott JJ, Jetté N, Pringsheim T, Makhani N, Morrow SA, Fisk JD, Evans C, Béland SG, Kulaga S, Dykeman J, Wolfson C, Koch MW, Marrie RA. Incidence and prevalence of multiple sclerosis in Europe: a systematic review. *BMC Neurol* 2013;13:128.

Knight RA, Scarabelli TM, Stephanou A. STAT transcription in the ischemic heart. *JAKSTAT* 2012;1(2):111–7.

Kono H, Rock KL. How dying cells alert the immune system to danger. *Nat Rev Immunol* 2008;8(4):279–89.

Korn T, Bettelli E, Gao W, Awasthi A, Jäger A, Strom TB, Oukka M, Kuchroo VK. IL-21 initiates an alternative pathway to induce proinflammatory T(H)17 cells. *Nature* 2007;448(7152):484–7.

Kotenko SV, Gallagher G, Baurin VV, Lewis-Antes A, Shen M, Shah NK, Langer JA, Sheikh F, Dickensheets H, Donnelly RP. IFN-lambdas mediate antiviral protection through a distinct class II cytokine receptor complex. *Nat Immunol* 2003;4(1):69–77.

Krakowski M, Owens T. Interferon-gamma confers resistance to experimental allergic encephalomyelitis. *Eur J Immunol* 1996;26(7):1641–6.

Krenger W, Falzarano G, Delmonte J Jr, Snyder KM, Byon JC, Ferrara JL. Interferon-gamma suppresses T-cell proliferation to mitogen via the nitric oxide pathway during experimental acute graft-versus-host disease. *Blood* 1996;88(3):1113–21.

Kroenke MA, Carlson TJ, Andjelkovic AV, Segal BM. IL-12- and IL-23-modulated T cells induce distinct types of EAE based on histology, CNS chemokine profile, and response to cytokine inhibition. *J Exp Med* 2008;205(7):1535–41.

Kurihara T, Warr G, Loy J, Bravo R. Defects in macrophage recruitment and host defense in mice lacking the CCR2 chemokine receptor. *J Exp Med* 1997;186(10):1757–62.

Lagresle-Peyrou C, Luce S, Ouchani F, Soheili TS, Sadek H, Chouteau M, Durand A, Pic I, Majewski J, Brouzes C, Lambert N, Bohineust A, Verhoeven E, Cosset FL, Magerus-Chatinet A, Rieux-Laucat F, Gandemer V, Monnier D, Heijmans C, van Gijn M, Dalm VA, Mahlaoui N, Stephan JL, Picard C, Durandy A, Kracker S, Hivroz C, Jabado N, de Saint Basile G, Fischer A, Cavazzana M, André-Schmutz I. X-linked primary immunodeficiency associated with hemizygous mutations in the moesin (MSN) gene. *J Allergy Clin Immunol* 2016 S0091-6749(16)30423–7.

Lamb RF, Ozanne BW, Roy C, McGarry L, Stipp C, Mangeat P, Jay DG. Essential functions of ezrin in maintenance of cell shape and lamellipodial extension in normal and transformed fibroblasts. *Curr Biol* 1997;7(9):682–8.

Langer JA, Pestka S. Interferon receptors. *Immunol Today* 1988;9(12):393–400.

Larner AC, David M, Feldman GM, Igarashi K, Hackett RH, Webb DS, Sweitzer SM, Petricoin EF 3rd, Finbloom DS. Tyrosine phosphorylation of DNA binding proteins by multiple cytokines. *Science* 1993;261(5129):1730–3.

Lazear HM, Nice TJ, Diamond MS. Interferon-lambda: immune functions at barrier surfaces and beyond. *Immunity* 2015;43(1):15–28.

Lee J, Katakai T, Hara T, Gonda H, Sugai M, Shimizu A. Roles of p-ERM and Rho-ROCK signaling in lymphocyte polarity and uropod formation. *J Cell Biol* 2004;167(2):327–37.

Leiphrakpam PD, Rajput A, Mathiesen M, Agarwal E, Lazenby AJ, Are C, Brattain MG, Chowdhury S. Ezrin expression and cell survival regulation in colorectal cancer. *Cell Signal* 2014;26(5):868–79.

Leung S, Li X, Stark GR. STATs find that hanging together can be stimulating. *Science* 1996;273(5276):750–1.

Levy DE, Darnell JE Jr. Stats: transcriptional control and biological impact. *Nat Rev Mol Cell Biol* 2002;3(9):651–62.

Li XL, Lv J, Xi NN, Wang T, Shang XF, Xu HQ, Han Z, O'Byrne KT, Li XF, Zheng RY. Neonatal endotoxin exposure suppresses experimental autoimmune encephalomyelitis through regulating the immune cells responsivity in the central nervous system of adult rats. *Biochem Biophys Res Commun* 2010;398(2):302–8.

Li Y, Harada T, Juang YT, Kyttaris VC, Wang Y, Zidanic M, Tung K, Tsokos GC. Phosphorylated ERM is responsible for increased T cell polarization, adhesion, and migration in patients with systemic lupus erythematosus. *J Immunol* 2007;178(3):1938–47.

Lighvani AA, Frucht DM, Jankovic D, Yamane H, Aliberti J, Hissong BD, Nguyen BV, Gadina M, Sher A, Paul WE, O'Shea JJ. T-bet is rapidly induced by interferon-gamma in lymphoid and myeloid cells. *Proc Natl Acad Sci U S A* 2001;98(26):15137–42.

Lin JX, Li P, Liu D, Jin HT, He J, Ata Ur Rasheed M, Rochman Y, Wang L, Cui K, Liu C, Kelsall BL, Ahmed R, Leonard WJ. Critical role of STAT5 transcription factor tetramerization for cytokine responses and normal immune function. *Immunity* 2012;36(4):586–99.

Linossi EM, Nicholson SE. Kinase inhibition, competitive binding and proteasomal degradation: resolving the molecular function of the suppressor of cytokine signaling (SOCS) proteins. *Immunol Rev* 2015;266(1):123–33.

Liu B, Mink S, Wong KA, Stein N, Getman C, Dempsey PW, Wu H, Shuai K. PIAS1 selectively inhibits interferon-inducible genes and is important in innate immunity. *Nat Immunol* 2004;5(9):891–8.

Liu X, Robinson GW, Wagner KU, Garrett L, Wynshaw-Boris A, Hennighausen L. Stat5a is mandatory for adult mammary gland development and lactogenesis. *Genes Dev* 1997;11(2):179–86.

Livak KJ, Schmittgen TD. Analysis of relative gene expression data using real-time quantitative PCR and the 2(-Delta Delta C(T)) Method. *Methods* 2001;25(4):402–8.

Lödige I, Marg A, Wiesner B, Malecová B, Oelgeschläger T, Vinkemeier U. Nuclear export determines the cytokine sensitivity of STAT transcription factors. *J Biol Chem* 2005;280(52):43087–99.

Ma CS, Wong N, Rao G, Nguyen A, Avery DT, Payne K, Torpy J, O'Young P, Deenick E, Bustamante J, Puel A, Okada S, Kobayashi M, Martinez-Barricarte R, Elliott M, Sebnem Kilic S, El Baghdadi J, Minegishi Y, Bousfiha A, Robertson N, Hambleton S, Arkwright PD, French M,

Blincoe AK, Hsu P, Campbell DE, Stormon MO, Wong M, Adelstein S, Fulcher DA, Cook MC, Stepensky P, Boztug K, Beier R, Ikincioğullari A, Ziegler JB, Gray P, Picard C, Boisson-Dupuis S, Phan TG, Grimbacher B, Warnatz K, Holland SM, Uzel G, Casanova JL, Tangye SG. Unique and shared signaling pathways cooperate to regulate the differentiation of human CD4+ T cells into distinct effector subsets. *J Exp Med* 2016 213(8):1589–608.

Majoros A, Platanitis E, Szappanos D, Cheon H, Vogl C, Shukla P, Stark GR, Sexl V, Schreiber R, Schindler C, Müller M, Decker T. Response to interferons and antibacterial innate immunity in the absence of tyrosine-phosphorylated STAT1. *EMBO Rep* 2016;17(3):367–82.

Mao X, Ren Z, Parker GN, Sondermann H, Pastorello MA, Wang W, McMurray JS, Demeler B, Darnell JE Jr, Chen X. Structural bases of unphosphorylated STAT1 association and receptor binding. *Mol Cell* 2005;17(6):761–71.

Marcelo P, Lefèvre F. Induction of the IFN-gamma gene and protein is linked to the establishment of cell polarity in a porcine epithelial cell line. *Exp Cell Res* 2002;280(1):33–44.

Matsui T, Maeda M, Doi Y, Yonemura S, Amano M, Kaibuchi K, Tsukita S, Tsukita S. Rho-kinase phosphorylates COOH-terminal threonines of ezrin/radixin/moesin (ERM) proteins and regulates their head-to-tail association. *J Cell Biol* 1998;140(3):647–57.

Matsumoto M, Hirata T. Moesin regulates neutrophil rolling velocity in vivo. *Cell Immunol* 2016;304-305:59–62.

McBride KM, Banninger G, McDonald C, Reich NC. Regulated nuclear import of the STAT1 transcription factor by direct binding of importin-alpha. *EMBO J* 2002;21(7):1754–63.

McCormick J, Barry SP, Sivarajah A, Stefanutti G, Townsend PA, Lawrence KM, Eaton S, Knight RA, Thiemermann C, Latchman DS, Stephanou A. Free radical scavenging inhibits STAT phosphorylation following in vivo ischemia/reperfusion injury. *FASEB J* 2006;20(12):2115–7.

McCormick J, Suleman N, Scarabelli TM, Knight RA, Latchman DS, Stephanou A. STAT1 deficiency in the heart protects against myocardial infarction by enhancing autophagy. *J Cell Mol Med* 2012;16(2):386–93.

McKendry R, John J, Flavell D, Müller M, Kerr IM, Stark GR. High-frequency mutagenesis of human cells and characterization of a mutant unresponsive to both alpha and gamma interferons. *Proc Natl Acad Sci U S A* 1991;88(24):11455–9.

McWhorter FY, Wang T, Nguyen P, Chung T, Liu WF. Modulation of macrophage phenotype by cell shape. *Proc Natl Acad Sci U S A* 2013;110(43):17253–8.

Menager C, Vassy J, Doliger C, Legrand Y, Karniguian A. Subcellular localization of RhoA and ezrin at membrane ruffles of human endothelial cells: differential role of collagen and fibronectin. *Exp Cell Res* 1999;249(2):221–30.

Meraz MA, White JM, Sheehan KC, Bach EA, Rodig SJ, Dighe AS, Kaplan DH, Riley JK, Greenlund AC, Campbell D, Carver-Moore K, DuBois RN, Clark R, Aguet M, Schreiber RD. Targeted disruption of the Stat1 gene in mice reveals unexpected physiologic specificity in the JAK–STAT signaling pathway. *Cell* 1996;84(3):431–42.

Mertens C, Haripal B, Klinge S, Darnell JE Jr. Mutations in the linker domain affect phospho-STAT3 function and suggest targets for interrupting STAT3 activity. *Proc Natl Acad Sci U S A* 2015;112(48):14811–6.

Mertens C, Zhong M, Krishnaraj R, Zou W, Chen X, Darnell JE Jr. Dephosphorylation of phosphotyrosine on STAT1 dimers requires extensive spatial reorientation of the monomers facilitated by the N-terminal domain. *Genes Dev* 2006;20(24):3372–81.

Meyer T, Begitt A, Lödige I, van Rossum M, Vinkemeier U. Constitutive and IFN-gamma-induced nuclear import of STAT1 proceed through independent pathways. *EMBO J* 2002;21(3):344–54.

Meyer T, Begitt A, Vinkemeier U. Green fluorescent protein-tagging reduces the nucleocytoplasmic shuttling specifically of unphosphorylated STAT1. *FEBS J* 2007;274(3):815–26.

Meyer T, Hendry L, Begitt A, John S, Vinkemeier U. A single residue modulates tyrosine dephosphorylation, oligomerization, and nuclear accumulation of stat transcription factors. *J Biol Chem* 2004;279(18):18998–9007.

Meyer T, Marg A, Lemke P, Wiesner B, Vinkemeier U. DNA binding controls inactivation and nuclear accumulation of the transcription factor Stat1. *Genes Dev* 2003;17(16):1992–2005.

Moriggl R, Topham DJ, Teglund S, Sexl V, McKay C, Wang D, Hoffmeyer A, van Deursen J, Sangster MY, Bunting KD, Grosveld GC, Ihle JN. Stat5 is required for IL-2-induced cell cycle progression of peripheral T cells. *Immunity* 1999;10(2):249–59.

Mosmann TR, Cherwinski H, Bond MW, Giedlin MA, Coffman RL. Two types of murine helper T cell clone. I. Definition according to profiles of lymphokine activities and secreted proteins. *J Immunol* 1986;136(7):2348–57.

Murphy TL, Geissal ED, Farrar JD, Murphy KM. Role of the Stat4 N domain in receptor proximal tyrosine phosphorylation. *Mol Cell Biol* 2000;20(19):7121–31.

Nefedova Y, Huang M, Kusmartsev S, Bhattacharya R, Cheng P, Salup R, Jove R, Gabrilovich D. Hyperactivation of STAT3 is involved in abnormal differentiation of dendritic cells in cancer. *J Immunol* 2004;172(1):464–74.

Niggli V. Insights into the mechanism for dictating polarity in migrating T-cells. *Int Rev Cell Mol Biol* 2014;312:201–70.

Nishibori T, Tanabe Y, Su L, David M. Impaired development of CD4+ CD25+ regulatory T cells in the absence of STAT1: increased susceptibility to autoimmune disease. *J Exp Med* 2004;199(1):25–34.

Nogai A, Siffrin V, Bonhagen K, Pfueller CF, Hohnstein T, Volkmer-Engert R, Brück W, Stadelmann C, Kamradt T. Lipopolysaccharide injection induces relapses of experimental autoimmune encephalomyelitis in nontransgenic mice via bystander activation of autoreactive CD4+ cells. *J Immunol* 2005;175(2):959–66.

Novick D, Cohen B, Rubinstein M. The human interferon alpha/beta receptor: characterization and molecular cloning. *Cell* 1994;77(3):391–400.

Okamoto I, Kawano Y, Matsumoto M, Suga M, Kaibuchi K, Ando M, Saya H. Regulated CD44 cleavage under the control of protein kinase C, calcium influx, and the Rho family of small G proteins. *J Biol Chem* 1999;274(36):25525–34.

Ouadrhiri Y, Sibille Y, Tulkens PM. Modulation of intracellular growth of Listeria monocytogenes in human enterocyte Caco-2 cells by interferon-gamma and interleukin-6: role of nitric oxide and cooperation with antibiotics. *J Infect Dis* 1999;180(4):1195–204.

Park C, Li S, Cha E, Schindler C. Immune response in Stat2 knockout mice. *Immunity* 2000;13(6):795–804.

Park H, Li Z, Yang XO, Chang SH, Nurieva R, Wang YH, Wang Y, Hood L, Zhu Z, Tian Q, Dong C. A distinct lineage of CD4 T cells regulates tissue inflammation by producing interleukin 17. *Nat Immunol* 2005;6(11):1133–41.

Park JH, Jeong SY, Choi AJ, Kim SJ. Lipopolysaccharide directly stimulates Th17 differentiation in vitro modulating phosphorylation of RelB and NF-kappaB1. *Immunol Lett* 2015;165(1):10–9.

Pérez-Rivero G, Cascio G, Soriano SF, Sanz ÁG, Guinoa JS de, Rodríguez-Frade JM, Gomariz RP, Holgado BL, Cabañas C, Carrasco YR, Stein JV, Mellado M. Janus kinases 1 and 2 regulate chemokine-mediated integrin activation and naive T-cell homing. *Eur J Immunol* 2013;43(7):1745–57.

Pestonjamasp K, Amieva MR, Strassel CP, Nauseef WM, Furthmayr H, Luna EJ. Moesin, ezrin, and p205 are actin-binding proteins associated with neutrophil plasma membranes. *Mol Biol Cell* 1995;6(3):247–59.

Peters A, Fowler KD, Chalmin F, Merkler D, Kuchroo VK, Pot C. IL-27 induces Th17 differentiation in the absence of STAT1 signaling. *J Immunol* 2015;195(9):4144–53.

Piro M, Della Bona R, Abbate A, Biasucci LM, Crea F. Sex-related differences in myocardial remodeling. *J Am Coll Cardiol* 2010;55(11):1057–65.

Platanias LC. Mechanisms of type-I- and type-II-interferon-mediated signalling. *Nat Rev Immunol* 2005;5(5):375–86.

Pore D, Gupta N. The ezrin-radixin-moesin family of proteins in the regulation of B-cell immune response. *Crit Rev Immunol* 2015;35(1):15–31.

Potter DA, Tirnauer JS, Janssen R, Croall DE, Hughes CN, Fiacco KA, Mier JW, Maki M, Herman IM. Calpain regulates actin remodeling during cell spreading. *J Cell Biol* 1998;141(3):647–62.

Puddu P, Fais S, Luciani F, Gherardi G, Dupuis ML, Romagnoli G, Ramoni C, Cianfriglia M, Gessani S. Interferon-gamma up-regulates expression and activity of P-glycoprotein in human peripheral blood monocyte-derived macrophages. *Lab Invest* 1999;79(10):1299–309.

Qing Y, Stark GR. Alternative activation of STAT1 and STAT3 in response to interferon-gamma. *J Biol Chem* 2004;279(40):41679–85.

Rangachari M, Kuchroo VK. Using EAE to better understand principles of immune function and autoimmune pathology. *J Autoimmun* 2013;45:31–9.

Rawlings JS, Rosler KM, Harrison DA. The JAK/STAT signaling pathway. *J Cell Sci* 2004;117(Pt 8):1281–3.

Raziuddin S, Morrison DC. Prolonged suppression of experimental allergic encephalomyelitis in the Lewis rats: the effect of lipopolysaccharides. *J Immunol* 1982;128(3):1486–9.

Refaeli Y, van Parijs L, Alexander SI, Abbas AK. Interferon gamma is required for activation-induced death of T lymphocytes. *J Exp Med* 2002;196(7):999–1005.

Riley JK, Takeda K, Akira S, Schreiber RD. Interleukin-10 receptor signaling through the JAK-STAT pathway. Requirement for two distinct receptor-derived signals for anti-inflammatory action. *J Biol Chem* 1999;274(23):16513–21.

Sahrbacher UC, Lechner F, Eugster HP, Frei K, Lassmann H, Fontana A. Mice with an inactivation of the inducible nitric oxide synthase gene are susceptible to experimental autoimmune encephalomyelitis. *Eur J Immunol* 1998;28(4):1332–8.

Sauvé M, Ban K, Momen MA, Zhou YQ, Henkelman RM, Husain M, Drucker DJ. Genetic deletion or pharmacological inhibition of dipeptidyl peptidase-4 improves cardiovascular outcomes after myocardial infarction in mice. *Diabetes* 2010;59(4):1063–73.

Saygideğer-Kont Y, Minas TZ, Jones H, Hour S, Çelik H, Temel I, Han J, Atabey N, Erkizan HV, Toretsky JA, Üren A. Ezrin enhances EGFR signaling and modulates Erlotinib sensitivity in non-small cell lung cancer cells. *Neoplasia* 2016;18(2):111–20.

Scaffidi P, Misteli T, Bianchi ME. Release of chromatin protein HMGB1 by necrotic cells triggers inflammation. *Nature* 2002;418(6894):191–5.

Scarabelli TM, Gottlieb RA. Functional and clinical repercussions of myocyte apoptosis in the multifaceted damage by ischemia/reperfusion injury: old and new concepts after 10 years of contributions. *Cell Death Differ* 2004;11 Suppl 2:S144-52.

Scarabelli TM, Mariotto S, Abdel-Azeim S, Shoji K, Darra E, Stephanou A, Chen-Scarabelli C, Marechal JD, Knight R, Ciampa A, Saravolatz L, de Prati AC, Yuan Z, Cavalieri E, Menegazzi M, Latchman D, Pizza C, Perahia D, Suzuki H. Targeting STAT1 by myricetin and delphinidin provides efficient protection of the heart from ischemia/reperfusion-induced injury. *FEBS Lett* 2009;583(3):531–41.

Schaefer TS, Sanders LK, Nathans D. Cooperative transcriptional activity of Jun and Stat3 beta, a short form of Stat3. *Proc Natl Acad Sci U S A* 1995;92(20):9097–101.

Scherer WF, Syverton JT, Gey GO. Studies on the propagation in vitro of poliomyelitis viruses IV. Viral mltiplication in a stable strain of human malignant epithelial cells (strain HeLa) derived from an epidermoid carcinoma of the cervix. *J Exp Med* 1953(97(5)):695–710.

Scherrer-Crosbie M, Ullrich R, Bloch KD, Nakajima H, Nasseri B, Aretz HT, Lindsey ML, Vançon AC, Huang PL, Lee RT, Zapol WM, Picard MH. Endothelial nitric oxide synthase limits left ventricular remodeling after myocardial infarction in mice. *Circulation* 2001;104(11):1286–91.

Schindelin J, Arganda-Carreras I, Frise E, Kaynig V, Longair M, Pietzsch T, Preibisch S, Rueden C, Saalfeld S, Schmid B, Tinevez JY, White DJ, Hartenstein V, Eliceiri K, Tomacak P, Cardona A. Fiji: an open-source platform for biological-image analysis. *Nat Methods* 2012;9(7):676–82.

Schindler C, Fu XY, Improta T, Aebersold R, Darnell JE Jr. Proteins of transcription factor ISGF-3: one gene encodes the 91-and 84-kDa ISGF-3 proteins that are activated by interferon alpha. *Proc Natl Acad Sci U S A* 1992a;89(16):7836–9.

Schindler C, Shuai K, Prezioso VR, Darnell JE Jr. Interferon-dependent tyrosine phosphorylation of a latent cytoplasmic transcription factor. *Science* 1992b;257(5071):809–13.

Schneider CA, Rasband WS, Eliceiri KW. NIH Image to ImageJ: 25 years of image analysis. *Nat Methods* 2012;9(7):671–5.

Sheppard P, Kindsvogel W, Xu W, Henderson K, Schlutsmeyer S, Whitmore TE, Kuestner R, Garrigues U, Birks C, Roraback J, Ostrander C, Dong D, Shin J, Presnell S, Fox B, Haldeman B, Cooper E, Taft D, Gilbert T, Grant FJ, Tackett M, Krivan W, McKnight G, Clegg C, Foster D,

Klucher KM. IL-28, IL-29 and their class II cytokine receptor IL-28R. *Nat Immunol* 2003;4(1):63–8.

Shimoda K, van Deursen J, Sangster MY, Sarawar SR, Carson RT, Tripp RA, Chu C, Quelle FW, Nosaka T, Vignali DA, Doherty PC, Grosveld G, Paul WE, Ihle JN. Lack of IL-4-induced Th2 response and IgE class switching in mice with disrupted Stat6 gene. *Nature* 1996;380(6575):630–3.

Shuai K. Modulation of STAT signaling by STAT-interacting proteins. *Oncogene* 2000;19(21):2638–44.

Shuai K. Regulation of cytokine signaling pathways by PIAS proteins. *Cell Res* 2006;16(2):196–202.

Shuai K, Schindler C, Prezioso VR, Darnell JE Jr. Activation of transcription by IFN-gamma: tyrosine phosphorylation of a 91-kD DNA binding protein. *Science* 1992;258(5089):1808–12.

Shuai K, Stark GR, Kerr IM, Darnell JE Jr. A single phosphotyrosine residue of Stat91 required for gene activation by interferon-gamma. *Science* 1993a;261(5129):1744–6.

Shuai K, Ziemiecki A, Wilks AF, Harpur AG, Sadowski HB, Gilman MZ, Darnell JE Jr. Polypeptide signalling to the nucleus through tyrosine phosphorylation of Jak and Stat proteins. *Nature* 1993b;366(6455):580–3.

Slavin AJ, Soos JM, Stuve O, Patarroyo JC, Weiner HL, Fontana A, Bikoff EK, Zamvil SS. Requirement for endocytic antigen processing and influence of invariant chain and H-2M deficiencies in CNS autoimmunity. *J Clin Invest* 2001;108(8):1133–9.

Soulika AM, Lee E, McCauley E, Miers L, Bannerman P, Pleasure D. Initiation and progression of axonopathy in experimental autoimmune encephalomyelitis. *J Neurosci* 2009;29(47):14965–79.

Speil J, Baumgart E, Siebrasse JP, Veith R, Vinkemeier U, Kubitscheck U. Activated STAT1 transcription factors conduct distinct saltatory movements in the cell nucleus. *Biophys J* 2011;101(11):2592–600.

Staab J, Riebeling T, Koch V, Herrmann-Lingen C, Meyer T. The two interfaces of the STAT1 N-terminus exhibit opposite functions in IFNgamma-regulated gene expression. *Mol Immunol* 2015;67(2 Pt B):596–606.

Stark GR. How cells respond to interferons revisited: from early history to current complexity. *Cytokine Growth Factor Rev* 2007;18(5-6):419–23.

Starr R, Hilton DJ. Negative regulation of the JAK/STAT pathway. *Bioessays* 1999;21(1):47–52.

Stephanou A, Brar BK, Scarabelli TM, Jonassen AK, Yellon DM, Marber MS, Knight RA, Latchman DS. *J Biol Chem* 2000;275(14):10002–8.

Stephanou A, Scarabelli TM, Townsend PA, Bell R, Yellon D, Knight RA, Latchman DS. The carboxyl-terminal activation domain of the STAT-1 transcription factor enhances ischemia/reperfusion-induced apoptosis in cardiac myocytes. *FASEB J* 2002;16(13):1841–3.

Strehlow I, Schindler C. Amino-terminal signal transducer and activator of transcription (STAT) domains regulate nuclear translocation and STAT deactivation. *J Biol Chem* 1998;273(43):28049–56.

Stritesky GL, Yeh N, Kaplan MH. IL-23 promotes maintenance but not commitment to the Th17 lineage. *J Immunol* 2008;181(9):5948–55.

Su SB, Grajewski RS, Luger D, Agarwal RK, Silver PB, Tang J, Tuo J, Chan CC, Caspi RR. Altered chemokine profile associated with exacerbated autoimmune pathology under conditions of genetic interferon-gamma deficiency. *Invest Ophthalmol Vis Sci* 2007;48(10):4616–25.

Surin B, Rouillard D, Bauvois B. Loss of alpha5beta1-mediated adhesion of monocytic cells to fibronectin by interferons beta and gamma is associated with changes in actin and paxillin cytoskeleton. *Hematol J* 2000;1(3):172–80.

Takeda K, Akira S. STAT family of transcription factors in cytokine-mediated biological responses. *Cytokine Growth Factor Rev* 2000;11(3):199–207.

Takeda K, Kishimoto T, Akira S. STAT6: its role in interleukin 4-mediated biological functions. *J Mol Med (Berl)* 1997a;75(5):317–26.

Takeda K, Noguchi K, Shi W, Tanaka T, Matsumoto M, Yoshida N, Kishimoto T, Akira S. Targeted disruption of the mouse Stat3 gene leads to early embryonic lethality. *Proc Natl Acad Sci U S A* 1997b;94(8):3801–4.

Takeuchi K, Sato N, Kasahara H, Funayama N, Nagafuchi A, Yonemura S, Tsukita S, Tsukita S. Perturbation of cell adhesion and microvilli formation by antisense oligonucleotides to ERM family members. *J Cell Biol* 1994;125(6):1371–84.

Tamura A, Kikuchi S, Hata M, Katsuno T, Matsui T, Hayashi H, Suzuki Y, Noda T, Tsukita S, Tsukita S. Achlorhydria by ezrin knockdown: defects in the formation/expansion of apical canaliculi in gastric parietal cells. *J Cell Biol* 2005;169(1):21–8.

Tojo SJ, Yokota S, Koike H, Schultz J, Hamazume Y, Misugi E, Yamada K, Hayashi M, Paulson JC, Morooka S. Reduction of rat myocardial ischemia and reperfusion injury by sialyl Lewis x oligosaccharide and anti-rat P-selectin antibodies. *Glycobiology* 1996;6(4):463–9.

Tran EH, Prince EN, Owens T. IFN-gamma shapes immune invasion of the central nervous system via regulation of chemokines. *J Immunol* 2000;164(5):2759–68.

Udy GB, Towers RP, Snell RG, Wilkins RJ, Park SH, Ram PA, Waxman DJ, Davey HW. Requirement of STAT5b for sexual dimorphism of body growth rates and liver gene expression. *Proc Natl Acad Sci U S A* 1997;94(14):7239–44.

Utech M, Ivanov AI, Samarin SN, Bruewer M, Turner JR, Mrsny RJ, Parkos CA, Nusrat A. Mechanism of IFN-gamma-induced endocytosis of tight junction proteins: myosin II-dependent vacuolarization of the apical plasma membrane. *Mol Biol Cell* 2005;16(10):5040–52.

Valitutti S, Dessing M, Aktories K, Gallati H, Lanzavecchia A. Sustained signaling leading to T cell activation results from prolonged T cell receptor occupancy. Role of T cell actin cytoskeleton. *J Exp Med* 1995;181(2):577–84.

van der Veen RC, Dietlin TA, Pen L, Gray JD, Hofman FM. Antigen presentation to Th1 but not Th2 cells by macrophages results in nitric oxide production and inhibition of T cell proliferation: interferon-gamma is essential but insufficient. *Cell Immunol* 2000;206(2):125–35.

Villarino AV, Gallo E, Abbas AK. STAT1-activating cytokines limit Th17 responses through both T-bet-dependent and -independent mechanisms. *J Immunol* 2010;185(11):6461–71.

Vilmos P, Kristó I, Szikora S, Jankovics F, Lukácsovich T, Kari B, Erdélyi M. The actin-binding ERM protein moesin directly regulates spindle assembly and function during mitosis. *Cell Biol Int* 2016;40(6):696–707.

Vinkemeier U, Cohen SL, Moarefi I, Chait BT, Kuriyan J, Darnell JE Jr. DNA binding of in vitro activated Stat1 alpha, Stat1 beta and truncated Stat1: interaction between NH2-terminal domains stabilizes binding of two dimers to tandem DNA sites. *EMBO J* 1996;15(20):5616–26.

Vinkemeier U, Moarefi I, Darnell JE Jr, Kuriyan J. Structure of the amino-terminal protein interaction domain of STAT-4. *Science* 1998;279(5353):1048–52.

Wan CK, Andraski AB, Spolski R, Li P, Kazemian M, Oh J, Samsel L, Swanson PA 2nd, McGavern DB, Sampaio EP, Freeman AF, Milner JD, Holland SM, Leonard WJ. Opposing roles of STAT1 and STAT3 in IL-21 function in CD4+ T cells. *Proc Natl Acad Sci U S A* 2015;112(30):9394–9.

Wang C, Morley SC, Donermeyer D, Peng I, Lee WP, Devoss J, Danilenko DM, Lin Z, Zhang J, Zhou J, Allen PM, Brown EJ. Actin-bundling protein L-plastin regulates T cell activation. *J Immunol* 2010;185(12):7487–97.

Wang D, Stravopodis D, Teglund S, Kitazawa J, Ihle JN. Naturally occurring dominant negative variants of Stat5. *Mol Cell Biol* 1996;16(11):6141–8.

Wang Y, Yago T, Zhang N, Abdisalaam S, Alexandrakis G, Rodgers W, McEver RP. Cytoskeletal regulation of CD44 membrane organization and interactions with E-selectin. *J Biol Chem* 2014;289(51):35159–71.

Wang Z, Hong J, Sun W, Xu G, Li N, Chen X, Liu A, Xu L, Sun B, Zhang JZ. Role of IFN-gamma in induction of Foxp3 and conversion of CD4+ CD25- T cells to CD4+ Tregs. *J Clin Invest* 2006;116(9):2434–41.

Watanabe K, Tachibana M, Kim S, Watarai M. Participation of ezrin in bacterial uptake by trophoblast giant cells. *Reprod Biol Endocrinol* 2009;7:95.

Webb JL, Harvey MW, Holden DW, Evans TJ. Macrophage nitric oxide synthase associates with cortical actin but is not recruited to phagosomes. *Infect Immun* 2001;69(10):6391–400.

Wegenka UM, Buschmann J, Lütticken C, Heinrich PC, Horn F. Acute-phase response factor, a nuclear factor binding to acute-phase response elements, is rapidly activated by interleukin-6 at the posttranslational level. *Mol Cell Biol* 1993;13(1):276–88.

Wegrzyn J, Potla R, Chwae YJ, Sepuri NB, Zhang Q, Koeck T, Drecka M, Szczepanek K, Szelag M, Gornicka A, Moh A, Moghaddas S, Chen Q, Bobbili S, Cichy J, Dulak J, Baker DP, Wolfman A, Stuehr D, Hassan MO, Fu XY, Avadhani N, Drake JI, Fawcett P, Lesnefsky EJ, Larner AC. Function of mitochondrial Stat3 in cellular respiration. *Science* 2009;323(5915):793–7.

Wenta N, Strauss H, Meyer S, Vinkemeier U. Tyrosine phosphorylation regulates the partitioning of STAT1 between different dimer conformations. *Proc Natl Acad Sci U S A* 2008;105(27):9238–43.

White HD, Norris RM, Brown MA, Brandt PW, Whitlock RM, Wild CJ. Left ventricular end-systolic volume as the major determinant of survival after recovery from myocardial infarction. *Circulation* 1987;76(1):44–51.

Willenborg DO, Fordham S, Bernard CC, Cowden WB, Ramshaw IA. IFN-gamma plays a critical down-regulatory role in the induction and effector phase of myelin oligodendrocyte glycoprotein-induced autoimmune encephalomyelitis. *J Immunol* 1996;157(8):3223–7.

Willenborg DO, Fordham SA, Staykova MA, Ramshaw IA, Cowden WB. IFN-gamma is critical to the control of murine autoimmune encephalomyelitis and regulates both in the periphery and in the target tissue: a possible role for nitric oxide. *J Immunol* 1999;163(10):5278–86.

Wurster AL, Tanaka T, Grusby MJ. The biology of Stat4 and Stat6. *Oncogene* 2000;19(21):2577–84.

Xiang FL, Lu X, Hammoud L, Zhu P, Chidiac P, Robbins J, Feng Q. Cardiomyocyte-specific overexpression of human stem cell factor improves cardiac function and survival after myocardial infarction in mice. *Circulation* 2009;120(12):1065-74, 9 p following 1074.

Yamaoka K, Saharinen P, Pesu M, HoltVE 3rd, Silvennoinen O, O'Shea JJ. The Janus kinases (Jaks). *Genome Biol* 2004;5(12):253.

Yamazaki T, Seko Y, Tamatani T, Miyasaka M, Yagita H, Okumura K, Nagai R, Yazaki Y. Expression of intercellular adhesion molecule-1 in rat heart with ischemia/reperfusion and limitation of infarct size by treatment with antibodies against cell adhesion molecules. *Am J Pathol* 1993;143(2):410–8.

Yan R, Small S, Desplan C, Dearolf CR, Darnell JE Jr. Identification of a Stat gene that functions in Drosophila development. *Cell* 1996;84(3):421–30.

Yang E, Henriksen MA, Schaefer O, Zakharova N, Darnell JE Jr. Dissociation time from DNA determines transcriptional function in a STAT1 linker mutant. *J Biol Chem* 2002;277(16):13455–62.

Yang J, Stark GR. Roles of unphosphorylated STATs in signaling. *Cell Res* 2008;18(4):443–51.

Yang XO, Panopoulos AD, Nurieva R, Chang SH, Wang D, Watowich SS, Dong C. STAT3 regulates cytokine-mediated generation of inflammatory helper T cells. *J Biol Chem* 2007;282(13):9358–63.

Yao X, Thibodeau A, Forte JG. Ezrin-calpain I interactions in gastric parietal cells. *Am J Physiol* 1993;265(1 Pt 1):C36-46.

Yeh WI, McWilliams IL, Harrington LE. Autoreactive Tbet-positive CD4 T cells develop independent of classic Th1 cytokine signaling during experimental autoimmune encephalomyelitis. *J Immunol* 2011;187(10):4998–5006.

Youakim A, Ahdieh M. Interferon-gamma decreases barrier function in T84 cells by reducing ZO-1 levels and disrupting apical actin. *Am J Physiol* 1999;276(5 Pt 1):G1279-88.

Zawawi KH, Kantarci A, Schulze-Späte U, Fujita T, Batista EL Jr, Amar S, van Dyke TE. Moesin-induced signaling in response to lipopolysaccharide in macrophages. *J Periodontal Res* 2010;45(5):589–601.

Zettl UK, Mix E, Zielasek J, Stangel M, Hartung HP, Gold R. Apoptosis of myelin-reactive T cells induced by reactive oxygen and nitrogen intermediates in vitro. *Cell Immunol* 1997;178(1):1–8.

Zhang SY, Boisson-Dupuis S, Chapgier A, Yang K, Bustamante J, Puel A, Picard C, Abel L, Jouanguy E, Casanova JL. Inborn errors of interferon (IFN)-mediated immunity in humans: insights into the respective roles of IFN-alpha/beta, IFN-gamma, and IFN-lambda in host defense. *Immunol Rev* 2008;226:29–40.

Zhang Y, Hu MY, Wu WZ, Wang ZJ, Zhou K, Zha XL, Liu KD. The membrane-cytoskeleton organizer ezrin is necessary for hepatocellular carcinoma cell growth and invasiveness. *J Cancer Res Clin Oncol* 2006;132(11):685–97.

Zheng SG, Wang JH, Gray JD, Soucier H, Horwitz DA. Natural and induced CD4+CD25+ cells educate CD4+CD25- cells to develop suppressive activity: the role of IL-2, TGF-beta, and IL-10. *J Immunol* 2004;172(9):5213–21.

Zhong M, Henriksen MA, Takeuchi K, Schaefer O, Liu B, Hoeve J ten, Ren Z, Mao X, Chen X, Shuai K, Darnell JE Jr. Implications of an antiparallel dimeric structure of nonphosphorylated STAT1 for the activation-inactivation cycle. *Proc Natl Acad Sci U S A* 2005;102(11):3966–71.

Zhou H, Wang Y, Lian Q, Yang B, Ma Y, Wu X, Sun S, Liu Y, Sun B. Differential IL-10 production by DCs determines the distinct adjuvant effects of LPS and PTX in EAE induction. *Eur J Immunol* 2014;44(5):1352–62.

Zouein FA, Altara R, Chen Q, Lesnefsky EJ, Kurdi M, Booz GW. Pivotal importance of STAT3 in protecting the heart from acute and chronic stress: new advancement and unresolved issues. *Front Cardiovasc Med* 2015;2:36.

Curriculum vitae

Name	Theresa Riebeling
Date of Birth	8 September 1988
Place of Birth	Schwalmstadt, Germany
Nationality	German

Education:

05/2013 – present	Doctorate student, Institute of Psychosomatic Medicine and Psychotherapy, Department of Molecular Psychocardiology, University Medical Centre Göttingen, Germany, PhD program "Molecular Medicine" Research project 10 of the IRTG1816
10/2011 – 04/2013	Master student, Molecular Medicine, Georg-August-University, Göttingen, Germany, Master thesis: Oxidative stress as a potential cause for residual DNA damage and adverse side effects of radiation therapy in cancer patients; Grade: 1.5
10/2008 – 08/2011	Bachelor student, Molecular Medicine, Georg-August-University, Göttingen, Germany, Bachelor thesis: Studies on the development of hypertrophic cardiomyopathy in *Hspa4*-deficient mice; Grade: 1.75
08/1999 – 06/2008	Abitur, Melanchthon-Schule, Willingshausen-Steinatal, Germany; Grade 1.4

Participation in conferences:

29 May – 03 June 2016: **Gordon Research Conference, 'Chemotactic Cytokines'**, Girona, Spain, poster presentation: Transription of the cytoskeletal protein ezrin is induced by interferon-γ-activated STAT1

15 – 16 September 2014: **Joint KCL-JCI International Symposium, 'Recent advances in heart failure'**, London, UK, poster presentation: Binding to High-Affinity DNA Sequences Prevents the Disruption of STAT1 dimers